TECHNISCHE UNIVERSITÄT MÜNCHEN

Lehrstuhl für Realzeit-Computersysteme

Multi-Scale System Design and Management for Battery Health Optimization

Alma Marie Pröbstl

Vollständiger Abdruck der von der Fakultät für Elektrotechnik und Informationstechnik der Technischen Universität München zur Erlangung des akademischen Grades eines

Doktor-Ingenieurs (Dr.-Ing.)

genehmigten Dissertation.

Vorsitzender:	Prof. Dr.-Ing. Gerhard Rigoll
Prüfer der Dissertation:	1. Prof. Dr. sc. Samarjit Chakraborty 2. Prof. Dr.-Ing. Andreas Jossen 3. Prof. Qi Zhu, Ph.D., Northwestern University, Illinois, USA

Die Dissertation wurde am 18.09.2019 bei der Technischen Universität München eingereicht und durch die Fakultät für Elektrotechnik und Informationstechnik am 05.06.2020 angenommen.

Abstract

This thesis deals with battery health management approaches that have the objective to prolong the useful life of devices powered with Lithium-Ion (Li-Ion) batteries. To that end, three novel aging mitigating techniques are proposed that cover different areas of application. These strategies make use of contextual information and significantly mitigate battery aging.

With this aim in mind, we present these mitigation techniques in combination with three typical use cases of battery health management and make the following contributions within this thesis. In our first use case, we introduce a State-of-Health (SOH)-aware active cell balancing technique for Electric Vehicles (EVs) that adapts load currents to reduce stress on already impaired cells. In the second use case, we develop a context-aware intelligent charging scheme for smartphones that delays charging based on usage predictions. Battery aging is mitigated by reducing the duration for which the battery stays on a full charge level. In addition to delayed charging, the target charge level is lowered, thereby further mitigating battery aging. In the third use case, we develop a control strategy for a system consisting of an Electrical Energy Storage (EES) and Photovoltaic (PV) that minimizes both financial cost, i.e., the sum of battery aging cost, PV depreciation and grid electricity costs, as well as the privacy leakage.

The design and development of rechargeable battery-powered devices are mainly driven by (i) fast system performance, e.g., high processor speeds in smartphones, high driving speeds and acceleration in EVs, (ii) lower economic impact, e.g., cheap phones or affordable EVs, and (iii) increased customer satisfaction, e.g., high single cycle runtime, high availability, and flexibility. Today Li-Ion batteries are the most prevalent type of secondary batteries. Their fields of application cover a wide power range including smartphones, tablets, laptops, EVs, and stationary storages. With the increasing importance of renewable energies and the rise of the Internet of Things (IoT), the number of devices that rely on Li-Ion batteries in the future will grow further. We have got used to a seemingly infinite supply of raw materials and complex products being sold at cheap prices. Often, devices are replaced long before they become unusable and battery health is commonly neglected in system design. However, there are very good reasons to focus on extending the useful life of devices: Electronic waste increases and contaminates the soil. Rare earth materials slowly get more expensive and make recycling an attractive alternative. Besides, the number of customers that care about sustainable products is on the rise. Furthermore, the mining of lithium unbalances sensitive ecosystems and land use rights have negative social impacts on the local population. Similarly, poor ethical conditions occur in cobalt mining, which comes with child labor and unsafe working conditions.

Battery health management has the objective to mitigate battery aging. Over time and usage, batteries suffer from resistance growth and capacity fading. Aging control parameters of Li-Ion batteries, that can be targeted by system designers, are average State-of-Charge (SOC),

SOC swing, and temperature. By leveraging usage patterns, high average SOC can be reduced, thereby mitigating battery aging. Similarly, reduced SOC swing can prolong battery cycle life. Lower charge and discharge currents are less detrimental and can be achieved by slow charging or by avoiding peak loads, e.g., through load shifting. Proper cooling of Li-Ion batteries is required to not expose the battery to overly high temperatures. In cold environments, preheating is required for battery health-aware usage. Even if not in use, battery health degrades due to calendar aging. Battery health management targets these factors and mitigates aging by applying operational limits and smart battery health-aware control algorithms.

For our battery health management strategies, contextual information is exploited to adjust the battery aging relevant control parameters. Within this thesis, three novel aging mitigation control strategies are proposed.

In our first use case, we develop an SOH-aware cell balancing strategy for EV battery packs. We find that the useful life of a battery pack depends on the weakest cell since the capacity of the weakest or least healthy cell determines the limits of charge and discharge processes. A way to compensate for the limitations induced by the weaker cells is active cell balancing. Mitigation of the degradation of the least healthy cell extends the useful life of the pack and therefore of the whole device. The time until End-of-Life (EOL) can be extended by unburdening the less healthy cells from detrimental conditions if an active cell balancing architecture is installed. Using active cell balancing, the balancing currents are adjusted such that healthy cells are stressed more than less healthy cells and therefore the useful life of the pack is extended as the less healthy cells experience a lower current and lower SOC swing. We find that in the first use case, the SOH-aware cell balancing scheme for large scale battery packs on module-level mitigates aging by up to $23.5\,\%$ over passive cell balancing and up to $17.6\,\%$ over active SOC cell balancing.

In our second use case, we discuss an intelligent charging strategy for smartphones. As smartphones are often charged overnight, the battery remains at high SOCs for long periods. The introduction of charge delays based on contextual information of device usage lowers the average SOC. Charging is delayed such that the phone reaches the full charge level only shortly before the phone is unplugged. In addition to charge delays, reduction of the charge level can be achieved if the required charge is known in advance and the upper charge limit is lowered. Lower average SOC results in less severe aging. The choice of the charge level needs to be made following the usage pattern, e.g., the target SOC should accommodate the energy required until the smartphone is recharged. The combination of charge delays and lowered target charge SOC almost doubles the cycle life of smartphones.

In the third use case, we propose a control strategy that trades-off privacy, electricity costs, and battery aging for a residential home set-up consisting of an EES, PV, and a smart meter. We find that health-aware operation often conflicts with system operation goals. Therefore, compromising strategies need to be developed. Co-optimization problems of battery health and the system objective, e.g., minimization of financial costs, need to be formulated. Either it is possible to reach optimality for both objectives using the appropriate control parameters or slightly lower system performance should be taken into consideration to gain battery health. As battery health is a longterm effect and environmental costs often are not easily quantified, battery health is often neglected these days. We find that the financial operation and degradation costs for a trade-off solution of privacy and financial cost lie in the range of USD 600-1700.

Li-Ion battery aging factors are mostly independent of the application domain. On the other hand, the implementability of strategies depends on the target system whose requirements and infrastructure need to be considered. For example in Android, access to the charger chip is limited, making it difficult for independent app developers to introduce charge delays. Another example are system components. If an active balancing architecture or an advanced thermal system are existent, balancing and cooling control strategies can be co-optimized with battery aging mitigation. Similarly, if known, the charging patterns can be exploited to prolong battery cycle life. Predictors are a way to estimate the usage pattern, e.g., PV generation estimation based on the weather forecast or prediction of smartphone energy consumption from statistical data.

Bringing all together, we present a holistic view of multi-scale battery health management and also discuss cross-scale approaches. The aging management strategies operate on four different abstraction levels, namely, module-, device- and system-level. The challenge lies in the identification of feasible modifications of the charge and discharge patterns, which often depend on the application requirements. The factors contributing to the aging need to be targeted while impairing as little as possible the user experience as well as other system components. Towards this, we propose a modular framework to rapidly evaluate the aging mitigation capabilities of our use cases. We quantify the effects of techniques applied on cell-, module-, device- and system-level and discuss cross-layer strategies and implications.

In summary, this thesis proposes battery health management strategies for EVs, smartphones, and stationary storages. The discussed techniques and cycle life gains shall help to develop further aging mitigating strategies for environment-friendly and economically efficient products with increased useful life.

Kurzfassung

Diese Dissertation befasst sich mit Ansätzen zum Batteriezustandsmanagement mit dem Ziel, die Lebensdauer von Geräten mit Lithium-Ionen Batterien zu verlängern. Zu diesem Zweck werden drei neuartige Techniken zur Verlängerung der Lebensdauer von Batterien vorgeschlagen, die in verschiedenen Anwendungen eingesetzt werden können. Diese Strategien nutzen Kontextinformationen und verringern die Alterung der Batterie erheblich.

Diesbezüglich stellen wir drei Strategien und Anwendungsfälle des Batteriezustandsmanagements vor und leisten in dieser Arbeit die folgenden Beiträge. In unserem ersten Anwendungsfall führen wir eine State-of-Health (SOH)-basierte Methode zum aktiven Ausgleich von Zellladungen (auch Active Cell Balancing genannt) für Elektroautos ein, welche Lastströme anpasst, um die Belastung bereits beeinträchtigter Zellen zu verringern. Im zweiten Anwendungsfall entwickeln wir ein kontextsensitives intelligentes Ladeschema für Smartphones, das die Ladung basierend auf Nutzungsvorhersagen verzögert und den Sollladezustand reduziert, wodurch die Batteriealterung gemindert wird. Im dritten Anwendungsfall entwickeln wir eine kostenminimierende Steuerungsstrategie für ein System, das aus einem stationären Energiespeicher und einer Photovoltaik-Anlage besteht. Konkret wird die Summe aus Batteriealterungskosten, der Photovoltaik-Abschreibung und der Netz-Stromkosten minimiert sowie die Privatsphäre maximiert.

Das Design und die Entwicklung von wiederaufladbaren batteriebetriebenen Geräten wird hauptsächlich angetrieben durch (i) schnelle Systemleistung, z.B. hohe Prozessorgeschwindigkeit in Smartphones, oder hohe Reichweite und Beschleunigung von Elektroautos, (ii) geringere Kosten, z.B. kostengünstige Mobiltelefone oder erschwingliche Elektrofahrzeuge, und (iii) erhöhte Kundenzufriedenheit, z.B. hohe Einzelzykluslaufzeit, hohe Verfügbarkeit und Flexibilität. Heutzutage sind Lithium-Ionen Batterien die am weitesten verbreitete Art von Sekundärbatterien. Ihre Anwendungsbereiche decken ein breites Spektrum ab, darunter Smartphones, Tablets, Laptops, Elektrofahrzeuge und stationäre Speicher. Mit der zunehmenden Bedeutung erneuerbarer Energien und dem Aufkommen des Internet-of-Things wird auch in Zukunft die Anzahl von Geräten steigen, die auf Lithium-Ionen Batterien angewiesen sind. Wir haben uns an ein scheinbar unendliches Angebot an Rohstoffen und komplexen Produkten gewöhnt, die zu günstigen Preisen angeboten werden. Oft werden Geräte ausgetauscht, lange bevor sie unbrauchbar sind, und der Zustand der Batterie wird beim Systemdesign häufig vernachlässigt. Es gibt jedoch gute Gründe, sich auf die Verlängerung der Nutzungsdauer von Geräten zu konzentrieren: Elektroschrott häuft sich, verschmutzt Böden, seltene Erden verteuern sich und erhöhen die Attraktivität des Recyclings. Dazu kommt, dass die Zahl der Kunden, die Interesse an nachhaltigen Produkten zeigen, steigt. Der Abbau von Lithium bringt außerdem empfindliche Ökosysteme aus dem Gleichgewicht und die Verteilung von Landnutzungsrechten hat negative

soziale Auswirkungen auf die lokale Bevölkerung. In ähnlicher Weise geht der Kobaltabbau mit Kinderarbeit und unsicheren Arbeitsbedingungen einher.

Das Batteriezustandsmanagement hat das Ziel, die Alterung der Batterie zu verringern. Im Laufe der Zeit leiden Batterien unter ansteigendem Innenwiderstand und Kapazitätsschwund. Die Alterungsfaktoren von Lithium-Ionen Batterien, die bei der Systementwicklung beachtet werden sollten, sind der durchschnittliche State-of-Charge (SOC), SOC-Abweichung und Temperatur. Durch die Berücksichtigung von Nutzungsverhalten kann ein hoher durchschnittlicher SOC reduziert werden, wodurch die Batteriealterung gemindert wird. In ähnlicher Weise können verringerte Entladezyklustiefen die Lebensdauer der Batterie verlängern. Niedrigere Lade- und Entladeströme sind weniger schädlich und können durch langsames Laden oder durch Vermeiden von Spitzenlasten, beispielsweise durch Lastverschiebung, erzielt werden. Ausreichende Wärmeabfuhr muss gewährleistet sein, damit die Lithium-Ionen Batterien keinen zu hohen Temperaturen ausgesetzt werden. In kalten Umgebungen ist ein Vorwärmen erforderlich, um der Batterie nicht zu schaden. Selbst ohne aktive Nutzung altern Batterien bei längerer Lagerung. Das Batteriezustandsmanagement zielt auf die oben genannten Faktoren ab und mindert die Alterung durch Betriebsgrenzen und Lebensdauer-verbessernde Regelungsstrategien.

Bei diesen Strategien zum Batteriezustandsmanagement werden Kontextinformationen genutzt, um die für die Alterung der Batterie relevanten Steuerungsparameter anzupassen. In dieser Arbeit werden drei neuartige Strategien zur Verringerung der Batteriealterung vorgeschlagen.

Im ersten Anwendungsfall entwickeln wir eine SOH-basierte Strategie für Batteriepacks in Elektrofahrzeugen. Wir nutzen die Beobachtung, dass die Lebensdauer eines Batteriepacks von der schwächsten Zelle abhängt, da die Kapazität der schwächsten Zelle die Grenzen der Lade- und Entladevorgänge bestimmt. Ein Weg, um die durch die schwächeren Zellen induzierten Einschränkungen zu kompensieren, ist Active Cell Balancing. Die Verringerung der Beanspruchung der schwächsten Zelle verlängert die Nutzungsdauer des Packs und damit des gesamten Geräts. Die Zeit bis zum Lebensende des Packs kann verlängert werden, indem die weniger gesunden Zellen von schädlichen Bedingungen entlastet werden. Eine Architektur für Active Cell Balancing ermöglicht zusätzlich die Anpassung der Ausgleichsströme. Dadurch werden gesunde Zellen mehr als schwächere Zellen belastet. Die Nutzungsdauer des Packs verlängert sich, wenn die schwächeren Zellen einen geringeren Strom und eine geringere SOC Veränderung erfahren. Wir stellen fest, dass das SOH-basierte Zellenausgleichsschema für große Batteriepacks die Alterung um bis zu $23.5\,\%$ gegenüber dem passiven Cell Balancing verringert und bis zu $17.6\,\%$ gegenüber aktivem Cell Balancing.

Im zweiten Anwendungsfall stellen wir eine intelligente Ladestrategie für Smartphones vor. Da Smartphones häufig über Nacht geladen werden, verbleibt die Batterie über lange Zeit auf hohem SOC. Durch Verzögerung des Ladens basierend auf dem Nutzungskontext kann der Durchschnitts-SOC verringert werden. Zusätzlich kann eine Reduzierung des Ladezustands erreicht werden, wenn die benötigte Energie im Voraus bekannt ist. Ein niedrigerer durchschnittlicher SOC führt zu einer geringeren Alterung. Die Wahl des Ladestands muss sich am Nutzerverhalten orientieren, z.B. sollte der Zielladezustand die erforderliche Energie bereitstellen können, die für den nächsten Entladezyklus eines Smartphones benötigt wird. Die Kombination aus Ladeverzögerungen und verringerter Zielladung führt nahezu zu einer Verdopplung der Lebensdauer von Smartphones.

Im dritten Anwendungsfall stellen wir eine Regelungsstrategie vor, welche die Privatsphäre, Elektrizitätskosten und die Batteriealterung in einem Set-up bestehend aus einem stationären Batteriespeicher, einer Photovoltaik-Anlage und einem Smart Meter abwägt. Wir beobachten, dass ein funktionsbewusster Betrieb häufig mit den Zielen des Systembetriebs kollidiert. Daher müssen Kompromissstrategien entwickelt werden. Co-Optimierung des Batteriezustands und des Systemziels, z.B. Minimierung der finanziellen Kosten, müssen formuliert werden. Entweder ist es möglich, mit den entsprechenden Steuerungsparametern ein Optimum für beide Ziele zu erzielen, oder es sollte eine geringfügig geringere Systemleistung in Betracht gezogen werden, um den Batteriezustand zu verbessern. Da die Batteriegesundheit eine langfristige Auswirkung hat und die Umweltkosten häufig nicht leicht zu beziffern sind, wird die Batteriegesundheit heutzutage häufig vernachlässigt. Schließlich stellen wir fest, dass die finanziellen Betriebs- und Alterungskosten für eine Kompromisslösung zwischen Privatsphäre und Kosten im Bereich von 600-1700 US Dollar liegen.

Die Alterungsfaktoren von Lithium-Ionen Akkus sind größtenteils unabhängig von der Anwendungsdomäne. Andererseits hängt die Umsetzbarkeit von Strategien vom Zielsystem ab, dessen Anforderungen und Infrastruktur berücksichtigt werden müssen. Beispielsweise ist der Zugriff auf den Ladechip in Android-Geräten begrenzt, was es unabhängigen App-Entwicklern erschwert, Ladeverzögerungen einzuführen. Ein weiteres Beispiel sind Systemkomponenten. Wenn eine Architektur für Active Cell Balancing oder ein aktives thermisches Managementsystem vorhanden sind, können Cell Balancing-Strategien zusammen mit einer Verringerung der Batteriealterung optimiert werden. Ebenso können, falls bekannt, die Lademuster ausgenutzt werden, um die Batterielebensdauer zu verlängern. Prädiktoren sind eine Möglichkeit das Nutzungsmuster zu bestimmen. Beispiele sind die Vorhersage der Photovoltaik-Erzeugung basierend auf der Wettervorhersage oder die Vorhersage des Smartphone-Energieverbrauchs aus statistischen Daten.

Im vorletzten Kapitel wird eine ganzheitliche Sichtweise des Multi-Scale-Battery-Health-Managements präsentiert und darüber hinaus werden übergreifende Systemansätze diskutiert. Die Herausforderung besteht darin, mögliche Änderungen der Lade- und Entlademuster zu identifizieren, die häufig von den Anwendungsanforderungen abhängen. Strategien zum Batteriezustandsmanagement arbeiten auf vier verschiedenen Abstraktionsebenen: Zell-, Modul-, Geräte- und Systemebene. Die Faktoren, die zur Lebensdauer der Batterie beitragen, müssen gezielt angegangen werden ohne das Benutzererlebnis sowie andere Systemkomponenten zu beeinträchtigen. Um dies zu erreichen, schlagen wir ein modulares Framework vor, um die Alterungsreduzierung unserer Anwendungsfälle effizient zu bewerten. Wir quantifizieren die Auswirkungen von Techniken auf Zellen-, Modul-, Geräte- und Systemebene und diskutieren ebenen-übergreifende Strategien und Implikationen.

Zusammenfassend schlägt diese Arbeit Strategien für das Batterielebensdauermanagement für eine Vielzahl von Anwendungen vor. Die diskutierten Techniken sollen dazu beitragen, weitere Strategien zur Verringerung der Alterung für umweltfreundliche und wirtschaftlich effiziente Produkte mit längerer Lebensdauer zu entwickeln.

Acknowledgements

This thesis is the outcome of my work at the Chair of Real-Time Computer Systems (RCS) at the Technical University of Munich (TUM). During that time, I received a lot of support and encouragement from many people who deserve my sincere gratitude.

First of all, I would like to thank my advisor Samarjit Chakraborty for his support throughout the years and his excellent guidance. I consider myself very fortunate to have received his valuable insights throughout our fruitful discussions. Furthermore, the collaborations and research stay he initiated for me are invaluable. My sincere thank goes to Naehyuck Chang for hosting me at Seoul National University (SNU), South Korea, and for the successful collaboration during my research stay. I would also like to thank Prof Jossen and Prof Zhu for being co-examiners and reviewers of this thesis as well as Prof Rigoll for heading the examination committee.

I am particularly grateful to Sebastian Steinhorst, Sanyoung Park, and Swaminathan Narayanaswamy with whom, I collaborated closely in my research. I very much appreciate their time spent on discussions, their extensive feedback, and the very helpful advice both on scientific as well as personal questions.

My warmest thank goes to all my wonderful colleagues, co-authors, lunch-buddies, and friends I had the opportunity to meet and work with at RCS. The deep discussions, joyful laughs, and encouraging talks we had made my time here enjoyable, brightened up my days, and helped me through stressful periods. Many persons should be named and the list below surely is not complete. I would like to thank Florian Rattei without whom I would have never considered pursuing a doctoral degree. In particular, I am overly grateful to my team-mate and friend Nadja Peters who always listened when needed, discussed all sorts of personal and work problems, and who is a great team-player.

A big thank you goes to the administrative staff of RCS for all help and support. Furthermore, I would like to thank my working students for their support in building hardware and conducting experiments. I am also fortunate to have met such friendly and welcoming colleagues at TUM-CREATE, who made my teaching stays in Singapore even more enjoyable.

Finally, I particularly thank my friends, my parents, and my sister for their great support, their love, and their continuous encouragement both in times of struggle and success.

Contents

Abstract iii

Kurzfassung (German abstract) vii

Acknowledgements xi

1 Introduction 1
- 1.1 Motivation . . . 1
- 1.2 Background on batteries . . . 3
  - 1.2.1 Secondary batteries . . . 4
  - 1.2.2 Battery health degradation . . . 5
  - 1.2.3 Safety . . . 6
  - 1.2.4 Battery management systems . . . 6
  - 1.2.5 Costs . . . 8
- 1.3 Application domains of Li-Ion batteries . . . 9
  - 1.3.1 Mobile devices . . . 9
  - 1.3.2 Electric vehicles . . . 11
  - 1.3.3 Stationary battery storages . . . 12
- 1.4 Battery health-aware multi-scale management . . . 13
- 1.5 Contributions and organization . . . 14
  - 1.5.1 SOH-aware cell balancing for EV battery packs . . . 15
  - 1.5.2 Smart charging for smartphones . . . 16
  - 1.5.3 Cost/privacy co-optimization for stationary storages . . . 16
  - 1.5.4 Summary of contributions . . . 17
- 1.6 List of publications . . . 17

2 Battery State-of-Health: Basics, models and management approaches 19
- 2.1 Health degradation of Li-Ion batteries . . . 19
  - 2.1.1 Electrochemical degradation mechanisms . . . 19
  - 2.1.2 Causes for battery aging . . . 22
  - 2.1.3 State-of-Health estimation techniques . . . 23
- 2.2 Battery aging models . . . 24
  - 2.2.1 Model types . . . 24
  - 2.2.2 Requirements . . . 25
  - 2.2.3 Model selection . . . 26

2.3 Related work on battery health management techniques 28

3 SOH-aware active cell balancing strategy for high power battery packs 33
3.1 Introduction 34
3.1.1 Motivation 34
3.1.2 Contributions 35
3.2 Related work 36
3.2.1 SOH degradation mitigation in electric vehicles 36
3.2.2 Active cell balancing 36
3.2.3 Online SOH measurement 37
3.3 Observations for active cell balancing 37
3.3.1 Active cell balancing operating principle 37
3.3.2 Observations with two cells 37
3.4 System modeling 39
3.4.1 Battery aging model 39
3.4.2 Cell balancing efficiency 40
3.5 SOH-aware active cell balancing 41
3.5.1 Overview 41
3.5.2 Charge transfer direction 42
3.5.3 Balancing currents 43
3.6 Simulation results 44
3.6.1 Dependency on balancing current 46
3.6.2 Dependency on aging-speed 46
3.6.3 Dependency on initial aging distribution 47
3.7 Concluding remarks 47

4 Smart^2: Smart charging for smart phones 51
4.1 Introduction 52
4.1.1 Motivation 52
4.1.2 Contributions 52
4.2 Related work and background 54
4.2.1 Battery aging in smartphones 54
4.2.2 Battery management applications 55
4.2.3 Smartphone usage predictors 55
4.3 Aging-aware charging 56
4.3.1 Aging mitigation by delayed charging 56
4.3.2 Smart charger Android application 57
4.3.3 Smart charger hardware 58
4.3.4 Alarm clock based charging delay 58
4.4 Plug duration model 60
4.4.1 Simple moving average predictor 60
4.4.2 Exponential smoothing 62
4.4.3 Probabilistic predictor 63
4.5 Evaluation 64

4.5.1 Smartphone application evaluation . . . 64
4.5.2 Smart charging with optimal predictor . . . 65
4.5.3 Smart charging with predictor . . . 67
4.5.4 Comparison of predictors . . . 69
4.6 Discussion and open issues towards intelligent charging . . . 69
4.6.1 Intelligent charging protocol . . . 71
4.6.2 Under-dimensioned chargers . . . 74
4.6.3 Open issues . . . 76
4.7 Concluding remarks . . . 77

5 Cost/privacy co-optimization in smart energy grids 79
5.1 Introduction . . . 80
5.1.1 Motivation and related works . . . 80
5.1.2 Contributions . . . 82
5.2 Motivational example and problem statement . . . 82
5.3 System models . . . 84
5.3.1 Battery cycle life and associated cost . . . 84
5.3.2 Residential load model . . . 84
5.3.3 PV power generation model and PV cost . . . 85
5.3.4 Dynamic energy pricing . . . 85
5.3.5 Mutual information . . . 86
5.4 Financial cost and privacy optimization . . . 86
5.4.1 States, actions and reward . . . 86
5.4.2 Transition probability matrix . . . 87
5.4.3 Transition reward matrix . . . 87
5.4.4 Battery aging, grid and privacy cost . . . 87
5.4.5 Solution . . . 88
5.5 Simulation results . . . 88
5.5.1 Privacy-cost trade-off . . . 89
5.5.2 Dimensioning of PV . . . 90
5.5.3 Dimensioning of electrical energy storage and quantification of costs . 90
5.5.4 Cost overhead for existing installations . . . 92
5.5.5 Cost splitting . . . 92
5.6 Concluding remarks . . . 93

6 Battery health-aware multi-scale design and management 95
6.1 Introduction . . . 96
6.2 Multi-scale health management techniques . . . 98
6.2.1 Cell-level . . . 99
6.2.2 Module-level . . . 100
6.2.3 Device-level . . . 102
6.2.4 System-level . . . 103
6.2.5 Cross-layer health management . . . 103
6.2.6 Battery health management framework . . . 104

6.3 Results 106
6.3.1 Experimental set-up 106
6.3.2 Combination of cell- and module-level 107
6.3.3 Combination of cell- and device-level 108
6.3.4 Combination of module- and device-level 108
6.3.5 Combination of cell-, module- and device level 109
6.4 Concluding remarks 112

7 Concluding remarks **117**
7.1 Summary 117
7.2 Future work 119

Bibliography **121**

List of Tables **137**

List of Figures **140**

Nomenclature **141**

Abbreviations **147**

1 Introduction

Battery-powered systems are ubiquitous. They are present in various fields of applications, such as smartphones, laptops, Electric Vehicles (EVs), and stationary storages. Lithium-Ion (Li-Ion) batteries are frequently used in such systems, due to their high power capability and energy density. However, batteries suffer from aging and often are the prevalent reason for device replacement once the end of useful life has been reached. The old devices become obsolete and are discarded even though many parts remain to be in a working condition. This raises both economical as well as environmental concerns. The primary focus of energy and power management for battery-powered devices is to enhance the runtime in a single cycle, whereas battery aging mitigation and cycle life improvement have often been neglected. We propose to increase the focus on battery health management to achieve extended useful life, reduced waste, and sustainable system design.

This chapter shall provide an introduction to rechargeable Li-Ion batteries, their characteristics, aging factors, mitigation strategies as well as areas of application, and respective challenges. Section 1.1 gives a general overview of the topic of battery health-aware management and explains the motivation for this thesis. Section 1.2 provides basic background on Li-Ion batteries. Section 1.3 reviews application domains of Li-Ion batteries and their respective requirements that should be considered when designing health management strategies. In Section 1.4, multi-scale battery health management levels, techniques, and challenges are introduced. Next, in Section 1.5, the main contributions of this thesis are summarized and the structure of the thesis is outlined. Finally, in Section 1.6, the associated publications are listed.

1.1 Motivation

Battery aging is a big concern in mobile devices such as laptops, tablets, or smartphones as well as in EVs and stationary storages. Battery aging results in premature device replacements

and the disposal of whole devices that still include many functioning parts. The resulting huge amount of electronic waste is highly poisonous for the environment. While in past decades, processor speed has been the limiting factor for the useful life of mobile devices, nowadays battery aging is the main reason for device replacement. In the case of EVs, increased capacity fading results in a lower driving range. As EV charging takes a comparatively long time, user satisfaction strongly depends on the available driving range. Stationary storages are probably less critical when it comes to capacity fading. Nevertheless, if placed in residential homes, the required storage space matters, and reduction in energy and power density are undesirable. The premature replacement of a device that suffers from insufficient runtime of the battery is economically undesirable from the consumer perspective. Manufacturers seem to win from this situation as they can sell more new devices. But sustainability gains more and more importance in product choice for a growing number of consumers and therefore has become a factor that needs to be considered by manufacturers.

Factors that contribute to battery aging are the average State-of-Charge (SOC), SOC swing, cell temperature, and the charge and discharge current. Generally, higher average SOC and higher discharge depth are detrimental for the battery. Therefore, the reduction of target charge SOC levels has a positive impact on battery health. Similarly, lower currents are the health friendlier choice and should be considered in intelligent charging and discharging approaches. Battery aging results in reduced available capacity and resistance growth. If recharges are required too often due to faded available capacity, the device becomes unusable and is discarded. On the upside, it is possible to treat batteries in a conscious way to significantly extend their cycle life. Towards this, we propose less detrimental battery health management techniques in this thesis.

While in previous days replacements of mobile devices were commonly triggered by insufficient processor speed, these days, battery capacities having decreased to an unacceptable level are the far more prominent reason for the purchase of a new device. Hence, batteries have become a limiting factor in many mobile devices. Not only that they run out of capacity before other parts of the device become unusable but also the size of Li-Ion batteries has not significantly reduced during the past few years. Other than for processors, there is no Moore's Law for batteries [132]. Some manufacturers even purposely slowed down smartphones through an update to account for aged batteries and got fined [54]. Given that many manufacturers have built-in non-removable batteries claiming that they can, therefore, offer thinner devices, a battery replacement is commonly not the option chosen by the user. Instead, they replace the whole device. EV manufacturers follow a different approach and commonly oversize batteries to not impair the driving range and the user experience [35]. To not violate the warranty, i.e., $80\,\%$ of the initial capacity remaining after eight years, only a fraction of the actual available capacity of an EV battery is used in the early life of the battery. As the overall capacity fades, the usable capacity fraction is then gradually increased over time such that the user does not notice any impairments on the driving range.

A survey published in 2017 has shown that only $8\,\%$ out of 1200 participating users had replaced their smartphone battery, and $13\,\%$ had exchanged their laptop battery at some point in time [131]. As a result, otherwise perfectly working devices are disposed of. Recycling is costly and the necessary infrastructure is not everywhere available. Besides, most users are unaware of how to treat their mobile devices in a battery health-aware manner. The same survey [131]

revealed that $27\,\%$ out of 1200 participating users commonly charge their device when they receive a low battery warning. Most likely these users also charge to full level, thereby exposing the battery to high SOC swing cycles which is detrimental for Li-Ion batteries. Furthermore, $61\,\%$ of the users are not aware of Li-Ion aging factors and therefore cannot apply proper battery treatment [131]. It is likely, that an equivalent survey for other battery-powered devices, such as EVs and stationary energy storages, would give similar results.

Yet, the potential for increased battery health-aware usage exists according to the survey in [131]. $25\,\%$ of smartphone users would find charging times of more than $2\,\mathrm{h}$ acceptable, hence a lower charging current could be applied. $36\,\%$ of smartphone users follow a fixed charging routine, which could be exploited by lower charging currents, delayed charging, and even longer charging time might still be acceptable if the user experience is not compromised. The survey shows that users care about battery health and are willing to compromise for increased health. Even though this study has focused on smartphone usage and batteries, we believe that similar observations could be made for other battery-powered devices, such as EVs and stationary storages, and that similar willingness for battery health-aware behavior exists.

In the context of this thesis, battery health management strategies are proposed. We introduce a State-of-Health (SOH)-aware cell balancing scheme for large scale battery packs making use of an existing active cell balancing infrastructure. Next, charge delays and lowering of the target SOC are evaluated concerning aging mitigation and implementability on smartphones. Finally, a trade-off between privacy, time-of-use electricity prices, and battery degradation in the context of smart metering in residential homes featuring a Photovoltaic (PV) and Electrical Energy Storage (EES) is analyzed. A co-optimization problem is formulated to find control strategies for the EES. The discussed techniques and cycle life gains shall help to develop further aging mitigating strategies for environmentally friendly and economically efficient products with increased useful life.

1.2 Background on batteries

In the following, we discuss some basic properties of batteries such as the general functioning of rechargeable batteries, battery health degradation, safety issues, cost, and battery management systems. Before we do so, some general terms and definitions are presented. The available charge of a battery depends on the amount of energy that has already been used within one cycle. It fades over time and with a growing number of charge and discharge cycles conducted. We refer to this phenomenon as capacity fading and describe it in terms of SOH. The SOH κ is defined as the ratio of the actual capacity of a cell C_0 and the nominal capacity of a new cell C_N.

$$\kappa = \frac{C_0}{C_\mathrm{N}} \tag{1.1}$$

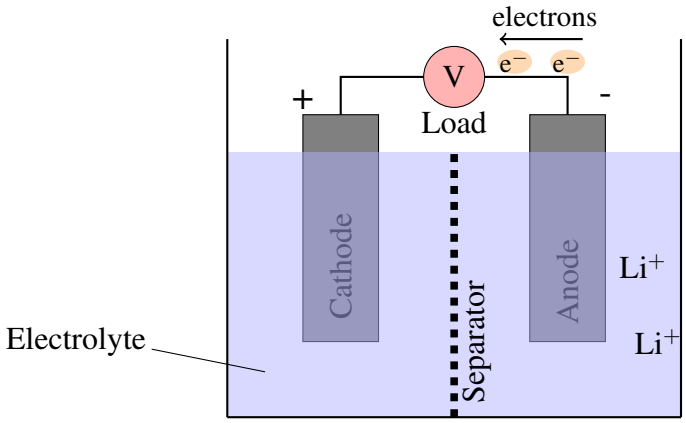

Figure 1.1: Discharging a battery: Electrons travel from anode to cathode.

The SOC S describes the ratio of available charge Q_0 of a cell and the usable capacity C_0 of a cell. The Depth of Discharge (DOD) δ is the percentage of discharged charge.

$$S = \frac{Q_0}{C_0} \tag{1.2}$$

$$\delta = 1 - \frac{Q_0}{C_0} \tag{1.3}$$

The voltage that is measured between the terminals of a battery under no-load conditions is referred to as Open Circuit Voltage (OCV). It increases with higher SOC. Charge and discharge current are often normalized against the capacity of a battery and are expressed in terms of C-rate. For example, discharging a battery with 1 C depletes the battery within $1\,\mathrm{h}$ while a rate of 2 C fully discharges the battery in $0.5\,\mathrm{h}$.

1.2.1 Secondary batteries

A battery is an electrochemical energy storage device consisting of one or more cells. Multiple cells connected in parallel and series are also called a battery *pack*. Two types need to be distinguished, *primary* and *secondary* batteries. While the former ones are disposed of after depletion, the latter ones can be recharged and can be used multiple times. In other words, their chemical reaction is reversible. In general, a battery consists of two electrodes, a positive and negative one called the *anode* and *cathode*, respectively. The electrolyte serves as a buffer through which ions travel between electrodes as shown in Figure 1.1. During discharge, the shuttle ions in the positive active material of the anode are oxidized and electrons are produced. These electrons move through the outer circuit and power a connected load. The shuttle ions move through the electrolyte to the cathode and are reduced. They consume the electrons coming in from the outer circuit. This process is reversed when charging the battery. The separator prevents the direct contact of anode and cathode but lets the shuttle ions pass.

Li-Ion batteries are nowadays widely employed in various application domains due to their favorable energy density, power capability, size, and weight characteristics. Compared to other cell chemistries, the advantages of Li-Ion batteries are their high specific energy and energy

density as well as their high power density. Some Li-Ion battery types, that were specifically developed for power applications, offer a high rate-capability. Furthermore, Li-Ion batteries have a low self-discharge rate and comparably good calendar life without memory effect [25]. They operate reliably in a broad temperature range. Due to all these properties, Li-Ion batteries are very cost-effective.

Within the group of Li-Ion batteries, different types exist which vary in their characteristics. In the following, we summarize the main features of selected, well known Li-Ion electrode materials as described in [127]. Lithium Cobalt Oxide (LCO)/Graphite electrodes are one of the most common types used in Li-Ion batteries. Typical areas of application are laptop computers, smartphones, and digital cameras. This electrode type is appreciated by system designers for its stable capacity and its high specific energy. On the downside, compared to other Li-Ion battery electrode materials, LCO batteries have a relatively short life cycle, low thermal stability, and smaller load capacity. Nickel-Mangan-Cobalt-Oxide (NMC) electrodes are used in high energy and high power applications. They come at a lower cost and better safety compared to LCO batteries. NMC cells that are optimized for energy have mostly average cycle life. However, some specialized cells for use in satellites have extremely good cycle life characteristics. NMC/Graphite batteries that are optimized for power characteristics are particularly suitable for high discharge rates. $LiMn_2O_4$/Graphite batteries are sometimes blended with NMC, which then results in good cycle life. Finally, Lithium Iron Phosphate (LFP) cells have a very long cycle life. They are thermally stable, in particular, if graphite is used as the negative electrode material. However, they have relatively low specific energy and low energy density. Within the scope of this thesis, we develop health management strategies for all types of Li-Ion batteries as the general aging characteristics are very similar.

1.2.2 Battery health degradation

Battery aging manifests itself in two ways: capacity and power fading. Capacity fading means the loss of usable capacity over time. Due to internal mechanisms, which will be discussed in Section 2.1.1, the capacity of a Li-Ion battery decreases over time. This is problematic as in most applications, it would negatively impact the user experience. Once capacity fading has advanced, the device becomes unusable and will be discarded even though other parts might still be in good condition. Capacity fading is induced by certain stress factors, such as elevated or very low temperatures, the usage pattern, i.e., average SOC and SOC swing. The current and C-rate are further factors influencing the battery aging. They can alternatively be expressed in terms of SOC pattern and time.

Power capability means the ability of a battery to effectively deliver the stored capacity. With a low internal resistance, the battery can better accommodate high loads. Power fading means the growth of the inner resistance resulting in the battery heating up and increased voltage drop under load. This may induce premature shut-downs of the device.

Battery aging not only happens during cycling but also during storage. The latter is called calendar aging. Unfavorable temperatures and storage voltage level or storage SOC lead to increased capacity fading during storage periods.

The End-of-Life (EOL) of a battery or device is reached once it has become unusable due to capacity fading or power fading. When considering capacity fading, the EOL is commonly

defined to be reached once $80\,\%$ (sometimes $70\,\%$) of the initial capacity remain. At that point, e.g., a smartphone no longer satisfies user needs by requiring too many recharges. In the case of EVs, the EOL manifests when driving distances decrease notably and the weight of the battery, that needs to be carried, is in no relation to the energy that is required to carry it. Sometimes a battery that has reached its EOL can be used in a second life application, which is an active area of research. However, commonly it will be discarded and sometimes not even properly recycled due to missing infrastructure.

Unfortunately, battery aging currently cannot be avoided, and hopefully, advances in electrochemistry and battery manufacturing will, in the future, bring batteries to the market which suffer from lesser or no aging. In the meantime, we should use the battery as gently as possible without remarkably impairing user experience and come up with battery health management strategies.

1.2.3 Safety

While aging reduces the usability of the battery, unsafe operation conditions potentially destroy the battery. Therefore, it is important to keep the battery within its Safe Operating Area (SOA). Firstly, violation of voltage bounds harms the battery. During charging, an upper voltage bound may not be exceeded and during discharge, the voltage may not fall below a certain level. Secondly, the temperature needs to be maintained within safe levels. High temperatures can cause severe damage and may impose safety risks. Similarly, temperatures that drop below a certain level may severely damage the battery. Finally, the load current may not exceed a certain threshold.

Effects of operating outside the SOA can be irreversible damage done to the battery, performance loss or continuous operation fail up to the point of catching fire and causing dangerous and threatening situations. The Battery Management System (BMS) may take different measures to handle such situations. It can actively send a request to the load controller to request a lower load current. A fuse or switch may be included in the design, such that loads are disconnected if operated outside the SOA. In many applications such as EVs or stationary storages, the BMS actively controls the environment through heaters or cooling systems to ensure stable and safe conditions.

1.2.4 Battery management systems

The BMS can be seen as the digital representation of the physical battery. Its tasks are *monitoring and control* of the current battery state, *computation* of parameters, and in some cases *cell balancing*. It should ensure that the battery stays within its SOA and that the battery is optimally used. There is no standard set of features for a BMS. Depending on the battery-powered device, its requirements, and overall costs, varying functionality needs to be included in the BMS.

Monitoring and control of parameters such as voltage, current, and temperature help to determine failures, malfunctions, and operation outside the safe bounds. Jointly with other control units, the BMS ensures, that the battery does not leave the limits of safe operation. The monitoring of voltage, current, and temperature further helps to estimate SOC and SOH. In case of a failure, the BMS would disconnect the battery. Of course, failure detection should not

rely on software only, and therefore, additional safety hardware circuits are used. To ensure safe operation, the charge and discharge current should not exceed an upper limit. Also, temperature deviations could indicate malfunctions.

Two important **computation** variables of the BMS are SOC and SOH as defined in Equations 1.2 and 1.1, respectively. The SOC represents the remaining charge in the battery and indicates the remaining runtime. The SOH marks the ability of a battery to meet power and energy requests. The estimate can also be used for maintenance and replacement planning.

A crucial and, at the same time, extremely difficult task of the BMS is to determine the remaining charge of a cell or pack. This parameter is required when estimating the remaining runtime of the device. It is also used to calculate the SOC. The SOC is the ratio of remaining capacity currently stored in the battery and either the rated or the available capacity. The rated capacity is provided by the manufacturer, while the available capacity is less due to aging. As determining the available capacity is usually very difficult and as the estimated value often contains huge inaccuracies, the relation of the currently stored capacity to the rated capacity is commonly implemented as the default solution. The available capacity is also an important indicator of the SOH. The lesser the available capacity gets, the more the health has degraded.

Determination of the available capacity is a very difficult task and therefore, often alternative and simpler means of SOH estimation are implemented in a BMS. Cycle counting is a simple and widely used method. It is, however, very inaccurate as important aging factors such as average SOC, SOC swing, and battery temperature are omitted. Furthermore, inconsistent definitions of a *cycle* exist. Some systems increase the cycle counter each time the device charges, while other systems only increase the counter when partial cycles add up to a full cycle. Few devices even use an expiry date of the battery. This makes sense in safety-critical applications, e.g., in the medical domain, to avoid that a device that stayed on the shelf for too long and has undergone severe calendar aging is used. Nevertheless, it bears the danger, that a device will age faster due to heavy usage and is still kept in use as the expiry date has not been reached. A common method for SOH estimation is coulomb counting. Here, the in- and outflowing current is measured to determine the number of cycles a device was exposed to but also to derive the remaining available capacity. The drawback of this method is that drifts occur and the results become unreliable. Usually, a full charge cycle delivers the best estimates on the capacity. However, in most applications, the users tend to charge their device long before the battery is fully depleted. Finally, advanced methods rely on precise measurements or are based on elaborate aging models.

Due to aging and manufacturing variances, cells built into a battery pack vary in their usable capacity. To increase the overall usable capacity of a pack, **cell balancing** techniques can be applied. The cell with the lowest usable capacity limits the overall pack capacity by setting the charge and discharge limits to remain in an SOA. The objective of cell balancing is to equalize individual cell SOCs in the series-connected battery pack. In passive cell balancing, the excess charge is transformed into heat over a resistor. This is also the cheapest solution. On the other hand, in active cell balancing, the charge of healthier cells is transferred towards cells with the lower usable capacity to improve charge and discharge limits. Hence, the overall usable capacity of a pack is increased, and therefore, the runtime of the battery-powered device is extended.

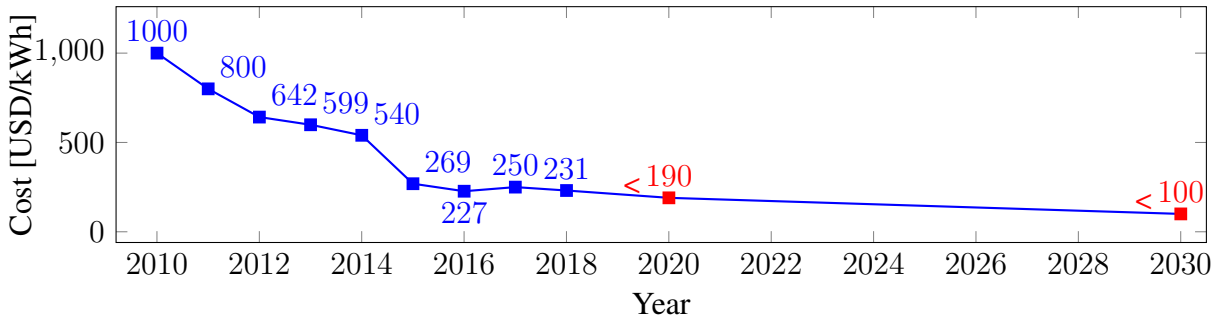

Figure 1.2: Past [85] and future [103] cost development of EV battery packs in USD per kW h.

BMS architectures can roughly be classified into *central* and *distributed* topologies. In central topologies, the BMS is implemented on a single master controller. This is very cost-effective but has the disadvantage that it introduces a single point of failure to the system. On the other hand, in a distributed system, each cell is equipped with a computation unit, which potentially allows implementing solutions that make the system more robust to failures. The battery health management strategies proposed in this thesis would ideally extend the functionalities of state-of-the-art BMSs.

1.2.5 Costs

Battery health management extends the cycle life and hence increases the monetary cost efficiency of battery-powered devices. A battery whose replacement is postponed by intelligent aging management will reduce long-term operating costs. As can be seen in Figure 1.2, the battery pack cost of EVs has dropped significantly over the past years [85] and is predicted to further decrease [103]. Reduced battery costs will induce further growth of the electro-mobility and stationary storage market.

Despite a drop in battery purchase prices, the costs of premature battery replacement are undesirable for both consumers as well as manufacturers. Countermeasures taken when batteries age, such as performance reduction to save energy, commonly impair user satisfaction. For example, Apple lowered system performance in devices with aged batteries, which seems to be a reasonable measure to avoid premature shut-downs due to power fading. However, many users would have preferred a battery replacement over sacrificing performance. As a result, Apple had to lower battery replacement costs from previously USD 79 to USD 29 as of December 2018 [109]. As average costs for new smartphones are high, i.e., USD 567 in northern America or USD 259 in Europe in 2017 [68], battery replacement might slowly become the cheaper option.

The situation for EVs is a bit different. Manufacturers usually give a warranty of eight to ten years on the battery. This is shorter than the lifespan of the vehicle itself. Over-dimensioned batteries account for future capacity fading and guarantee unrestrained driving range and user experience. Nevertheless, battery aging mitigation will additionally help to avoid warranty violation and to further extend the useful life of the battery.

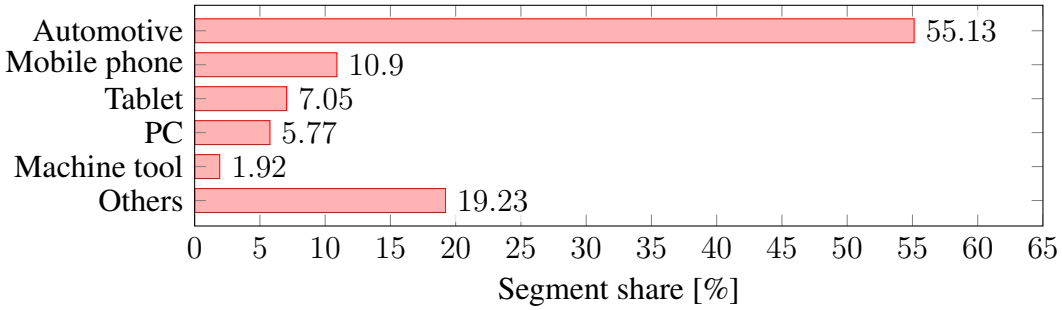

Figure 1.3: Projected split of the global Li-Ion battery market in 2020 by segment [55]

1.3 Application domains of Li-Ion batteries

With the introduction of smartphones and the rise of electro-mobility, an increase in secondary battery employments can be observed. Li-Ion batteries are widely used due to their high power capability and energy density. The application domains are manifold and all have specific requirements and characteristics. While in 2014, the highest share of Li-Ion batteries was applied in mobile devices [108], in 2020, it is assumed that the automotive segment will dominate the market split, followed by mobile phones [55] as shown in Figure 1.3. Battery health management is relevant for all application domains. In the following, we identify the respective requirements. Namely, we discuss EVs, stationary storages, and mobile devices, such as smartphones and laptop computers. From our analysis of load patterns and aging behavior, we conclude potential control parameters for battery health management.

1.3.1 Mobile devices

In Germany, 57 million people used smartphones in 2018 [12]. Worldwide, 37 % of the global population is expected to use smartphones in 2019 with further growth predicted [41]. All these smartphones as well as other mobile devices, such as tablets and laptops, are commonly equipped with Li-Ion batteries. Also common oversizing of smartphone batteries [48] could be further reduced if proper health management was in place. In the following, we discuss battery load characteristics and thermal conditions of mobile devices to identify aging mitigation measures that prolong battery cycle life.

The main power-consuming entities within mobile phones are the Global System for Mobile Communications (GSM) unit, Central Processing Unit (CPU), Random Access Memory (RAM), WiFi, Graphics, Liquid Crystal Display (LCD) and audio [19, 71, 118]. The GSM unit contributes to total power consumption in the form of a high as well as a continuous ratio. The share of other entities depends on the respective usage. Carroll et al. [19] find that in a phone call, GSM is the highest contributor to energy consumption, whereas during video playback the LCD shows the highest consumption, which also depends on its backlight settings. Similarly, during an audio playback, the graphics unit holds a high share in power consumption. The usage patterns depend, on the one hand, on the entity, e.g., wireless communication protocols create specific power patterns. On the other hand, depending on the Operating System (OS) task scheduler and resulting running applications, required hardware units are active and thus

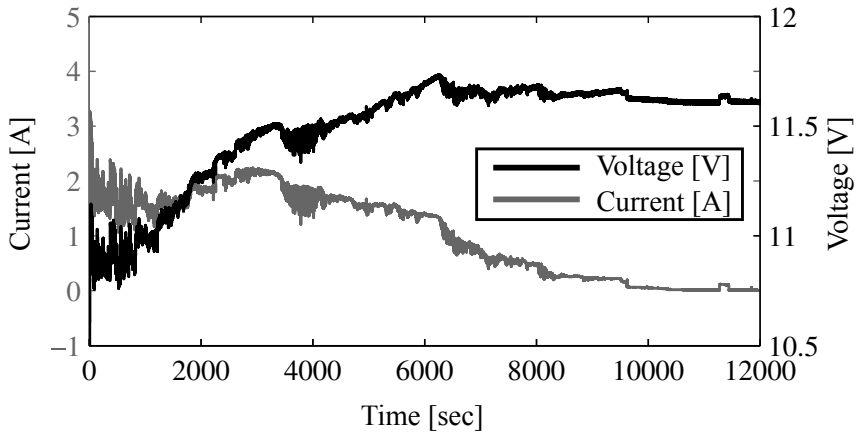

Figure 1.4: CC-CV charging measurement of a laptop battery [83]

result in specific power consumption patterns. Most active applications depend on the human user, who decides when and how to use the phone. While regularly scheduled tasks follow a predictable pattern, incoming communication energy requirements and the human user induced energy consumption is less deterministic. These load patterns affect the average SOC and SOC swing as well as temperature since hardware components transfer heat.

The Constant-Current-Constant-Voltage (CC-CV) protocol is used to charge smartphones and laptops and, if applicable, the Universal Serial Bus (USB) battery charging specification [148] is applied. In CC-CV charging, the phone is first charged with constant current until a predefined voltage limit is reached. Then, the voltage is kept constant and the remaining charge is slowly topped up as shown for a laptop computer in Figure 1.4. Many users charge their mobile phones to full SOC overnight [45]. Over the day, the phone is discharged and discharges are interleaved with states when the phone is not in active use but still receives messages, etc. This charge and discharge patterns affect the average SOC and SOC swing and are therefore relevant for battery aging.

High battery temperature increases aging. The battery cell temperature is influenced by the ambient temperature during standby and additionally by thermal coupling with other heat sources, such as CPU and Graphics Processing Unit (GPU), during usage [156, 157]. In smartphones, commonly no active cooling is implemented, while laptop computers include fans for CPU cooling. The speed-dependent energy consumption of the fan needs to be carefully chosen to mitigate aging without significantly compromising device runtime [160]. In the case of smartphones, manufacturers often place the battery at the backside of the smartphone with high distance to heat sources such as the CPU.

The constraints when designing a battery management system and in particular, the health management part are on the one hand safety. The BMS should ensure both, compliance with the SOA as well as user experience. Explosions of batteries as having occurred in Samsung Galaxy 7 phones, immediately end the useful life of a device [9]. Gradual capacity fading leads to a less sudden end but impairs usability, flexibility, and performance. On the other hand, health management measures should be designed such that good user experience is maintained.

In the case of notebook computers, the energy-consuming loads such as CPU, GPU, display, etc. are of a similar type as in the case of smartphones. The performance of laptops, and therefore, the resulting power consumption, is usually higher compared to a smartphone. This means that the battery capacity needs to be higher and a battery pack usually consists of more than just one cell. Naturally, the average power and energy consumption depends on typical usage. Office applications commonly consume less power compared to gaming applications or power-intensive simulations. Similar to the case of smartphones, the charging follows the CC-CV protocol, but it is not handled over USB and hence the absolute charging current is higher compared to smartphones. For example, highly demanding usage can result in premature aging even when the laptop is plugged into a power outlet [83]. Other than in smartphones, a fan is used for CPU cooling on laptops. Some manufacturers attach the battery outside the main case to dissipate battery waste heat to the environment. In the office, many notebooks spend most of the time in their docking stations and are taken out only for travel or meetings. Battery charging could be scheduled very flexibly for improved battery health. In summary, charge and discharge prediction for improved health management in the case of laptops needs to consider different factors compared to smartphones.

1.3.2 Electric vehicles

Pack size and the usage pattern make the design of health-aware battery management systems for EVs differ from the ones for consumer electronics. Nevertheless, some of the constraints can be transferred. The battery packs in EVs usually consist of multiple cells connected in series and parallel. The exact amount of cells and connection topology vary among manufacturers. Most automotive manufacturers over-dimension the EV battery packs to accommodate the expected degradation of the battery. For example, an EV that nominally requires a $12\,\mathrm{kW\,h}$ battery, is commonly equipped with a $20\,\mathrm{kW\,h}$ battery to accommodate for about $40\,\%$ health degradation within the expected 10 years usage time [35]. As a result, the user will not notice any changes in operation.

The size and high power of EV battery packs necessitate active cooling mechanisms. Airflow cooling and liquid cooling are common options. Nevertheless, uneven temperature distribution occurs in battery packs even if active cooling is used. Along with manufacturing variations, such temperature inhomogeneities result in imbalanced charge levels among cells. Active cell balancing deals with the symptoms of this situation. The temperature distribution within battery packs not only depends on thermal coupling and excess heat from charging or discharging the cell but it is also influenced by the ambient temperature. EVs are used in all kinds of climate zones. A globally operating manufacturer not only needs to consider tropical zones with high temperatures and humidity all year round but also colder zones with degrees far below zero for several months in winter. In the latter case, the preheating of batteries becomes necessary to avoid damage.

Charging currents and charge duration depend on the type of charging used: Level 1, Level 2, or Level 3 charging [22]. In Level 1 charging, the charging power is usually $1\,\mathrm{kW}$ and the charge time for a full charge amounts to $8\,\mathrm{h}$ to $15\,\mathrm{h}$. In Level 2 charging, the charging power ranges from $3\,\mathrm{kW}$ to $20\,\mathrm{kW}$ and the time for a full charge is $3\,\mathrm{h}$ to $8\,\mathrm{h}$. Finally, fast charging, also referred to as Level 3 charging, provides charging power of typically $50\,\mathrm{kW}$ and a full

charge takes 20 min to 1 h. Charging opportunities exist at home with Level 1 or Level 2, at work with Level 2 charging and at charging station networks with Level 2 or Level 3 charging. Charging at work can take place during several hours and charging at home would often happen overnight. In both cases, long periods of detrimental high SOC occur if charged immediately when plugged-in. On the other hand, delaying charge is undesirable when charging at network charger stations. The disadvantage of fast charging is the damaging influence of high charging currents [79, 145]. Regenerative braking also recharges batteries during driving. Interestingly, regenerative braking has been found to mitigate aging due to lower SOC swing [78, 80].

Advisable operation modes of EVs consist of low depth cycles at low average SOC. Power consumption of the electrical engine in EVs depends on velocity, acceleration, and roadway grade [155]. Additional power drain results from the air conditioning, heating system, and multimedia system, etc. Standardized drive cycles, such as New European Driving Cycle (NEDC), Artemis European driving cycle [2], or Worldwide Harmonized Light Vehicles Test Procedure (WLTP) simulate typical drive scenarios like city trips, highway trips, high speed, use of air conditioning, cold temperature, etc. Average SOC and SOC swing can be estimated from such data. The approximation of battery usage is sufficient since it has been observed that the aging of batteries cycled with realistic dynamic drive cycles is equivalent to static cycling with identical average current and cycle depth [80].

The typical usage of an EV differs from combustion engine vehicles. Firstly, range anxiety is a widespread phenomenon among EV users [49]. As a result, users tend to recharge earlier than necessary. This behavior results in increased average SOC, which is detrimental for battery health and is likely to be the dominant aging factor. However, the SOC swing is also reduced, which results in less severe aging. The overall effect of range anxiety on battery health remains an open question. Secondly, due to their limited driving range, EVs are commonly used for city trips and less for long-distance journeys. However, expected advances in battery technology will impact the typical usage patterns. EVs that are part of taxi fleets have a much higher degree of utilization compared to privately owned EVs that spend most of the time unused in a parking place. Similarly, EVs that are part of car-sharing pools differ in usage and utilization.

1.3.3 Stationary battery storages

While in the mobile applications discussed above, the purpose of the battery was to provide energy in times of no access to an outlet, stationary battery storages are used to store excess energy to use it at some later point in time to, for example, reduce costs in time-of-use pricing schemes or to increase the degree of autarky. Residential EESs are often used along with PV or wind turbines. Considering the case of PV, charging happens at times of energy generation, and hence times of high sun irradiation. Discharge, on the other hand, happens at times of low generation but high demand, i.e., the morning and evening hours. Charging or discharging of the storage often is motivated by reducing the financial cost of electricity through leveraging time-of-use prices.

Same as battery packs in EVs, EESs contain many cells connected in parallel and series, which are potentially imbalanced and radiate heat. Cell balancing measures, as well as active cooling, is required. Imbalance can be an even bigger challenge in second life scenarios, which are often discussed in the context of stationary storages. Appropriate sizing of the storage is

crucial as otherwise the full charge level will be prematurely reached and excess energy cannot be stored. From an aging perspective, long storage times at a high SOC should be avoided. By including forecast information on required usage, the average SOC during storage times can be lowered [75].

1.4 Battery health-aware multi-scale management

Having discussed the characteristics and requirements for health management from the application perspective, we now outline strategies and control parameters for aging mitigation on multiple levels. We identify four abstraction levels, namely cell-, module-, device- and system level. The battery health management strategies presented in this thesis cover all of these abstraction levels. Each level has specific constraints and parameters for aging mitigation, which are detailed in this section. In the following, we shortly introduce the levels for battery health management. A detailed description of multi-scale battery health management and cross-scale strategies will be presented in Chapter 6.

Cell-level

Chemists continue to experiment with new battery cell chemistries to improve the characteristics of batteries. Cycle life is one of the concerns which new inventions try to improve. However, system engineers can only select from existing battery types and need to consider the respective properties for optimal system design. On cell-level, operational parameters such as high and low voltage cutoffs and the maximum allowed current play an important role to protect the cell from premature health degradation and damage. Selecting appropriate SOC levels and charging currents can significantly mitigate aging.

Module-level

On battery module-level, more fine-tuning can be done. In particular, as cells age at different speeds, a high discrepancy between the health of individual cells exists. Discharge conditions often increase this discrepancy. Aging mitigating measures on module-level include active cell balancing, which compensates for capacity variations, and aging-aware charge transfer strategies, that try to reduce the capacity imbalance. Furthermore, if heterogeneous hybrid energy storages are employed, aging optimal energy sources should be selected based on present load characteristics, thereby protecting the Li-Ion battery from detrimental conditions.

Device-level

Battery health management on device-level leverages application-specific usage patterns and modifies them to provide battery health-aware operation conditions. This usually means trading-off battery cycle life improvement and performance or usability. Sacrificing too much usability is not acceptable from the user perspective. Therefore, design parameters have to be carefully decided. Battery charging optimization has a high potential for such modifications. EVs and smartphones are often plugged-in for longer durations than required and have long idle times.

These idle times can be leveraged and the charging process can be rescheduled or the charging current can be reduced. As high average SOC levels are detrimental for the battery, reaching the full charge level too early results in long storage times at a high SOC and therefore faster aging. Charge delays depending on the predicted usage can help to enhance battery cycle life.

System-level

Finally, in systems consisting of multiple components, aging mitigating control strategies are required. Such control strategies need to trade-off battery aging with other system optimization objectives. Co-optimization of battery cycle life with system objectives such as financial cost, performance, or privacy needs to be done. For example, a residential home equipped with an EES and PV requires a battery health optimal as well as a financial cost-optimal strategy. Another example could be a fleet of EVs whose trips should be scheduled such that batteries age at the same speed.

Within this thesis, we present three use cases of battery health-aware management that include techniques from all four levels.

1.5 Contributions and organization

Having introduced Li-Ion battery basics, application domains of battery cells and packs as well as their respective requirements in the previous section, contributions, and organization of the thesis at hand are detailed in this section. This is followed by the list of publications this thesis is based on in Section 1.6.

This thesis is organized into seven chapters. Chapter 1 gives an overview of Li-Ion battery properties and their management systems, it outlines characteristics of application domains of Li-Ion batteries and introduces the multiple levels on which battery health management can be performed. Chapter 2 provides background information on Li-Ion health degradation factors and aging modeling. Battery aging depends on a multitude of factors including average SOC, SOC swing, and temperature. Aging models capture aging mechanisms on different levels. While electrochemical models describe battery dynamics and internal degradation mechanisms – some even on an atomistic or molecular level – data-driven models use analytical data obtained from experimental investigation and measurements to approximate degradation. Very fine-grained modeling requires high runtime which is not desirable in fast prototyping and complex system-level simulations. In particular, for control algorithm design and strategy evaluation, a relatively fast model that nevertheless covers a broad amount of aging factors is required. We conclude that chapter by justifying the selection of models used within the scope of this thesis.

Chapters 3, 4, and 5 present use cases of multi-scale battery health management as detailed in Sections 1.5.1, 1.5.2, and 1.5.3. An SOH-aware cell balancing scheme for EV battery packs is presented in Chapter 3. Then in Chapter 4, we discuss charge delays and lower charge SOC. In Chapter 5, we present a system-level co-optimization of cost and privacy in residential homes that are equipped with smart meters. The use cases cover three different application domains, namely, EV, smartphones, and stationary storages to demonstrate the wide range of

importance and potential of battery health management. Furthermore, the presented strategies are not necessarily restricted to the application, and often the same or similar strategies may be applied to other applications that use Li-Ion batteries.

In Chapter 6, we introduce the holistic view of multi-scale battery health management. We identify health management strategies on cell-, pack-, device- and system-level as follows. Operational limits to ensure safe and health-aware battery operation are imposed on cell-level. Cell balancing strategies and architectures as well as cooling system choices along with thermal management strategies impact the battery health on module-level. Their design and dimensioning needs to be carefully decided to extend cycle life. The battery loads and their operation patterns can be leveraged to mitigate battery aging on the device-level. This can be achieved by, e.g., hybrid energy storages to reduce peak currents drawn from the battery. Furthermore, intelligent charging strategies lower the average SOC and apply lower charge currents. On system-level, trade-offs between aging and other system constraints such as financial costs, the scheduling of loads and energy generation, etc. need to be considered. A framework is developed to simulate battery aging as well as the impact of health management strategies and component choices. The presented framework can be applied in various application domains and allows for rapid analysis of various health management techniques at different abstraction levels. We revisit the use case of the EV battery pack and discuss health management strategies on all levels as well as cross-scale effects.

Finally, in Chapter 7, we summarize the results and conclude this work. We outline open issues in the field of battery health-aware management. Battery health management enables more sustainable device and system design as well as environmental benefits. Further research in this direction is required as the demand for sustainable products is continuously growing these days.

Now, we describe the main technical contributions of this thesis in more detail.

1.5.1 SOH-aware cell balancing for EV battery packs

Chapter 3 introduces an SOH-aware cell balancing technique that extends the cycle life of battery packs in EVs. While state-of-the-art active cell balancing solely focuses on equalizing SOC levels, the proposed SOH-aware technique reduces the load current of cells with low SOH using an active cell balancing architecture. Based on the observation that assigning the smallest possible load current to cells with lower SOH extends cycle life, the technique identifies the most beneficial charge transfers. The technique leverages the fact that the EV batteries are not always fully discharged during a trip, and hence, it is not necessary to keep the SOC equalized at all times.

The main technical challenge that we solve is to show how cell balancing can be further exploited to significantly extend battery cycle life. This can be achieved by reduction of the charge drawn from less healthy cells while stressing healthy cells more. Thereby, the C-rate as well as the SOC swing are reduced on less healthy cells, resulting in mitigation of the battery pack EOL. The presented algorithm mitigates aging by up to $23.5\,\%$ over passive cell balancing and up to $17.6\,\%$ over active SOC cell balancing.

We further investigate the component choices and find that given a certain variance in initial SOH levels, a minimum required balancing current can be found to achieve reasonable health

improvement. The initial SOH variance plays a big role in the effectiveness of aging mitigation. Therefore, thermal management should be closely coupled to the balancing strategy. The SOH-aware cell balancing strategy and the respective evaluations have been published in [122].

1.5.2 Smart charging for smartphones

Chapter 4 discusses an intelligent charging strategy for smartphones. Smartphone batteries are often charged overnight and in these cases, the battery remains at a high average SOC for a long duration which accelerates battery degradation. We identify a charging scheme that adaptively delays the charging and as a result, the average SOC is lowered and aging is mitigated. The main technical challenge that we solve is to find a feasible implementation of this scheme on Android phones that takes both the limitations of the operating system as well as the nondeterministic nature of the user behavior into consideration. To avoid insufficient battery charge levels when the user unplugs the phone, the smartphone alarm is used to estimate the unplug time. Furthermore, past usage is statistically analyzed and the performance of three predictors is evaluated. Namely a Simple Moving Average (SMA), an Exponential Moving Average (EMA), and a probabilistic predictor are investigated.

Lowering the target SOC reduces the average SOC as well. Similar to charge delays, the required charge level can be determined through analysis of the past usage data to adapt the target SOC level while charging. We discuss the combined effects of delayed charging and lower charge levels. Next, the implementation challenges on currently available smartphones are discussed and we find that the operating system does not provide any mechanisms to implement a solution that can be applied independently of the charger chip type. A modified battery charging device is proposed that can be used with almost all existing smartphone models.

Furthermore, we conduct a user study to evaluate our proposed scheme based on the collected smartphone usage routines. The collection of real smartphone usage profiles reveals that cycle life can almost be doubled by the intelligent charging scheme. We conclude the chapter with an extensive discussion of advances being made in intelligent chargers of mobile devices and outline remaining issues. The proposed intelligent charging strategy and evaluation have been published in [121] and [120].

1.5.3 Cost/privacy co-optimization for stationary storages

In Chapter 5, a system-level control strategy is proposed for a set-up consisting of an EES and a PV in a residential home that is part of the smart energy grid. Within the smart energy grid, smart meters continuously monitor the electricity usage of customers such that the energy provider receives real-time information on energy consumption or generation based on which dynamic pricing can be offered. However, communication of such information raises privacy concerns concerning undesired exposure of human activity and the use of home appliances. The combination of EES and PV is effective in hiding such privacy revealing information. Privacy protection however comes at the cost of EES and PV installation, increased EES aging, and possibly increased electricity cost. The control strategy of the system should, therefore, minimize both financial cost, i.e., the sum of battery and PV depreciation and grid electricity costs, and privacy exposure.

The main technical challenge that we solve is to build an extensive simulation framework and to identify suitable control strategies that trade-off cost and privacy. Our analysis shows that a strategy solely focusing on privacy results in high financial costs, while for a typical residential setting, the costs for a trade-off solution lie in the range of USD 600-1700.

It has been shown that one possibility to achieve privacy enhancement is load flattening. This has the positive side effect that it simultaneously results in peak shaving which is beneficial for the electricity provider as the complexity of demand-side management is reduced. Due to high battery depreciation costs, the costs of privacy enhancement are higher than a purely financial cost-optimal strategy. As increasing privacy is mutually beneficial for both, customers and electricity providers, a new business model could be introduced, where the costs for peak shaving could be shared among both parties. The results have been published in [123].

1.5.4 Summary of contributions

The main contributions of this work are summarized as follows.

- Introduction and evaluation of an SOH-aware active cell balancing technique that adapts load currents to reduce stress on already impaired cells. It thereby mitigates the aging of EV batteries on module-level.
- Development of a context-aware intelligent charging scheme for smartphones that delays charge and reduces the target charge level and thereby mitigates battery aging on device-level.
- Evaluation of smartphone usage predictors for the implementation of a prototype of the intelligent charging system.
- Development of a control strategy for a system consisting of EES and PV that minimizes both financial cost, i.e., the sum of battery aging cost, PV depreciation and grid electricity costs, as well as the privacy enhancement. This strategy simultaneously results in peak shaving.
- Identification of the trade-off of privacy and financial cost, where a controlled cost/privacy strategy reduces costs by more than half. Due to the correlation of privacy enhancement and peak shaving, which mutually benefits consumer and Utility Provider (UP), costs can be split, which potentially creates a new business model.
- Discussion of the holistic view of multi-scale battery health management and evaluation of cross-scale health management strategies.

1.6 List of publications

The research that has lead to this thesis has resulted in the following publications.

- Wanli Chang, Alma Pröbstl, Dip Goswami, Majid Zamani and Samarjit Chakraborty: *Battery- and Aging-Aware Embedded Control Systems for Electric Vehicles*. In: Proceedings of the IEEE Real-Time Systems Symposium (RTSS), 2014.

- Jaemin Kim, Alma Pröbstl, Samarjit Chakraborty and Naehyuck Chang: *Aging mitigation of power supply-connected batteries*. In: Proceedings of the IEEE/ACM International Symposium on Low Power Electronics and Design (ISLPED), 2014.

- Alma Pröbstl, Philipp Kindt, Emanuel Regnath and Samarjit Chakraborty: *Smart^2: Smart Charging for Smart Phones*. In: Proceedings of the 21st International Conference on Embedded and Real-Time Computing Systems and Applications (RTCSA), 2015.

- Wanli Chang, Alma Pröbstl, Dip Goswami, Majid Zamani and Samarjit Chakraborty: *Reliable CPS Design for Mitigating Semiconductor and Battery Aging in Electric Vehicles*. In: Proceedings of the IEEE 3rd International Conference on Cyber-Physical Systems, Networks, and Applications (CPSNA), 2015.

- Alma Pröbstl, Sangyoung Park, Swaminathan Narayanaswamy, Sebastian Steinhorst, and Samarjit Chakraborty: *SOH-aware active cell balancing strategy for high power battery packs*. In: Proceedings of the Design, Automation Test in Europe Conference and Exhibition (DATE), 2018.

- Alma Pröbstl, Sangyoung Park, Sebastian Steinhorst and Samarjit Chakraborty: *Cost/ Privacy Co-optimization in Smart Energy Grids*. In: Proceedings of Design, Automation and Test in Europe Conference and Exhibition (DATE), 2019.

- Wanli Chang, Swaminathan Narayanaswamy, Alma Pröbstl and Samarjit Chakraborty: *Reliable CPS Design for Unreliable Hardware Platforms*. In: Jörg Henkel and Nikil Dutt (Eds.), Dependable Embedded Systems. Springer, Heidelberg, 2021. ISBN 978-3-030-52017-5. (*In press.*)

- Debayan Roy, Swaminathan Narayanaswamy, Alma Pröbstl and Samarjit Chakraborty: *Multi-Stage Optimization for Energy-Efficient Active Cell Balancing in Battery Packs*. In: Proceedings of the IEEE/ACM International Conference on Computer-Aided Design (ICCAD), 2019.

- Debayan Roy, Swaminathan Narayanaswamy, Alma Pröbstl and Samarjit Chakraborty: *Optimal scheduling for active cell balancing*. In: Proceedings of the IEEE Real-Time Systems Symposium (RTSS), 2019

- Alma Pröbstl, Bashima Islam, Shahriar Nirjon, Naehyuck Chang, and Samarjit Chakraborty: *Intelligent Chargers Will Make Mobile Devices Live Longer.*. In: IEEE Design & Test, 2020

2

Battery State-of-Health: Basics, models and management approaches

This chapter discusses aging mechanisms and degradation factors in Li-Ion batteries in Section 2.1 and then outlines existing model types and their suitability for designing multi-scale battery health management systems in Section 2.2. A multitude of model types exists, making it difficult to decide on the best choice. Also, the specific design goals play a role in model selection. Furthermore, not only different cell chemistries impact the aging behavior of a cell but also manufacturing variances, thermal conditions inside a pack as well as the load pattern. We outline various existing battery aging models and summarize the ones used within this thesis, thereby justifying our choice.

2.1 Health degradation of Li-Ion batteries

To discuss the suitability of different model types, we first need to understand the degradation factors present in a battery. In this section, we therefore first discuss the electrochemical degradation mechanisms in Section 2.1.1 and then link them to the respective aging causes and effects in Section 2.1.2.

2.1.1 Electrochemical degradation mechanisms

In the following, we give an overview of the electrochemical effects taking place inside the battery that lead to battery aging and in particular to capacity fading. The two main effects of Li-Ion battery aging are capacity fade and power fade. Three degradation modes of Li-Ion cells can be distinguished: Loss of Li-Ion inventory, loss of active material of the negative electrode,

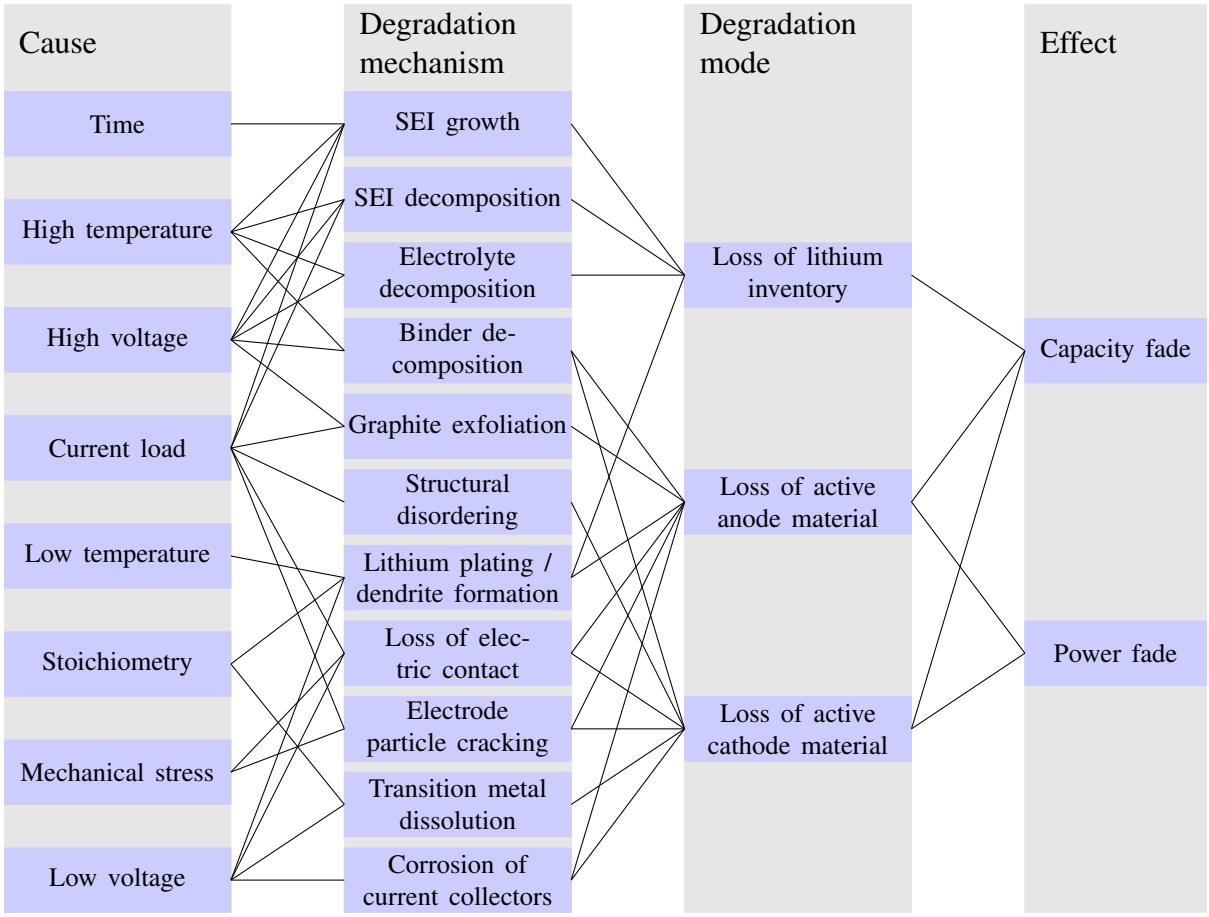

Figure 2.1: Effects and causes of battery degradation [11]

and loss of active material of the positive electrode [11]. Several aging mechanisms add to these losses. They are shown in Figure 2.1 and are briefly described in the following.

Loss of Li-Ion inventory

Due to side reactions, cyclable lithium can be consumed and therefore is no longer available for cycling between the electrodes. Hence, the capacity of the cell decreases. Two important degradation mechanisms that lead to a loss of lithium are *Solid Electrolyte Interphase (SEI) growth* and *lithium plating*. Other effects are *SEI decomposition* and *electrolyte decomposition*. As the former two, namely SEI growth and lithium plating, have a higher impact on capacity fade, we focus on their description.

The SEI is a film between the negative electrode and the electrolyte, which usually builds up during the first charge. During the first charges, the built-up of SEI is wanted, but during later cycles, further *SEI growth* leads to capacity fade and is undesired. The SEI is seen as protection for the negative electrode from corrosion and the electrolyte. Normally, it is electrically insulating but allows the conduction of lithium ions. However, some solvents pass through the SEI even after the first cycles and the SEI keeps growing. The more the SEI growths, the more

lithium ions will be irreversibly bound, and when growing too much, kinetics slow down. As an effect, the available capacity fades. The stability of the SEI is an important factor for the health of a battery [11].

Lithium plating [151] occasionally occurs instead of normal intercalation. Intercalation means the reversible insertion of lithium ions from the cathode into materials with layered structures, e.g., the graphite anode. Lithium plating happens on the one hand at low temperatures when the reaction rate slows down and on the other hand at high charge currents, which lead to a fast reaction rate. This results in the anode partially being unavailable for the actual process and also imposes security threats such as short-circuits and inflammation of metallic lithium. To avoid lithium plating, over-voltage when charging and usage of the battery at low temperatures should be avoided.

Loss of active material at the negative electrode (anode)

When the active mass of the anode vanishes, lithium ions can no longer be inserted into the anode. Degradation mechanisms contributing to the loss of active anode material are binder decomposition, graphite exfoliation (in case graphite is used as the anode material), lithium plating, electrode particle cracking, and corrosion of current collectors.

The *decomposition of the binder*, which connects the battery to the current collector, contributes to the battery's degradation as lithium gets lost and the mechanical stability is reduced. *Graphite exfoliation* is the complete separation of material layers instead of normal intercalation. As a result, the capacity of the battery decreases. In Li-Ion batteries, the anode is commonly made of graphite but other anode materials exist.

Another degradation mechanism is the *loss of electrical contact* of active material particles. It results from volume changes during cycling. It has a very high impact on capacity fading [151]. Contact loss can happen at multiple places: between carbon particles, between the current collector and carbon, between the binder and carbon, and finally between the binder and current collector.

Due to gas evolution and co-intercalation of the active material and the solvent, *particle cracking* occurs and leads to loss of active material, loss of lithium, and graphite exfoliation [151]. And finally, the overpotentials resulting from the *corrosion of current collectors* primarily result in power fade. However, the corrosion also comes along with an inhomogeneous distribution of current and potential, thereby intensifying other health degradation mechanisms [151].

Loss of active material of the positive electrode (cathode)

In the case of the cathode, several aging factors are the same as for the anode and have been explained above. These factors are binder decomposition, loss of electric contact, electrode particle cracking, corrosion of current collectors. Additionally, *structural disordering* and *transition-metal dissolution* from the cathode and resulting dendrite formation on the (carbon) anode may occur [11].

2.1.2 Causes for battery aging

Above, we explained the electrochemical degradation *mechanisms* for capacity and power fade. As for system-level design, analytical models often are more suitable due to their reduced complexity and faster simulation time, we summarize in the following the *causes* of battery aging. This is also useful for the identification of potential target points in intelligent battery health management. The interested reader may refer to Uddin et al. [146] who give a comprehensive overview of the relationship of degradation causes, such as temperature, voltage, current, SOC, etc. and the electrochemical degradation modes.

Usually one distinguishes between calendar and cycle aging. The first one describes the aging causes during storage, where certain storage conditions impact the severeness of battery degradation. The latter refers to additional causes that occur when the battery undergoes charge and discharge cycles. The causes are summarized in Figure 2.1.

Barré et al. [7] summarize the causes that degrade the battery during *calendar aging*. The storage temperature has a huge impact: Moderate temperatures should be preferred as too high and too low temperature causes increased aging. The second most important aging cause is the SOC level. Again, moderate levels are best for the battery, and too high as well as too low levels should be avoided. The combined effect of temperature and SOC level on aging needs further investigation to fully understand the interdependencies. Finally, time plays a role as non-linearities in aging can be observed. Health dependency during calendar aging on a low temperature and low cell voltage and corresponding SOC is experimentally confirmed by Ecker et al. through measurements of a cell with a hard carbon anode and a $LiNiMnCoO_2$ cathode [38]. The same holds for $LiCoO_2$ cells as shown in [91]. In [141], increased degradation is found when the cell voltage is above $4\,\mathrm{V}$, which relates, in this case, to an SOC of approximately $50\,\%$ or higher.

During *cycle aging*, the same factors as during calendar aging play a role but at the same time, additional ones influence the aging rate as explained by Barré et al. [7]. While during storage, only the ambient temperature influences the cell temperature, the cell temperature during cycling, increased by the reactions inside the battery, additionally impacts the cell temperature and hence, the aging rate [47]. Very high as well as very low temperatures are detrimental for the battery cell. During cycling, the battery undergoes an SOC swing. The lower the SOC swing, the better for the battery health [152]. Also, a higher charge/discharge voltage as well as high currents negatively impact battery health. Savoye et al. [130] could show the detrimental effects of current pulses on Li-Ion battery cells. Measurements on cycle aging of a $900\,\mathrm{mA\,h}$ $LiCoO_2$ battery at $25\,^{\circ}\mathrm{C}$ [28] reveal that a higher cut-off voltage while charging to full charge level increases the capacity fading. However, no dependence on the cut-off voltage while discharging to the empty charge level was found. Furthermore, lower charging and discharging rates decrease aging. Similarly, a longer duration of top-up charging, which compensates the self-discharge of a fully charged battery and maintains the full charge level as long as the battery is connected to the charger, increases the capacity fading.

2.1.3 State-of-Health estimation techniques

Battery health estimation and measurement are required to evaluate the health management techniques offline but also to monitor the effectiveness of operation modes and to adjust strategies to the respective battery characteristics during runtime. Generally, physics-based and empirical models can be distinguished [128]. The internal resistance and the remaining charge capacity are typical measures for SOH, where a rise of $100\,\%$ of the internal resistance over the initial value or a decrease of $20\,\%$ of the capacity are commonly defined as the EOL of the respective device [64]. Through measurements, battery SOH can be concluded from changes in the OCV curve [11, 98]. Hereby, voltage characteristics and voltage plateau lengths are related to degradation modes. Another widely employed method for SOH diagnosis is Electrochemical Impedance Spectroscopy (EIS) [139]. Finally, incremental capacity vs. differential voltage curves are another option for SOH estimation [115]. For online SOH estimation, the typical usage characteristics need to be considered. For example, while an EV needs to be parked while being charged and hence almost no load occurs, a smartphone can well be used during charging which potentially influences the voltage and current measurements. Overviews of Li-Ion battery health estimation and measurement techniques are provided in [10, 116, 128, 163].

EIS is a very reliable and widely employed method for battery health measurements in laboratory environments. EIS is a non-destructive method, where a sinusoidal current and voltage of a specific amplitude and frequency is applied to the battery. The phase shift and amplitude of the output voltage (galvanostatic mode) or current (potentiostatic mode) are obtained for various frequencies. Hereby, the impedance spectrum is measured [139]. More recently, real-time EIS methods for online applications have been developed [34, 63, 105, 125].

Within the scope of this thesis, we define the SOH as the ratio of remaining to nominal capacity. The straight forward solution for estimation of capacity is to discharge the battery with the nominal current at the nominal temperature from a fully charged state to the cut-off voltage [43, 117, 163]. Unfortunately, such nominal conditions are only available in laboratory environments not within real application measurements. Therefore, accuracy is low when using this method.

Measurement-based techniques have drawbacks in robustness and accuracy. Model-based approaches overcome these drawbacks by modeling the physical dependencies of parameters on the SOH [31]. Such model-based SOH estimation methods mostly rely on current, voltage, and sometimes temperature measurements [64, 117, 154, 162]. For example, a data-model fusion method is applied in [111, 154] to fit a Resistor-Capacitor (RC) model with current and voltage measurements obtained online with an adaptive forgetting recursive model. Thermal dynamics are leveraged by Zhang et al. [162] for a real-time model-based capacity estimation scheme. Gholizadeh et al. [52] also include nonlinearities and uncertainties for improved results. Further schemes include Fractional-Order Calculus [64].

Data-driven online SOH estimation methods extract features and employ machine learning approaches [31]. Existing approaches include genetic algorithms [27], Dynamic Bayesian Networks [60], prior knowledge-based neural network with Markov chains [31], Support Vector Machine (SVM)-based approaches [84], Artificial Neural Networks (ANNs) [39, 92], Kalman filters [1] and dual sliding mode observers [82], etc.

Lee et al. [87] present an SOH estimation scheme where the battery aging of smartphones is expressed as battery efficiency. Reduced efficiency means the progression of the degradation process. However, this metric does not reveal information about the remaining capacity.

Within the scope of this thesis, offline SOH estimation is relevant to evaluate the proposed degradation mitigation approaches. Online SOH estimation on the other hand is mainly relevant for the SOH-aware cell balancing algorithm discussed in Chapter 3. The above mentioned techniques should give an overview of the existing approaches but we expect further improvements in this domain enabling even better and more adaptive health management strategies in the future.

2.2 Battery aging models

The aging factors discussed above are reflected in varying levels of detail in existing aging models. Depending on the design goal and application, a different kind of model is required. In Section 2.2.1, we first discuss different model types that estimate the amount of aging on different levels of detail: Ranging from a very fine-grained level where the electrochemical mechanisms are correctly reproduced to black-box models that are based on statistics and no representation of the electrochemical mechanisms is included. Then, in Section 2.2.2, we discuss several models and their suitability for system-level design. Finally, in Section 2.2.3, we summarize two models that are used for the case studies in this thesis.

2.2.1 Model types

For the design of battery health management systems, we require models of battery SOH that help us to understand the impact of design decisions on the real battery. Such models should not be confused with SOH estimators that run online and determine the current SOH of a specific battery. Nevertheless, the algorithms are often similar for both purposes. A huge variety of models exists for this task, which estimate the impact of aging factors on different levels of abstraction. In the following, we present two categorization approaches and afterward discuss which kind of models are required for multi-scale battery health management systems.

Hu et. al [65] use a three-level categorization of available battery models. Firstly, white-box models describe the internal degradation mechanisms. A typical example is the electrochemical models. Secondly, black-box models are data-driven or model-free approaches. Neural networks are part of this group. In between white- and black-box models, gray-box models are located. The nature of models within this group is the approximation of internal dynamics. Equivalent circuit models represent these kinds of models.

Barré et al. [7] present more fine-grained categories for aging models: The first group is formed by electrochemical models. They are the most complex type of models as they describe the dynamics of the cell based on the degradation mechanisms. Some do this even at an atomistic or molecular level. The second type is the equivalent circuit-based models. They approximate the internal dynamics through equivalent circuits. The parameters are commonly estimated from experimental investigation and measurements. Thirdly, performance-based models implement the modeling of physical relations, e.g., by describing temperature dependencies,

etc. The fourth category is analytical models with empirical data fitting. They describe cause-effect relations, where parameters are obtained from measurement data. Big data-bases are required to fit such predictors. Finally, statistical methods are the most abstract group. Here, no understanding of underlying aging mechanisms is required and the models are purely data-based.

In system-level design, we usually require models that have reasonable simulation times for fast prototyping. Therefore, the fine grained insights of electrochemical models are not required. Accuracy is an issue that still requires much investigation. At the moment, we should note that not only aging models but also the environment imposes a large degree of inaccuracy and even more uncertainty. We often want to evaluate strategies independent of the specific cell chemistry, e.g., LCO, LFP, etc. Which means, that we cannot always reliably quantify degradation. Nevertheless, we often can draw qualitative conclusions. Simplicity in algorithmic structure, e.g., the pros and cons of recursion, can also be a criterion for model selection. In particular, for the development of control algorithms, light-weight and fast models that can potentially run online are preferable. The models to be chosen within this thesis are, therefore, gray-box or black-box models in the classification scheme by Hu et al. [65].

2.2.2 Requirements

In the following, we discuss a selection of existing battery aging models. We then select two models that are used for designing and evaluating the health management approaches in the subsequent chapters. The presented models have in common that they are either publicly available or else the respective publications include sufficient information to easily implement the model.

CAEBAT

Within the Computer Aided Engineering for Batteries (CAEBAT) project a *multi-scale multi-domain model* for system-level design was developed [81]. The model follows a multi-physics approach and includes thermal, electrical, and electrochemical calculations. The openly available software parts are the Open Architecture Software (OAS) and Virtual Integrated Battery Environment (VIBE) [72]. However, in the meantime, several parts have been integrated into commercial tools, i.e., ANSYS, and the free version is no longer maintained. The advantage of this model is its presumably high accuracy due to the underlying physiochemical descriptions. However, the documentation for the publicly available parts is rather limited at the time of investigation and no direct interface to MATLAB, where we develop the control strategies, is available. Nevertheless, investigation of the ANSYS system design tools, which include parts of the CAEBAT project results, is seen as an interesting option for future work.

LIONSIMBA

The LIONSIMBA framework [144] can be used for Li-Ion battery design, simulation tasks, and control application development. The framework is implemented in MATLAB and is openly available. The model uses complex partial differential equations to describe the electrochemical

processes inside the battery. It also offers very fine grained parametrization for battery input parameters such as the thickness of the current collector or porosity of the separator. However, the runtime and complexity are also relatively high and therefore, fast prototyping is difficult.

SIMSCAPE battery model

The SIMSCAPE battery model [99] is a generic model for various battery types including Li-Ion batteries. Control algorithms developed in MATLAB can be easily incorporated. Not only standard electrical behavior is implemented but also thermal as well as aging characteristics. Parameterizations for several batteries are available. However, the battery aging functionality was not available when the research for this thesis was started. Therefore, we decided to implement a custom-built model as described in the next paragraph.

Millner aging model

The Millner [104] model implements battery aging based on crack propagation calculations and uses empirical data of LFP batteries to fit the model. This model considers multiple aging factors such as temperature, average SOC, SOC swing, and time. On the downside, the model introduces complexity by recursively calculating the degradation. This results in difficulties when designing control applications. We select this model for evaluation purposes of our work due to its broad coverage of aging factors.

Suri et al. aging model

The Suri et al. [140] battery aging model was particularly developed for control applications. In this model, a severity factor rates the severeness of damage induced by a combination of aging factors, namely the SOC, the applied C-rate, and the temperature. The empirical data was gained from measurements with an LFP cell. We select this model for the design of an EES controller.

Conclusion

As the latter two models are lightweight while considering a wide range of the relevant aging factors, they are used in the analysis of the health management use cases developed within this thesis. The SOH-aware balancing strategy in Chapter 3 and the smart charging scheme in Chapter 4 are evaluated using the Millner model. The Suri et al. model is used for controller design in the cost/privacy co-optimization of a residential EES with PV in Chapter 5.

2.2.3 Model selection

In the following, we summarize the Millner model [104] and the Suri et al. model [140] and shortly discuss their commonalities and differences.

Millner model

The Millner model [104] is a widely-adopted SOH model, which describes electrochemical degradation processes by physical crack propagation mechanisms over cycling and time. Stress parameters are the cell temperature θ_{B}, the SOC swing σ, and average SOC $\overline{S}$, where the latter two along with the time interval T_m are equivalent descriptions of the charge/discharge current. The original Millner model considers single charge and discharge cycles of an identical pattern.

To derive the average SOC $\overline{S}$ within the m-th interval of duration T_{m}, we calculate

$$\overline{S} = \left(\int_{T_{\mathrm{m}}} S(t) dt \right) / T, \tag{2.1}$$

where T is the duration of the time interval. The normalized SOC swing σ within the time interval m is calculated by

$$\sigma = 2 \sqrt{3 \int_{T_{\mathrm{m}}} (S(t) - \overline{S})^2 dt / T}. \tag{2.2}$$

As the cycle interval T_{m} may start and end at arbitrary SOC states, the effective number of throughput cycles

$$N_{\mathrm{TP}} = \int_{T_{\mathrm{m}}} \frac{|i(t)| dt}{2 Q_{\mathrm{nom}}}, \tag{2.3}$$

needs to be calculated, where $i(t)$ is the charge- or discharge-current, Q_{nom} is the nominal amount of charge that can be stored in the battery and m denotes the m-th time the cell is discharged and recharged between arbitrary SOCs.

A first degradation parameter accounts for the damage in mid-centered cycles

$$D_1 = K_{\mathrm{co}} N_{\mathrm{TP}} \exp\left((\sigma - 1) \frac{\theta_{\mathrm{ref}} + 273}{K_{\mathrm{ex}} (\theta_{\mathrm{B}} + 273)} \right) + 0.2 \frac{T_{\mathrm{cycle}}}{T_{\mathrm{life}}}, \tag{2.4}$$

where K_{co} is a normalization coefficient for N_{TP} and K_{ex} is a constant exponent for SOC swing. θ_{ref} is the reference battery temperature of $25\,$°C. θ_{B} is the battery temperature. The duration of one cycle is denoted by T_{cycle} and T_{life} is the shelf life at $25\,$°C and $50\,\%$ SOC until EOL, which we set to 10 years.

Adjustment of the average SOC S is done in the second degradation parameter

$$D_2 = D_1 \exp\big(4 K_{\mathrm{soc}} (\overline{S} - 0.5)\big) \left(1 - D(T_{\mathrm{m}-1})\right), \tag{2.5}$$

using a constant K_{soc} to account for the average SOC. Finally, the total increase in the degradation parameter D is given by

$$D(T_{\mathrm{m}}) = D_2 \exp\left(K_{\mathrm{t}} (\theta_{\mathrm{B}} - \theta_{\mathrm{ref}}) \frac{\theta_{\mathrm{ref}} + 273}{\theta_{\mathrm{B}} + 273} \right), \tag{2.6}$$

where K_{t} accounts for a doubling of the decay rate for each $10\,$°C rise in temperature. Summing up the damage done by each cycle, one can derive the remaining life of the battery. Table 2.1 shows the values for the constants from [104].

Table 2.1: Aging parameters [104]

parameter	value	parameter	value	parameter	value
K_{co}	3.66 e-5	K_{t}	0.0693	θ_{ref}	25 °C
K_{ex}	0.717	K_{soc}	0.916	T_{life}	10 years

Suri et al. model

In the Suri et al. model [140], the cycle life degradation is determined in terms of an empirically fitted severity factor map, as depicted in Figure 2.2. The severity factor ζ_{funct} describes the amount of damage done to a battery by its current SOC, the applied C-rate, and the temperature. This cycle life model was particularly developed for control applications as the computational effort is comparably low and no iterative dependencies exist. The model is derived for Li-Ion batteries, which are commonly used in hybrid electric vehicles but also stationary storages. The framework can be easily adapted to other cell chemistries by using a similar data fitting approach as in [15].

We will reproduce some of the relevant formulae from [140]. Usually, the EOL of a battery is assumed to be reached at $80\,\%$ of its initial capacity. Battery aging in general has two occurrences: Capacity fading and resistance growth. From an economic perspective, the dominating problem is the capacity loss in percent $Q_{\text{loss},\%}$ and therefore it is the only aging type considered in this model:

$$Q_{\text{loss},\%} = \zeta_{\text{funct}} Q_{\mathrm{tp,Ah}}^{K_{\mathrm{pl}}}. \tag{2.7}$$

$Q_{\mathrm{tp,Ah}}$ is the accumulated throughput in and out of the battery in ampere-hours and K_{pl} is a power-law exponent retrieved from measurement data. The severity factor function ζ_{funct} describes the dependence on the three main factors that contribute to aging: C-rate ι_C, temperature θ_{B} and SOC S:

$$\zeta_{\text{funct}} = (K_{\mathrm{a}} S + K_{\mathrm{b}}) \exp\left(\frac{-E_a + K_{\mathrm{c}} \iota_C}{R_{\mathrm{gas}}(273.15 + \theta_{\mathrm{B}})}\right). \tag{2.8}$$

The variables K_{a} and K_{b} model the SOC dependence, E_a is the activation energy and R_{gas} is the universal gas constant. The variable K_{c} describes the dependence on the C-rate ι_C, where the C-rate is the ratio of current and battery capacity.

2.3 Related work on battery health management techniques

In this section, we survey related works on battery health management approaches. The related work targets control parameters and techniques, such as hybrid storages, thermal management, charge patterns, multi-objective optimization goals, etc. In the following, we discuss the proposed techniques and highlight the addressed abstraction layers and cross-level dependencies.

Management of multi-cell and hybrid energy storages

Multi-cell and hybrid energy storages provide the opportunity to distribute loads among the storage elements and thereby create less detrimental conditions for the individual battery cells.

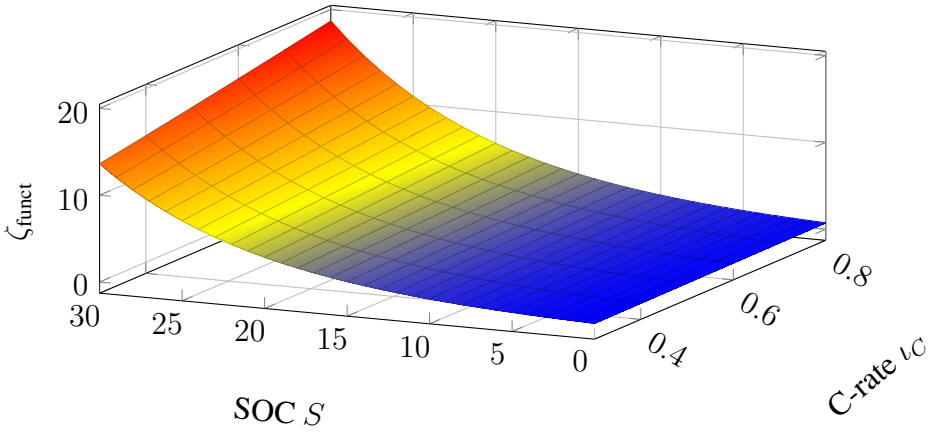

Figure 2.2: Severity factor map for 25 °C

In hybrid energy storages, the Li-Ion batteries are used in combination with other storage types that can compensate for the aging characteristics of Li-Ion batteries. For example, supercapacitors age at a slower rate compared to a Li-Ion battery cell. Therefore, they can be used to satisfy detrimental peak currents. Cell balancing architectures and reconfigurable systems can be used to distribute the load among battery cells with varying initial SOH. In Chapter 3, we present an SOH-aware cell balancing strategy in combination with a cell balancing architecture. Bouchima et al. [16] apply a strategy on reconfigurable systems that stresses healthier cells more than weaker cells, which is the same strategy, we apply for the SOH-aware cell balancing technique in Chapter 3. They confirm our findings that such a strategy results in the decreased spread of the available capacity and increased battery cycle life as well as better usability in second-life applications.

By using such balancing or reconfigurable systems on module-level, the cell-level boundaries are adjusted during runtime. Information from cell-level, such as the current SOH can similarly be used on module-level to refine strategies. For example, the optimal scheduling of multi-cell batteries in mobile devices needs to consider the SOH of all cells to correctly estimate and exploit the recovery effect and rate capacity effect [4]. Thereby, the performance and single-cycle runtime are increased.

Hybrid storages can be used to compensate for Li-Ion battery aging factors by combining them with other storage types with different aging characteristics, e.g., supercapacitors. A charge management policy is required for such Hybrid Electrical Energy Storages (HEESs) to optimize towards single cycle runtime as well as cycle life. A possible strategy is to satisfy the baseload using the battery, while the spiky part of the load is satisfied by the supercapacitor. Additionally, the SOC swing and average SOC of the battery should be minimized [158]. Previous work show improvements in cycle life of up to six times if HEESs are used with SOH-aware strategies [153].

Kim et al. [83] show how hybrid energy storages successfully solve the problem of under-dimensioned laptop chargers. Nowadays, laptop chargers come at a small size and weight, which seems to be advantageous for the user. However, such under-dimensioned chargers cannot always fulfill the power demand from the device-level and the battery is used additionally.

Therefore, the battery is unnecessarily exposed to additional discharge currents and SOC swing, which increases aging. The use of a supercapacitor on module-level to satisfy the additional charge requirement reduces stress on the battery by adjusting cell-level usage and mitigates aging.

Thermal management

The thermal system and thermal management can help to mitigate aging on the module-level. Commonly, higher temperatures increase battery aging. On the other hand, very low temperatures can also damage the battery. Some EVs are equipped with battery preheating systems to prevent damaging operating conditions [119]. Through this measure, thermal conditions for cells are improved, resulting in extended cycle life.

Similarly, one would also like to optimize the energy output and keep the battery at a temperature, where most energy can be obtained while causing as little damage as possible. One possibility to improve positioning dependent cell aging could be to have a reciprocating cooling airflow instead of a unidirectional one [95].

Battery health-aware charge patterns

In Chapter 4, we will discuss that delayed charging and reduced target SOC significantly mitigates the aging of a smartphone. Similarly, the aging of EVs can be mitigated by adjusting the charge strategy. Hoke et al. [61] present a charge strategy that not only delays charging but additionally uses a reduced charge current. As a consequence, the temperature rise is reduced and the average SOC decreases, thereby reducing the battery aging. This strategy makes use of device-level information on the usage times of the EV and adjusts cell parameters to operate in an aging friendly range for most of the time.

Such intelligent charging strategies can be extended to include multiple devices from distinct types. For example, if an EV, laptop computer, tablet, and smartphone share a calendar from which an algorithm can conclude unplug times and required charge of the individual devices, the charge schedule of all devices could be concluded and optimized.

The cost and battery health optimal charge patterns determined by Bashash et al. [8] achieve the least battery health degradation by keeping the SOC at a low level all time and hence the battery should not be charged. However, this strategy cannot be practically applied in most cases. A trade-off tending towards battery health-friendly behavior is to charge the battery shortly before the trip starts to avoid high storage SOCs. However, the filling level depends on the current energy price and also health considerations. On the other hand, a trade-off with a higher focus on financial cost results in making use of off-peak charging prices and only delaying charging if prices are low. The fill levels can be below 100% SOC as lower SOC is less detrimental for battery health. Finally, a purely financial cost-optimal strategy is to fully charge the Plug-In Hybrid Electric Vehicle (PHEV) before the trip at off-peak times when low prices are available. These strategies not only use device-level information of EV usage times but additionally operate on system-level and co-optimize the charge pattern with the financial cost.

Battery health-aware load patterns

Just as the charge pattern, the discharge pattern can be optimized towards battery health improvement by adjusting load patterns based on device-level usage information. Valentini et al. [149] optimize the transmission times and power consumption on battery-powered wireless sensor nodes towards increased cycle life. In the case of PHEVs, Serrao et al. [135] find that the fuel consumption should be co-optimized with battery behavior and in particular the battery degradation.

In EVs, the Heating, Ventilation and Air Conditioning (HVAC) have a huge impact on power consumption and therefore, battery cycle life. A co-optimization to control the HVAC considering the driving range and cycle life has been presented by Vatanparvar et al. [150]. The HVAC is the second-highest power consumer in a vehicle after the electrical motor. In the presented work, the HVAC power consumption is controlled such that the SOC deviation is minimized and hence the SOH degradation is reduced. In other words, the HVAC consumption is reduced at times when the electrical motor consumption is very high. The authors achieve an improvement of SOH degradation of up to $14\,\%$ compared to conventional approaches. At the same time, the overall power consumption is reduced. Therefore, both driving range, as well as battery cycle life, are increased. Similarly, the HVAC control in a residential home or office can be designed to co-optimized the objectives and constraints from stationary battery storage, PV, and the preferred temperature levels in different rooms within a building [30].

Battery health co-optimization problems

On system-level, battery health should be co-optimized with the actual system objectives. In Chapter 5, we will present a cost/privacy co-optimization for joint PV and EES installations. Privacy is just one of many metrics that may be considered in the joint EES and PV scenario. Li et al. [89] compare different charge/discharge strategies such as cost optimality, maximizing self-consumption, or maximizing cycle life for such a system. They find that cycle life optimal strategies start charging the residential EES only in the afternoon to avoid long periods of high SOC and hence, reduce average SOC. On the other hand, they also find that multi-objective strategies achieve similar cycle life improvements but are accompanied by a significantly better financial gain from saving and selling grid electricity.

Scheduling the charging of batteries in a fleet of delivery drones has been discussed by Park et al. [113]. The problem is formulated as a multi-objective optimization problem which not only minimizes the overall SOH degradation of all battery packs within the fleet of drones but also the waiting times of the delivery tasks. The charging of individual batteries is scheduled such that idle times at high SOC are reduced and average SOC is minimized. Hence, battery aging is mitigated.

Further EV design aspects are discussed by Chang et al. [21]. They find that controllers in EVs need to be redesigned once the processor ages and the battery has degraded to maintain quality of control. When a processor ages, the delay of the critical path gets longer. As a result, the sampling period increases, and the quality of control gets deteriorated, which is highly undesired in safety-critical applications such as the control of the electric motor in an EV. As a remedy, re-optimization is proposed. Once the processor has aged, autonomous frequency scaling can be applied to ensure that signals are completely transmitted within one clock cycle.

Operating the aged processor at a higher frequency and shorter sampling period potentially results in a better quality of control but comes at the cost of higher battery usage. Higher battery usage is disadvantageous in terms of less available capacity during the current cycle due to the rate capacity effect and also higher battery aging in the long term due to increased C-rates. Therefore, multi-stage controller design and re-optimization should be applied.

3

SOH-aware active cell balancing strategy for high power battery packs

Short driving range due to limited battery capacity and high battery depreciation costs persist to be the main deterrents to the wide adoption of EVs. High power battery packs consisting of a large number of battery cells require extensive management, such as SOC balancing and thermal management, to keep the operating conditions within a safe and efficient range. In this chapter, we propose a novel SOH-aware active cell balancing technique, which is capable of extending the cycle life of the whole battery pack. In contrast to the state-of-the-art active cell balancing techniques, the proposed technique reduces the load current of cells with low SOH using the active cell balancing architecture. Based on the observation that assigning the smallest possible load current to cells with lower SOH extends cycle life, the technique identifies the most beneficial charge transfers. We find that with our proposed scheme, aging could be mitigated by up to $23.5\,\%$ over passive cell balancing and $17.6\,\%$ over active SOC cell balancing.

Chapter outline: Chapter 3 is organized as follows. Section 3.1 introduces the idea of the SOH-aware balancing algorithm and summarizes the contributions of this chapter. In Section 3.2, the required background on SOH degradation in EVs, active cell balancing architectures, and online SOH measurement techniques is provided. Next, in Section 3.3, the observation that active cell balancing reduces stress on less healthy cells and extends cycle life is investigated and an outline on how this effect can be further exploited to increase cycle life is given. The used models of the battery pack and cell balancing infrastructure are summarized in Section 3.4. The proposed SOH-aware active cell balancing technique that adapts load currents to further mitigate aging is explained in Section 3.5. The experimental results in Section 3.6 compare the approach to passive and conventional active balancing. The chapter concludes with Section 3.7.

The following text and figures are quoted mostly verbatim from [122]. Small adjustments have been made to ensure good readability and layout of the full thesis.

3.1 Introduction

This section provides the introduction to SOH-aware cell balancing. After a brief description of the general problem of imbalanced cell capacities and the solution provided by conventional balancing approaches, the overall idea and contributions of SOH-aware cell balancing are presented.

3.1.1 Motivation

EVs are seen as one of the promising alternatives to combustion engine vehicles as they have a very low cost per mile and less environmental impacts. The market share of EVs is still small, but signs of a transition towards a fully electrified powertrain are evident. Despite the optimistic forecasts, major shortcomings of EVs persist, such as i) the range anxiety due to limited battery capacity and ii) high battery depreciation costs due to SOH degradation. Even though battery prices are expected to drop soon, either manufacturers or EV owners bear the costs for a battery which will eventually become unusable within the EV and therefore be disposed of due to capacity loss. This is undesirable from both the economic and the environmental perspective. If implemented, our method can help in saving several thousands of dollars.

Typically, Li-Ion cells are preferred for such high power applications due to their high energy and power densities compared to other rechargeable battery chemistries. As shown in Figure 3.1, a high power battery pack is formed by connecting multiple Li-Ion cells in parallel to increase the capacity and connecting these parallel cell modules in series for achieving the required high operating voltage. To ensure safe and efficient operation, Li-Ion cells demand tight control over their operating conditions. Operation outside their defined set of safe thresholds will reduce their cycle life and probably damage them, causing fire or explosion due to thermal runaway.

The capacity fading rate of Li-Ion cells depends on various factors, such as operating temperature, average SOC, and SOC swing and it is generally known that high average SOC, high temperature, and large SOC swing are detrimental for battery health [104]. While the SOH of each cell degrades, the usable capacity of the series-connected cells is determined by the cell with the lowest SOH. With repeated charge/discharge cycles, the SOH of all cells tends to diverge due to manufacturing inhomogeneities and varying temperature distribution. This also contributes to early disposal of the battery pack from the vehicle, since current regulations demand replacement of the entire EV battery pack if any cell in the pack reaches $70\,\%$ of its SOH value.

Conventional balancing approaches are passive, where the excess charge of cells with higher SOC is dissipated as heat across a resistor, resulting in reduced energy efficiency. By contrast, active cell balancing approaches increase the energy output of the battery pack by transferring the excess charge between cells instead of dissipating it as heat. However, existing active cell balancing approaches only focus on equalizing the SOC at all times and inherently partially contribute to increased cycle life [136]. By optimizing the load current assignment, the cycle life can be significantly improved further.

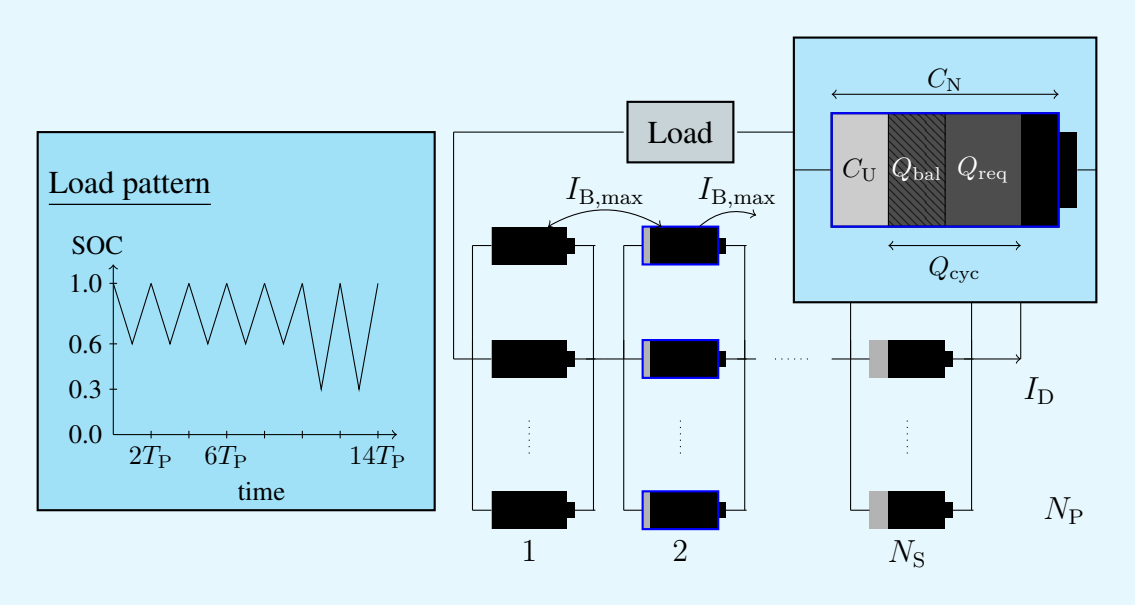

Figure 3.1: A battery pack consisting of N_P parallel electrically indistinguishable cells and N_S series-connected cells varying in SOH. C_U is the unusable capacity due to capacity fading. The required charge is $Q_{req} = I_D T_P$. Using an active cell balancing architecture, the amount of charge transferred is $Q_{bal} = I_{B,max} T_P$. The effective discharge of a cell is Q_{cyc}. The nominal capacity of a cell is denoted by C_N.

3.1.2 Contributions

In this chapter, we focus on the fact that the EV batteries are not always used to their full capacity in every drive cycle, and hence, it is not necessary to keep the SOC equalized at all times. For instance, a typical usage profile of an EV is shown in Figure 3.1 where the pack follows a driving pattern that consists of five small commuting trips during weekdays followed by two longer trips on the weekends. It is not mandatory to always maintain an equal SOC among all cells when the entire battery capacity will not be used within a single cycle. Existing methods of remaining range estimation [62] help to estimate the available SOC margin. Estimating the required charge to reach a predefined destination is crucial to enable autonomous driving and further advances are expected to be made in this domain. We propose to leverage this headroom for mitigating battery SOH degradation using a state-of-the-art active cell balancing architecture [110] by reducing the load current of the less healthy cells.

In particular, we propose the following contributions.

- Active cell balancing reduces stress on less healthy cells and extends cycle life. We show that this effect can be further exploited and cycle life is significantly extended (Section 3.3).

- We propose a novel SOH-aware active cell balancing technique that adapts load currents to further mitigate aging (Sections 3.4 and 3.5).

- Compared to passive and conventional active balancing, experimental results show that our technique improves cycle life by $23.5\,\%$ and $17.6\,\%$, respectively (Section 3.6).

3.2 Related work

In the following, related works in the field of SOH mitigation for EVs using other control knobs than active cell balancing are presented. Then, as our work is based on and extends active cell balancing strategies, available architectures and strategies are briefly explained. Finally, as the SOH-aware balancing algorithm relies on online SOH measurement, related work on suitable techniques is summarized.

3.2.1 SOH degradation mitigation in electric vehicles

There are various approaches to mitigate the SOH degradation of EV batteries. An often-used method for aging reduction is the charge pattern. A cost and SOH-degradation optimized charge pattern can be achieved by charging slowly and charging shortly before the trip starts, which reduces temperature rise, and lowers the average SOC, respectively [61]. Instead of the charging pattern, the authors of [150] control the EV's heating, ventilation, and air conditioning system to extend battery runtime and cycle life. Besides, battery pack reconfiguration techniques can also be used to improve the SOH. The work in [58] proposes to connect cells with similar SOH levels to increase available capacity in one cycle. However, such reconfigurable systems have significant efficiency limitations due to the on-resistance of reconfiguration switches. The work in [136] shows that compared to passive balancing, active SOC balancing narrows the capacity distribution among cells in the long term and increases cycle life. Our work overlays on this finding by proposing a methodology to even further increase this effect.

3.2.2 Active cell balancing

A comprehensive overview of different cell balancing architectures is provided in [18]. Typically, the existing active cell balancing approaches are classified into capacitor-based, inductor-based, and transformer-based, depending upon the type of energy storage element used for charge transfer [50]. Among them, the inductor-based approaches are more preferable since they provide a higher energy efficiency compared to the capacitor-based architectures and also occupy a smaller installation volume when compared to the transformer-based counterparts. In addition to the electrical architectures, several equalization strategies are proposed in the literature that determine the optimal charge transfer direction between the cells to equalize the SOC of the battery pack. For instance, four different request-driven equalization strategies are proposed in [138]. However, existing works in the domain of active cell balancing only focus on equalizing the SOC of all cells in the pack and do not consider SOH, which we do in this work for the first time.

3.2.3 Online SOH measurement

The proposed SOH-aware cell balancing technique requires an online SOH measurement that can be implemented in the BMS. An overview of existing methods is provided in [10]. Coulomb counting is a relatively simple online SOH estimation method, which integrates the amount of charge flowing in and out of the battery pack. However, it does not consider the temperature effects and the self-discharge current of the battery pack and therefore does not provide accurate results. On the other hand, electrochemical impedance spectroscopy techniques that directly measure the battery internal impedance are more accurate. However, due to their requirement of high accuracy measurements and complex signal processing tasks, they are typically performed offline in a laboratory. Recently, the work of [34] suggests a real-time electrochemical impedance spectroscopy technique, paving the way for high accuracy SOH estimation at the BMS level. SOH estimation is continuously improving. Moreover, SOH estimation techniques have been discussed in Chapter 2.1.3. Note that our proposed SOH-aware balancing methodology can be implemented in conjunction with any of the existing SOH estimation techniques in the literature.

3.3 Observations for active cell balancing

In this section, we first explain the operating principle of a state-of-the-art inductor-based active cell balancing architecture, upon which the proposed technique is built. Then, we provide some key observations, which form the groundwork for the strategies introduced in this chapter.

3.3.1 Active cell balancing operating principle

A state-of-the-art inductor-based active cell balancing architecture, as proposed in [86], is shown in Figure 3.2a. Each cell is associated with a balancing module that consists of two power Metal-Oxide-Semiconductor Field-Effect Transistor (MOSFET) switches (M_a^i and M_b^i) and an energy storage element, inductor L_i. Charge transfer between cells takes places in two phases, charging (Φ_1) and discharging (Φ_2) that are controlled by two high-frequency control signals ρ^1 and ρ^2, respectively. During the charging phase Φ_1, MOSFET M_b^1 is actuated with ρ^1 and the excess charge in cell B^1 is stored in inductor L_1. During the discharging phase, M_b^1 is turned *OFF* and M_a^2 is actuated with ρ^2 transferring the stored energy in the inductor L_1 to cell B^2. Short free-wheeling phases during which the inductor current flows through the body diode of the respective power MOSFETs are necessary to avoid short-circuit conditions between the cells. The balancing current ranges from $0\,\mathrm{A}$ to a maximum value $I_{\mathrm{B,max}}$ and is modified by adjusting the length of the Pulse Width Modulated (PWM) signal generated with ρ^1 and ρ^2.

3.3.2 Observations with two cells

We provide the key observations using a simple two-cell example. Two cells are discharged by a discharge current I_{D}. The balancing current $I_{\mathrm{B,max}}$, which is limited by hardware component constraints and costs, can now either increase or decrease the load current experienced by individual cells. When one cell B^1 transfers charge to another cell B^2 through $I_{\mathrm{B,max}}$, B^1

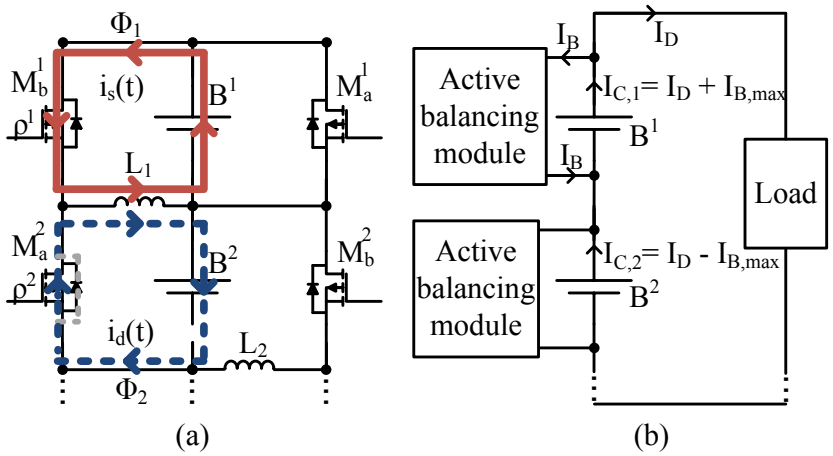

Figure 3.2: (a) Operating principle of an inductor-based active cell balancing architecture proposed in [86]. (b) A higher current ($I_{\mathrm{D}} + I_{\mathrm{B,max}}$) is discharged from healthier cell B^1 whereas cell B^2 sees a reduced current ($I_{\mathrm{D}} - I_{\mathrm{B,max}}$).

effectively has a higher load current $I_{C,1} = I_{\mathrm{D}} + I_{\mathrm{B,max}}$ and B^2, which receives the charge, has effectively a lower load current $I_{C,2} = I_{\mathrm{D}} - I_{\mathrm{B,max}}$ as shown in Figure 3.2. In this section, we ignore the transfer efficiency γ for the sake of simplicity. However, it will be considered in Section 3.5. We exploit the following observations for our SOH-aware balancing scheme.

Observation 1. *Battery aging depends on the average SOC and also the SOC swing.*

Therefore, avoiding high SOC levels helps to mitigate battery aging. Lower SOC swing means less severe capacity fading [56, 133] and is therefore preferable over higher variances in SOC levels. The effects are reflected in the used aging model [104].

Observation 2. *Cells in a pack degrade at different speeds.*

Temperature is the main contributor to this aging speed divergence [133]. In high power battery packs, cooling is usually not homogeneous. Especially in automotive applications, where the pack volume needs to be minimized, a trade-off exists between achievable temperature homogeneity and the overhead introduced by the cooling system hardware. Even the most efficient state-of-the-art cooling approaches still expose the batteries to temperature stress when being charged or discharged at high rates [66]. Manufacturing variations, while depending on the cell size and quality of the manufacturing process, are another significant contributor to cell inhomogeneity which eventually promotes different aging behavior between cells [5, 37]. Also, the aging-speed slightly reduces with decreased SOH [127, 133]. Due to permanent equalization currents, parallel cells can be assumed to be electrically indistinguishable. While serial cells built up a variation in capacity because of manufacturing inhomogeneities and temperature variations.

Observation 3. *Resting the less healthy cells mitigates the EOL.*

With active cell balancing, the individual cell current, and hence the average SOC and also SOC swing, can be adjusted. The work in [136] confirms that stressing the healthier cell more

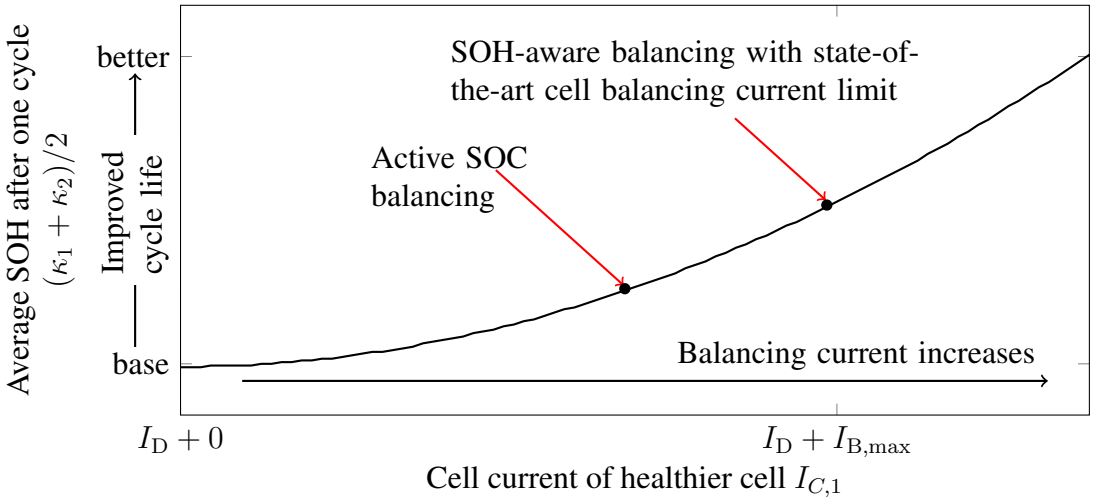

Figure 3.3: Average SOH of two series-connected cells after one charge/discharge cycle. Transferring charge from the healthier cell to the less healthy cell is beneficial in the long term and increases cycle life beyond SOC balancing.

than the less healthy cells reduces the SOH gap between the healthiest and the least healthy cell and prolongs cycle life. We observe the same behavior for two cells using the aging model from [104]. Figure 3.3 illustrates the effect of obtaining increased cycle life for higher balancing currents. In the long term, this preserves the less healthy cells as the EOL is determined by the least healthy cell reaching a predefined SOH value. Note that the gain achieved in a single cycle is small, but in the long term, the effect significantly contributes to increased cycle life as will be shown in Section 3.6. We propose a strategy that intensifies this effect by further optimizing the load current assignment. I.e., we use the maximum available balancing current, which is only limited by component constraints of the balancing architecture.

Based on the above observations, we develop an SOH-aware balancing strategy that increases the number of cycles of a battery pack until EOL in Section 3.5.

3.4 System modeling

In this section, we shortly explain the models used for battery behavior and aging simulation. We define the term *aging speed* and explain how cell balancing efficiency is considered in the simulations.

3.4.1 Battery aging model

Using the correct aging model is crucial for evaluating the proposed cell balancing technique. Hence, we employ a widely-adopted SOH model, the Millner model, which describes electrochemical degradation processes by physical crack propagation mechanisms over cycling and time [104]. The model has been summarized in Chapter 2.2.3. Further experimental evaluation in [136] supports the model behavior. Stress parameters are the cell temperature θ_{B}, SOC

swing σ, and average SOC $\overline{S}$, where the latter two along with the time interval T_{m} depict the charge/discharge current. We combine this with the equivalent electrical circuit model from [24] to account for short-term battery behaviors.

Besides the model, we define the aging-speed as degradation per cycle:

$$v_{\mathrm{a}} = \frac{\Delta\kappa}{\mathrm{cycle}}. \tag{3.1}$$

We specify the unit to be points per million and cycle: $\frac{1\times10^{-6}}{\mathrm{cycle}} = 1$ ppmc. I.e., a cell with an aging-speed of 50 ppmc will have lost 5% of its initial capacity after 1000 cycles.

3.4.2 Cell balancing efficiency

We use the existing analytical model from [77], which is derived for inductor-based active cell balancing architectures, to calculate the energy efficiency of the charge transfer process. We allow direct charge transfers only between neighboring cells. The energy efficiency of the charge transfer process is calculated as

$$\gamma = 1 - \frac{E_{\mathrm{diss}}}{E_{\mathrm{tx}}}, \tag{3.2}$$

where E_{diss} and E_{tx} is the energy dissipated and the energy transferred, respectively. The two major sources of energy dissipation in the cell balancing process are the conduction energy dissipation E^{cd}, due to the parasitic resistances of the circuit components and the switching energy dissipation E^{sw}, due to the non-zero ON and OFF times of the MOSFET switch. The conduction energy dissipation in a single charge transfer cycle is calculated as:

$$E^{\mathrm{cd}}_{\mathrm{cyc}} = Q_{\mathrm{tx}} \cdot V_{B^1} - Q_{\mathrm{rx}} \cdot V_{B^2}, \tag{3.3}$$

where Q_{tx} is the charge transferred by the source cell and Q_{rx} is the charge received by the destination cell in a single switching cycle. V_{B^1} and V_{B^2} are the voltages of the source and destination cells respectively. The energy dissipation due to the switching activity of MOSFETs in each charge transfer cycle is calculated as

$$E^{\mathrm{sw}}_{\mathrm{cyc}} = \frac{1}{2} I_{\mathrm{peak}} \{ t_{\mathrm{OFF}} \cdot V_{B^1} + t_{\mathrm{ON}} \cdot V_{B^2} \} + \frac{1}{2} C_{\mathrm{OSS}} \{ V^2_{B^1} + V^2_{B^2} \}, \tag{3.4}$$

where I_{peak} is the final inductor current during the charging phase, t_{ON} and t_{OFF} are the turn-ON and turn-OFF times of the MOSFET switch and C_{OSS} is the parasitic output capacitance of the MOSFET.

However, as we propose a high-level cell balancing strategy and simulate the long-term effects of batteries, it is impractical to consider circuit-level details. In the following sections, we use the average balancing current $I_{\mathrm{B,max}} = 1/4 \times I_{\mathrm{peak}}$. Also, based on our circuit-level simulations, we find that it is safe to assume a constant efficiency of 96% for typical V_B values and balancing currents.

Algorithm 1 SOH-aware cell balancing algorithm. *//Call this function at the start of each trip*

Input: destination, $C_i^{(k)}$, T_P
Output: $I_\mathrm{b}^{(k,k+1)} \forall k \in 1...N_\mathrm{S}-1$
1: Q_req = getQreq(destination, T_P);
2: I_D = getID(Q_req);
3: $\kappa_i^{(k)}$ = updateSOH($C_i^{(k)}$);
4: [healthList, i] = sortCellsAscendingSOH($\kappa_i^{(k)}$);
5: **for** all cells in healthList **do**
6: $[\eta^{(k-1,k-2)}, \eta^{(k-1,k)}, \eta^{(k,k-1)}, \eta^{(k,k+1)}, \eta^{(k+1,k)}, \eta^{(k+1,k+2)}]$ = getEta($C_i^{(k)}$); *// Table 3.1*
7: **end for**
8: **for** cell $k = 1...(N_\mathrm{S}-1)$ **do**
9: $[I_\mathrm{b}^{(k,k+1)}]$ = getBalancingCurrent($I_\mathrm{D}, \eta^{(k,k+1)}, C_i^{(k)}, C_i^{k+1}$); *// Table 3.2*
10: **end for**

3.5 SOH-aware active cell balancing

In the following, the algorithm for the SOH-aware cell balancing is presented. First, the algorithm is summarized. Then details on determination of the charge transfer direction and the amount of charge to be transferred are provided.

3.5.1 Overview

The basic idea of the SOH-aware cell balancing algorithm is to compensate the amount of charge that is discharged from cells with a lower SOH by transferring charge from neighboring cells with a relatively higher SOH. We assume that the battery management system is capable of reliably measuring the capacity of cells. The transfer is done using the active cell balancing architecture from Figure 3.2. We assume that the decision for the transfer direction and the amount of the cell balancing current is made at the beginning of each trip and remains fixed. This is sufficient as battery aging is a comparatively slow process. The algorithm is shown in Algorithm 1. We assume that the accumulated charge required from the battery pack Q_req is known at the beginning of each trip. In a real-world implementation, this could be determined by, e.g., the destination entered in the navigation system (Algorithm 1, line 1). For the remainder of this chapter, we consider a constant discharge current $I_\mathrm{D} = \frac{Q_\mathrm{req}}{T_\mathrm{P}}$ for our discussion of the algorithm (Algorithm 1, line 2), where T_P is the duration of a trip. This is safe to assume because using average I_D is sufficient for determining $I_\mathrm{b}^{(k,k+1)}$ in the algorithm. However, using a time-series of I_D values is possible without modifications.

The SOH $\kappa_i^{(k)} = \frac{C_i^{(k)}}{C_\mathrm{N}}$ of each cell is the ratio of available capacity $C_i^{(k)}$ and the nominal capacity C_N (Algorithm 1, line 3). The latter is the same for all cells. The superscript k indicates the physical location of the cell within the series connection, i.e., cell k is left of cell $k+1$. The subscript i denotes the position of the cell within the ordered list of cell SOHs, where $C_i^{(m)} \leq C_{i+1}^{(n)}$ (Algorithm 1, line 4). We assume that cells in parallel are electrically indistinguishable while cells in series vary in SOC. The discharge current of a cell $I_\mathrm{C}^{(k)}$ (and hence the SOC

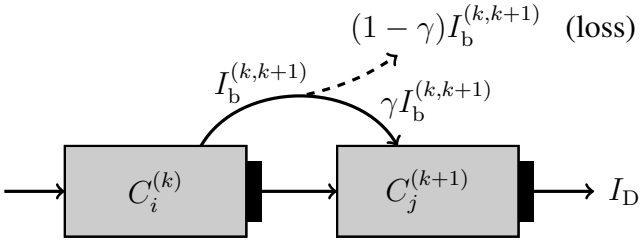

Figure 3.4: The left cell k is aged less than cell $k+1$. This is shown by indices $i > j$. The efficiency of the charge transfer is denoted by γ.

variation of cell k) depends on I_{D} but it is influenced by the balancing current $I_{\mathrm{b}}^{(k,k+1)}$ flowing between two cells k and $k+1$. The efficiency of the transfer is denoted by γ. Figure 3.4 shows a cell k being discharged by $I_{\mathrm{D}}T_{\mathrm{P}} + I_{\mathrm{b}}^{(k,k+1)}T_{\mathrm{P}}$ amount of charge while cell $k+1$ receives only $\gamma I_{\mathrm{b}}^{(k,k+1)}T_{\mathrm{P}}$. The algorithm calculates this under the assumption that the voltage difference among cells is not drastic as we discussed in Section 3.4.2. Accordingly, the current seen by cell k consists of I_{D} along with the current received by or transmitted to neighboring cells:

$$I_{\mathrm{C}}^{(k)} = I_{\mathrm{D}} + \eta^{(k,k-1)} I_{\mathrm{b}}^{(k-1,k)} + \eta^{(k,k+1)} I_{\mathrm{b}}^{(k,k+1)}, \tag{3.5}$$

where $\eta^{(m,n)} \in \{-\gamma, 0, 1\}$ indicates the charge transfer direction and loss. $I_{\mathrm{b}}^{(m,n)} = I_{\mathrm{b}}^{(n,m)}$ is independent of the direction. If $\eta^{(m,n)} = 1$ then m transmits and n receives charge. If $\eta^{(m,n)} = -\gamma$ then m receives and n transmits charge.

3.5.2 Charge transfer direction

The charge transfers between cells happen concurrently. However, a cell can only transfer charge to one neighboring cell at one time, not to both:

$$\eta^{(k,k-1)} \neq 0 \Rightarrow \eta^{(k,k+1)} = 0 \tag{3.6}$$

$$\eta^{(k,k+1)} \neq 0 \Rightarrow \eta^{(k-1,k)} = 0. \tag{3.7}$$

As aging is a very slow process, the SOH values are updated at a low rate, and transfer directions $\eta^{(k,k-1)}$ and $\eta^{(k,k+1)}$ are not adjusted during a trip but only at the beginning. The algorithm iterates through the cells sorted according to their $C_i^{(k)}$, denoted by subscript i (*health list*) (Algorithm 1, line 5). It marks the healthier neighbor as charge provider unless this neighbor is already grouped with another cell (Algorithm 1, line 6).

We illustrate the rules for cell groupings in the ***example*** in Figure 3.5. The formal formulation of the rules is given in Table 3.1. Due to space constraints, the special cases of cells $k = 1$ and $k = N_{\mathrm{S}}$ are omitted but can be easily derived.

In Iteration 1), the least healthy cell $C_1^{(3)}$ is grouped with its right neighbor $C_6^{(4)}$ as this is healthier than the left neighbor ($i = 6 > 2 > 1$). Accordingly, $\eta^{(3,4)} = -\gamma$ as the cell $C_1^{(3)}$ receives charge and $\eta^{(4,3)} = 1$ as cell $C_6^{(4)}$ transfers charge. Due to this grouping, cell $C_2^{(2)}$ cannot be grouped with cell $C_1^{(3)}$ and therefore, $\eta^{(3,2)} = 0$ and $\eta^{(2,3)} = 0$. Equally, cell $C_6^{(4)}$ cannot be grouped with cell $C_3^{(5)}$ and thus, $\eta^{(4,5)} = 0$ (Table 3.1, line 4).

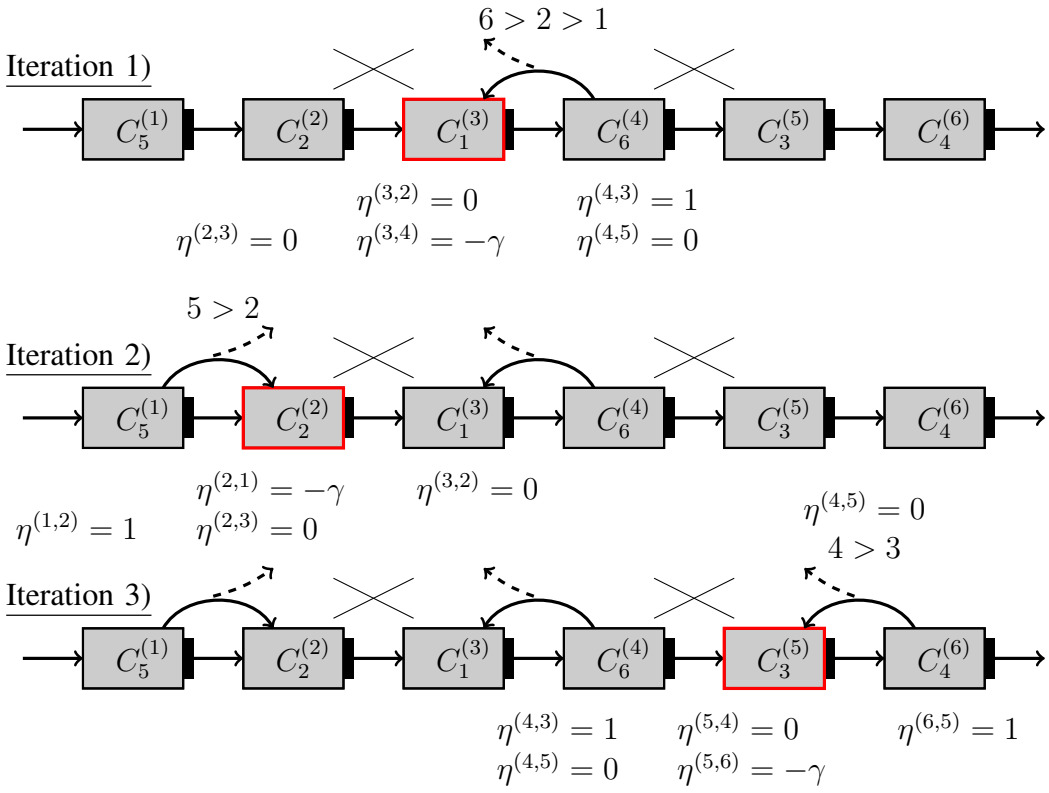

Figure 3.5: Finding the concurrent charge transfers. The grouping of cells is done by iterating through the ordered health list starting with the least healthy cell and grouping it with the healthier neighboring cell.

In Iteration 2), a grouping partner for the second least healthy cell $C_2^{(2)}$ is required and the healthier neighbor $C_5^{(1)}$ is selected (Table 3.1, line 6).

Finally in Iteration 3), the low health of cell $C_3^{(5)}$ should be compensated. The healthier neighbor $C_6^{(4)}$ is already grouped, which is indicated by $\eta^{(4,5)} = 0$. Therefore, the right neighbor $C_4^{(6)}$, which is also healthier than cell $C_3^{(5)}$ is selected and the $\eta^{(m,n)}$ is updated accordingly (Table 3.1, line 1+5).

3.5.3 Balancing currents

Next the balancing currents $I_\mathrm{b}^{(k,k+1)}$ are calculated (Algorithm 1, line 9). In general, the non-zero balancing currents should be set to the maximum balancing current allowed by the architecture, i.e., $I_\mathrm{B,max}$, to relieve the less healthy cell most as explained in Section 3.3, Observation 3).

$$I_\mathrm{b}^{(\nu)} = I_\mathrm{B,max}. \tag{3.8}$$

The variable ν is used as a placeholder for the cell pairs grouped, where

$$\eta^{(k,k-1)} \neq 0 \quad \Rightarrow \quad \nu = (k-1, k) \quad \text{and} \tag{3.9}$$

$$\eta^{(k,k+1)} \neq 0 \quad \Rightarrow \quad \nu = (k, k+1). \tag{3.10}$$

Table 3.1: Get the $\eta^{(m,n)}$ values depending on the already given η values and the available charge of the two neighbors of cell $C^{(k)}$: $C^{(k+1)}$ and $C^{(k-1)}$. A dash - means that the parameter remains unchanged.

	if	$\boldsymbol{C^{(k+1)}}$	$\boldsymbol{\eta^{(k-1,k-2)}}$/ $\boldsymbol{\eta^{(k-1,k)}}$	$\boldsymbol{\eta^{(k,k-1)}}$/ $\boldsymbol{\eta^{(k,k+1)}}$	$\boldsymbol{\eta^{(k+1,k)}}$/ $\boldsymbol{\eta^{(k+1,k+2)}}$
1:	$\eta^{(k-1,k)} = 0$	-	-/-	0/-	-/-
2:	$\eta^{(k+1,k)} = 0$	-	-/-	-/0	-/-
3:	$\eta^{(k,k-1)} =$ undef. $\eta^{(k,k+1)} =$ undef.	$> C^{(k-1)}$	-/0	0/$-\gamma$	1/0
4:	$\eta^{(k,k-1)} =$ undef. $\eta^{(k,k+1)} =$ undef.	$\leq C^{(k-1)}$	0/1	$-\gamma$/0	-/-
5:	$\eta^{(k,k-1)} = 0$ $\eta^{(k,k+1)} =$ undef.		-/-	-/$-\gamma$	1/-
6:	$\eta^{(k,k-1)} = 0$ $\eta^{(k,k+1)} =$ undef.		-/1	$-\gamma$/-	-/-

If both $\eta^{(k,k-1)} = 0$ and $\eta^{(k,k+1)} = 0$, then the balancing currents $I_{\mathrm{b}}^{(k-1,k)}$ and $I_{\mathrm{b}}^{(k,k+1)}$ are also zero. However, we need to consider two special cases. Firstly, if the current $I_{\mathrm{B,max}}$ applied over T_{P} would prematurely deplete the healthier cell, we need to apply a reduced current.

$$I_{\mathrm{b}}^{(\nu)} = \frac{C_{\mathrm{h}}}{T_{\mathrm{P}}} - I_{\mathrm{D}}. \tag{3.11}$$

Secondly, if the balancing current $I_{\mathrm{B,max}}$ is high and the discharge current I_{D} is small enough, the less healthy cell could rest and

$$I_{\mathrm{b}}^{(\nu)} = \frac{1}{\gamma} I_{\mathrm{D}}. \tag{3.12}$$

The decision criteria are depicted in Table 3.2. It takes into consideration the capacity of the healthier cell C_{h} and the less healthy cell C_{l}. Assuming that the $I_{\mathrm{b}}^{(\nu)}$ are calculated while iterating through the health list (i subscripts) (Algorithm 1, line 8), the following conditions apply:

$$\eta^{(k,k-1)} = -\gamma \quad \Rightarrow \quad C_{\mathrm{h}} = C^{(k-1)} \tag{3.13}$$

$$\eta^{(k,k+1)} = -\gamma \quad \Rightarrow \quad C_{\mathrm{h}} = C^{(k+1)} \tag{3.14}$$

$$C_{\mathrm{l}} = C^{(k)} \tag{3.15}$$

The case of $\eta^{(m,n)} = 1$ is similar.

3.6 Simulation results

We compare the SOH-aware cell balancing algorithm proposed in Section 3.5 with an active SOC balancing scheme and passive cell balancing. The active SOC balancing scheme equalizes

Table 3.2: The balancing current $I_{\mathrm{b}}^{(\nu)}$ depends on the available charge in the two neighboring cells.

	$I_{\mathrm{B,max}}$ relation	Charge Level Check $C_{\mathrm{h}}/T_{\mathrm{P}}$	Charge Level Check $C_{\mathrm{l}}/T_{\mathrm{P}}$	$I_{\mathrm{b}}^{(\nu)}$
1:	$I_{\mathrm{D}} > I_{\mathrm{B,max}}$	$> I_{\mathrm{D}} + I_{\mathrm{B,max}}$	$> I_D - \gamma I_{\mathrm{B,max}}$	Eq. 3.8
2:	$I_{\mathrm{D}} > I_{\mathrm{B,max}}$	$< I_{\mathrm{D}} + I_{\mathrm{B,max}}$	$> I_{\mathrm{D}} - \gamma \left(\frac{C_{\mathrm{h}}}{T_{\mathrm{P}}} - I_{\mathrm{D}} \right)$	Eq. 3.11
3:	$I_{\mathrm{D}} < I_{\mathrm{B,max}}$	$> I_{\mathrm{D}} \left(1 + \frac{1}{\gamma} \right)$		Eq. 3.12
4:	$I_{\mathrm{D}} < I_{\mathrm{B,max}}$	$< I_{\mathrm{D}} \left(1 + \frac{1}{\gamma} \right)$	$> I_{\mathrm{D}} - \gamma \left(\frac{C_{\mathrm{h}}}{T_{\mathrm{P}}} - I_{\mathrm{D}} \right)$	Eq. 3.11

only the SOC of all cells making use of the same cell balancing architecture for fair comparison [86]. We transfer charge between neighboring cells which have the larger SOC difference. But instead of applying the maximum $I_{\mathrm{B,max}}$, we equalize the SOC as much as possible. If that equalization should not be possible in T_{P} then Equation 3.11 and 3.12 are applied. We believe this baseline is reasonable enough, given the fact that most of the real-world battery packs utilize passive cell balancing, and active cell balancing is still a field of active research.

In passive cell balancing, no balancing happens during discharge. But when charging, all cells are charged to full SOC. Cells that reach full charge earlier are discharged by resistors. This scheme has the advantage that the architecture is simple and cheap. However, its energy efficiency is low as the excess charge is dissipated as heat. Furthermore, the usable capacity of the pack is smaller and requires that there are no outliers in cell parameters for acceptable system efficiency. However, SOH optimization cannot be performed with passive balancing.

We simulate a battery pack with an architecture similar to the one of the Nissan Leaf $24\,\mathrm{kW\,h}$ battery pack which features 96 cells in series and 2 in parallel (96s2p) enhanced with the active cell balancing architecture from Section 3.3. We simulate the battery pack in MATLAB. Our model includes the aging model from Section 3.4.1. The cells connected in series vary in SOH and aging-speed. We assume the cells' initial SOHs to be uniformly distributed in the interval $[0.9, 1]$ and an aging-speed range of $[54.352, 55.264]$ ppmc. This is a resemblance of the temperature inhomogeneity in a pack and the cells' manufacturing variations. If not mentioned otherwise, we assume a maximum balancing current $I_{\mathrm{B,max}}$ of $5\,\mathrm{A}$. We assume the period T_{P} to be $3600\,\mathrm{s}$. The simulation runtime of one charge-/discharge cycle is approximately $0.06\,\mathrm{s}$.

In the following, we investigate the dependency of our heuristics on (i) the balancing current, (ii) the aging-speed range, and (iii) the initial aging distribution. For the first two tests, we initialize the cells with a fixed initial age distribution. The EOL is reached when the SOH of the least healthy cell reaches 0.7. We compare three different user profiles: light, medium, and heavy. All three users repeat a pattern similar to the one shown in Figure 3.1. For all three users, the repeated pack SOC pattern starts from $S_{\mathrm{high}} = [1; 1; 1; 1; 1; 1; 1]$ and discharges to $S_{\mathrm{low}} = [S_2; S_2; S_2; S_2; S_2; 0.3; 0.3]$ with S_2 being 0.8, 0.6 and 0.3 for light, medium and heavy user, respectively. As the capacity fades, S_{low} is adjusted.

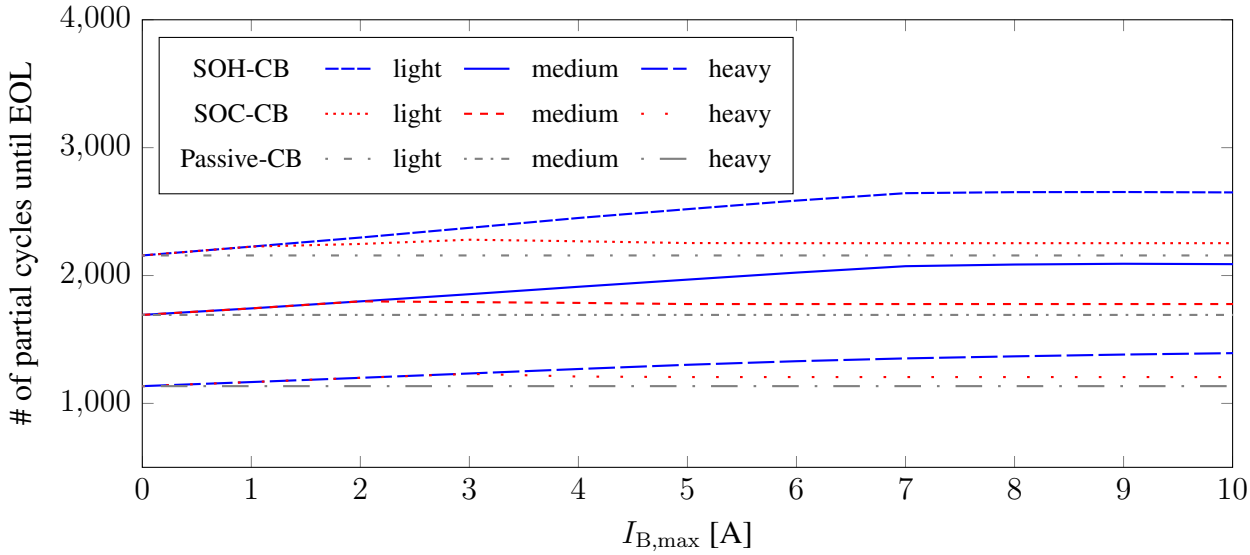

Figure 3.6: Comparison of balancing schemes with varying balancing current $I_{\mathrm{B,max}}$. The aging-speed is 54.674 ppmc.

3.6.1 Dependency on balancing current

The gain of the balancing schemes strongly depends on the balancing current. For the given initial SOH distribution, Figure 3.6 shows that for low balancing currents, the SOH-aware cell balancing performs very similar to SOC cell balancing. For balancing currents $I_{\mathrm{B,max}}$ greater than 1 A, 2 A, or 3 A the SOH-aware cell balancing clearly outperforms conventional SOC balancing. This is the case for all three user profiles, the heavy, medium, or light user profile. For approximately $I_{\mathrm{B,max}}$ =7 A, the SOH-aware scheme stabilizes at a gain of up to 23.5 % over the passive cell balancing. The gain is similar for all profiles. The results clearly suggest that the balancing architecture is an important design decision. Investing in a stronger balancing infrastructure can be rewarded by the increased cycle life of the battery pack. The main difference between user profiles is the total number of cycles until EOL, where, as expected, the battery pack of the heavy user ages much faster compared to the pack of the light user.

3.6.2 Dependency on aging-speed

Next, we investigate the impact of aging-speed variations induced by temperature inhomogeneities by increasing the interval from zero variation (all cells have an identical aging-speed) to a doubling of the aging-speed (the least healthy cell ages twice as fast as the slowest aging cell). The x-axis in Figure 3.7 shows the maximum aging-speed among a pack, normalized to a minimum aging-speed of $v_{\mathrm{a,min}} = 54.352$ ppmc. For example, a variation of 1.6 denotes a normalized aging speed distribution from 1 to 1.6. The balancing current equals 5 A. As expected, the number of cycles decreases with increasing aging-speed. Additionally, the gap between SOH-aware and passive cell balancing is almost constant at a gain of up to 14.7 %,

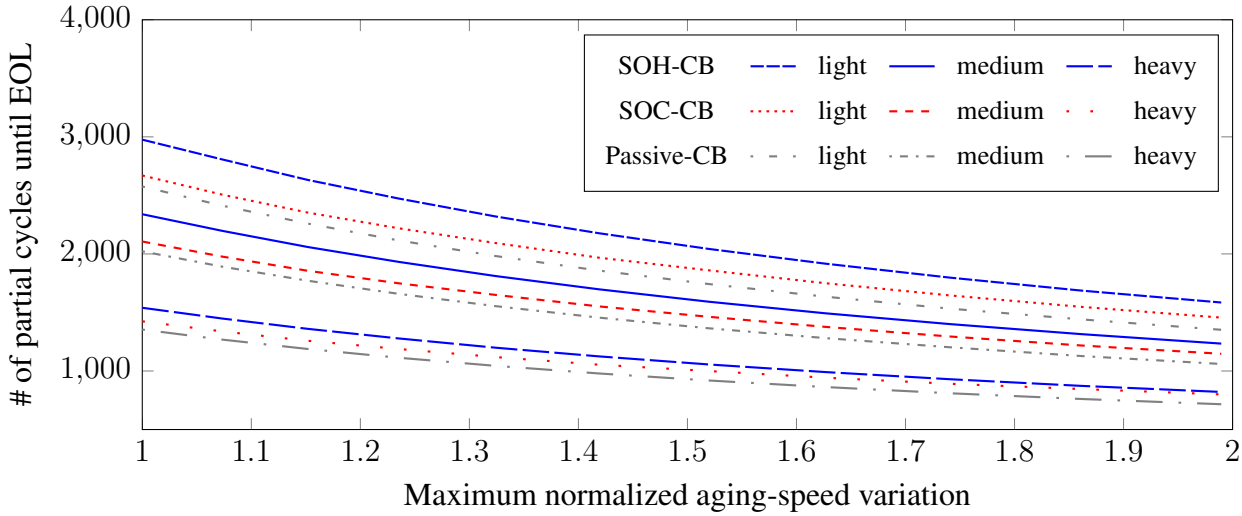

Figure 3.7: Comparison of balancing schemes with varying normalized aging-speed, where 1 means that all cells age at the same speed.

16.4 %, 17.2 % for heavy, medium, and light users, respectively. The gain of SOC balancing over passive cell balancing reaches up to 11.7 %, 8.2 %, 7.7 % for heavy, medium and light user, respectively.

3.6.3 Dependency on initial aging distribution

As we investigate the *neighbor-only* balancing techniques, the initial SOH distribution strongly influences the cycle life of the pack. In the following, we fix the balancing current to 5 A, which is a typical current achieved by state-of-the-art architectures, and the aging-speed v_{a} to 54.674 ppmc, randomly generate 20 uniform SOH distributions and calculate the mean cycle life. The performance in terms of cycle life of the proposed algorithm as well as passive and SOC balancing strongly depends on the initial distribution of differently aged cells within a pack. On average, the SOH-aware cell balancing outperforms the passive cell balancing by approximately 12.5 % for the heavy user, 13.3 % for both the medium and light user while the SOC balancing yields gains of approximately 4.4 %, 3.8 %, 3.4 % over passive cell balancing on average for heavy, medium and light user, respectively (Figure 3.8). The results suggest that the arrangement of cells varying in SOH and aging-speed within a pack is an important criterion to be considered.

3.7 Concluding remarks

Cell balancing architectures in large battery packs equalize SOC differences between cells stemming from manufacturing variances and temperature distribution within the pack to increase the usable capacity within a single cycle. We show that conventional active SOC balancing algo-

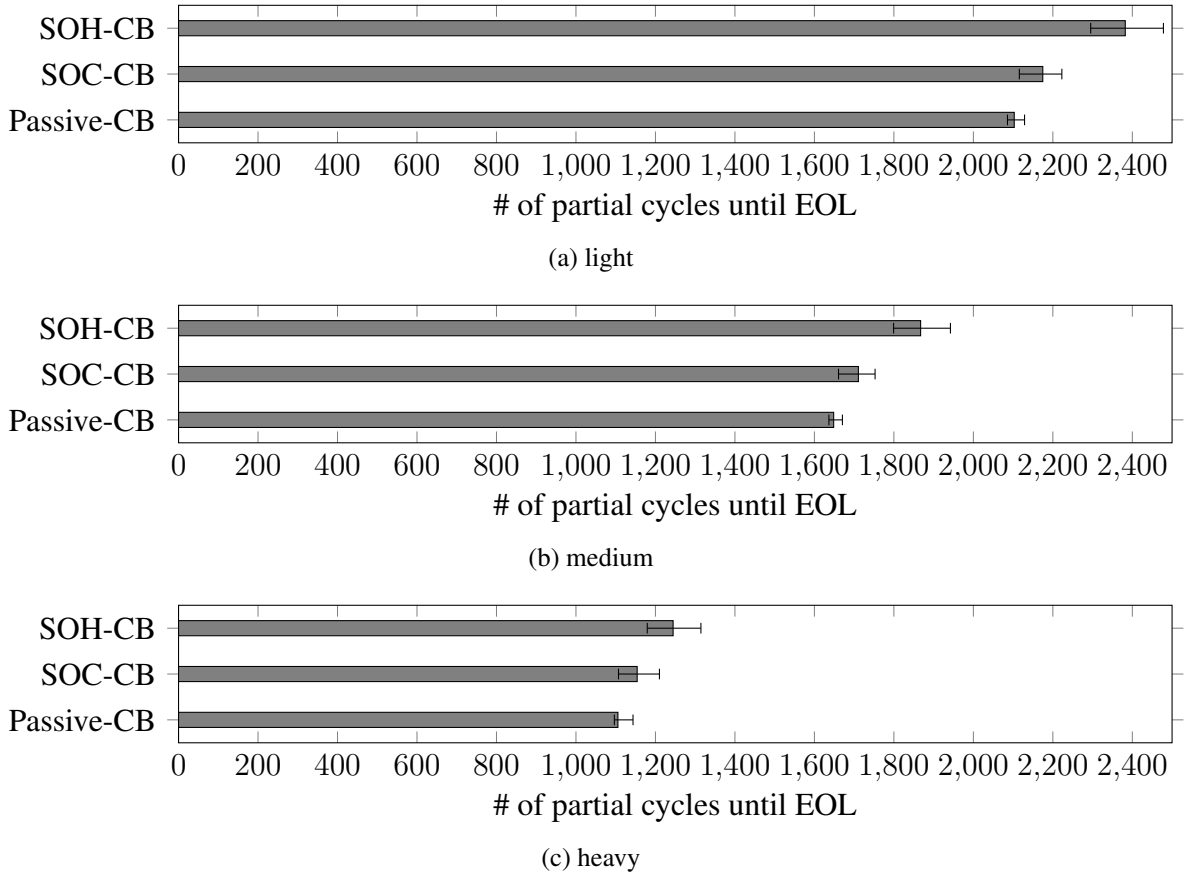

(a) light

(b) medium

(c) heavy

Figure 3.8: Mean number of cycles until EOL for 20 random initial distributions of aged cells for light, medium, and heavy users, respectively.

rithms do not make use of the full potential of the balancing architecture in terms of increasing cycle life. We propose a novel SOH-aware balancing scheme that increases the cycle life of the battery pack by up to $23\,\%$ by reducing the load current on cells with lower SOH. Considering the high prices for battery packs this leads to a massive benefit.

At the time of writing, no clear distinction of the impact of the cooling system and manufacturing inhomogeneities on SOH degradation can be made. Therefore, once advances have been made it would be interesting to refine the modeling. Moreover, in addition to balancing currents, the cooling flow could be optimized to further mitigate the aging of individual cells. Furthermore, the monetary cost aspects need to be discussed. Balancing architectures that allow higher maximum balancing currents are more expensive. A trade-off with the cooling capability of the thermal system needs to be discussed.

Next, the algorithm could be extended to non-neighbor architectures. Non-neighbor architectures allow charge transfers to non-neighboring cells with higher efficiency compared to multi-hop charge transfers. An optimization problem needs to be formulated that maximizes the pack SOH while complying with concurrency constraints.

Another interesting implication that can be made is the correlation between aging speed and pack quality. The current practice is to sort cells and include only cells of similar quality into a

pack. Pack costs can be lowered if cells of different quality are assembled into the same pack. Due to varying aging speeds among cells, the SOH spread of such a mixed quality pack will increase even faster compared to a pack consisting of cells with the same quality. However, with an active cell balancing architecture, a suitable maximum balancing current, and an SOH-aware strategy, these higher initial SOH deviations can be acceptable. The associated costs for sorting cells to only include cells of similar quality in a pack need to be studied. Based on this, a trade-off of sorting costs and cell balancing costs could be formulated.

4

Smart^2: Smart charging for smart phones

In this chapter, we present Smart^2, an advanced smartphone charger that mitigates the capacity fading of the battery, which until now has usually been ignored. Smart^2 exploits the fact that many users charge their phones overnight. Since the overnight charging duration is unnecessarily long, the battery is subjected to a high average SOC, which accelerates battery aging. Therefore, we delay the charging adaptively to be done shortly before the phone is unplugged. With this scheme, when averaged over the duration of the night, the average SOC is lower, and hence aging is reduced. Indicators are a set alarm clock and/or statistics of the previous usage. Similarly, we lower the maximum target SOC. To enable this, the main challenges are firstly, to find a solution that does not negatively influence the usability and secondly, to quantify the achieved savings in terms of aging mitigation. Towards this, we propose a novel charging scheme which can be implemented in the smartphone's firmware. Furthermore, we propose a modified battery charging device that can be used with almost all existing smartphone models. Using our proposed techniques, the average battery cycle life can be nearly doubled from 3.7 to 6.6 years.

Chapter outline: Chapter 4 is organized as follows. In Section 4.1, we outline typical smartphone usage scenarios to motivate this work and then summarize the contributions made in this chapter. In Section 4.2, we present related work including previously known aging aware charging systems. Next, in Section 4.3, we present our proposed system and describe multiple implementation possibilities. Then, in Section 4.4, we give details on the three predictors. To demonstrate the smart charger's effectiveness, we evaluate its impact on the battery aging in Section 4.5. After having presented the smart charger user study, we discuss the topic of intelligent chargers for mobile devices on a broader scale in Section 4.6 and point out open issues to be addressed in the future. Finally, we conclude this chapter in Section 4.7.

The following text and figures in Sections 4.1 to 4.5 and partly Section 4.7 are quoted mostly verbatim from [121]. Small adjustments have been made to ensure good readability and layout of the full thesis.

4.1 Introduction

One of the most important limitations of smartphones is their battery runtime. Even though batteries have evolved during the last years and despite the high-capacity Li-Ion cells that smartphones are equipped with nowadays, smartphones usually have to be recharged every day. Whereas the available runtime might be sufficient shortly after the purchase of the device, the capacity fading effect reduces the available capacity over time until after 2-3 years only $80\,\%$ of the initial capacity might be available and the battery gets empty before the user usually recharges it.

4.1.1 Motivation

Battery aging usually means power and capacity fading. In this work, we are interested in the latter and use the terms aging and capacity fading interchangeably. Battery aging is influenced by the battery temperature, average SOC, SOC swing, and charge-/discharge current. While the battery's capacity decreases even when not in use, the reduction of remaining available capacity increases whenever the battery is cycled, in other words, when it is charged or discharged.

As a result of capacity fading, either larger batteries are built into the phone that will last for a whole day even when aged or the battery needs to be replaced, which imposes a significant cost. Moreover, there are many phones which have batteries that cannot be replaced by the user. If the battery runtime decreases below an acceptable value, the whole device usually is replaced. In addition to the additional expenses, the high amount of electrical waste is of concern. Considering a decreasing innovation rate on the smartphone's hardware and resulting longer usage time, a fast-aging battery remains the bottleneck in smartphone disposal and resulting environmental issues.

Hence, battery aging needs to be mitigated. We propose a novel aging aware charging scheme that mitigates the capacity fading by reducing the average SOC because a high average SOC is one of the factors that increase capacity fading. Intelligent software components already exist in other device classes such as laptop computers that manage the charging process to increase the cycle life of the battery. For example, the Lenovo Battery Manager [88] allows one to select a maximum SOC. For smartphones, simply reducing the maximum SOC would reduce the battery aging, but in some cases, it would artificially shorten the battery runtime below the acceptable level. However, the detailed personal data available on smartphones, viz., a detailed history of the phone usage and recharging behavior can be exploited to make predictions to optimize the charging procedure towards reducing the battery aging without impairing the usability of the device.

4.1.2 Contributions

In this chapter, we for the first time present a novel context-aware scheme for aging aware battery charging that achieves the reduction of the average SOC and hence contributes to the mitigation of the battery's capacity fading. This is done by shifting the start of the charging process in time and by lowering the maximum SOC. Since smartphones are usually charged during the night, batteries usually reach $100\,\%$ of their maximum SOC a long time before their

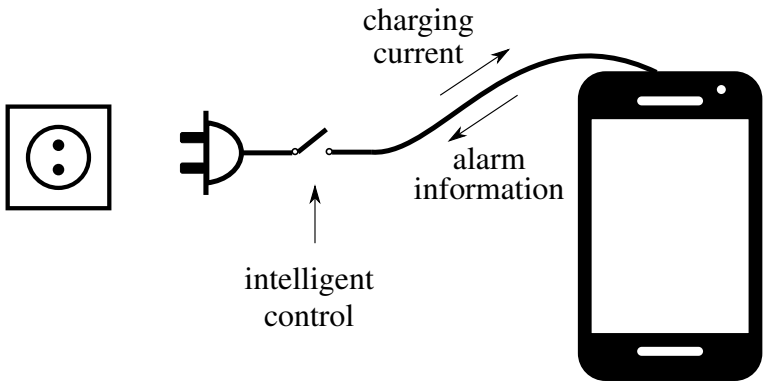

Figure 4.1: Intelligent smartphone charger. Charging is adapted to the use pattern to reduce battery degradation.

chargers are unplugged. During this time, the SOC remains at its maximum level thereby accelerating battery aging. By shifting the charging process to be done shortly before the phone is unplugged, the phone remains at a much lower SOC for most hours of the night. The average SOC is lower without harming the user experience. To address an unexpected need for phone energy overnight, we propose a two-stage charging process. When the charger is plugged-in, the battery is charged to a lower SOC first (e.g., $50\,\%$) and the remaining charge is provided in a second charging process that finishes shortly before the phone is unplugged from the charger. The unplugging time is estimated based on the alarm clock a user has configured in his/her mobile phone (see Figure 4.1) as well as statistical usage data. Besides, the charge which is consumed during the day is predicted to allow for an adaptive reduction of the maximum SOC while still providing enough charge to keep the phone operative during the whole day. Combining both, shifting the charging in time and lowering the maximum target SOC, the battery cycle life can be almost doubled from 3.7 to 6.6 years, as shown in Section 4.5.

Using our scheme allows for building batteries with smaller capacity into phones that due to less aging, will be usable for a longer time. Another advantage of these batteries is their smaller size and lower weight. Furthermore, the amount of electronic waste can be reduced.

In this work, we make the following contributions:

- We present a novel context-aware charging scheme that uses a combination of shifting the charging process in time and adaptively lowering the maximum charging SOC according to the required amount of charge needed per day. Hereby, the average SOC is reduced, which results in the mitigation of the battery's capacity fading.

- Towards this, we compare three predictors that exploit the available usage data and the regularity of usage patterns on smartphones to adaptively adjust the charging process. We compare an SMA, an EMA, and a probabilistic predictor.

- We describe two different implementations of this system. One has been realized as a pure software solution running as an application on an Android smartphone, the other

one is an external charger that works independently of the specific charger chip of the smartphone for all Android devices.

- We evaluate our proposed scheme using real-world measurements combined with a battery aging simulation model and estimate the impact of our system on the battery aging.

- Finally, we conduct a user study to support our assumptions on usage patterns and test the usability of our smart charger.

4.2 Related work and background

In this section, we present previous work on battery aging and derived models that are used to evaluate the aging mitigation of our approach. Also, we summarize other aging aware applications for laptops and smartphones. Finally, we give an overview of works that analyze and predict battery usage patterns of smartphone users.

4.2.1 Battery aging in smartphones

As described in Section 2.1.1, battery aging of Li-Ion batteries means either loss of power capability due to the increase of the internal resistance, or capacity fading. Our work aims at the mitigation of the latter.

Measurements on cycle aging of a $900\,\mathrm{mA\,h}$ LCO battery at $25\,^{\circ}\mathrm{C}$, which are presented in [28], show that a lower upper charging voltage limit, lower charging and discharging rates, and also shorter durations of top-up charging decrease the capacity fading. This part of the charging protocol compensates for the self-discharge of a fully charged battery and maintains a full charge level as long as the battery is still connected to the charger. The cell voltage limit corresponds to the battery SOC limits, where a lower voltage or a lower maximum SOC is preferable [91, 141]. In this chapter, we aim at several of these factors that can be targeted during the charging period to reduce battery aging. The proposed smart charger not only delays charging to reduce idle times at a high SOC but also stops charging at a lower maximum SOC where applicable.

In this work, an aging model is used for quantifying the amount of battery degradation with and without our proposed scheme. We select the Millner aging model [104], which uses average SOC, SOC deviation, and temperature as inputs and simulates the capacity fading over time. The model is summarized in Section 2.2.3. The parameter fitting in this model is done for an LFP cell, while the typical cell chemistry used in portable devices is LCO. Most available and already fitted battery aging models do use other cell chemistries than LCO and instead take data of batteries developed for use in EVs that are optimized for high power and slower aging. According to [127], the cycle life of LFP cells is more than two times higher than the one of LCO. Therefore, our results on battery aging presented in Section 4.5 can be seen as an upper bound, while the real cycle life is likely to be even shorter and hence the beneficial impact of our proposed charging technique is expected to be even higher. Also, from a consumer perspective, building batteries with improved degradation profiles into portable devices would be desirable.

A sign that battery aging awareness also is of concern to manufacturers is a patent filed by *Apple Inc.* that describes a tracking procedure for capacity fading in portable devices [101].

4.2.2 Battery management applications

From the studies and models described above, it is clear that lowering the maximum SOC would help to reduce the battery aging. For notebook computers, programs already exist that stop the charging after a predefined maximum SOC has been reached. This maximum SOC can be chosen manually by the user. Examples for such notebook applications are the Lenovo Power Manager [88] and the Samsung Battery Life Extender [129], which work only on notebooks of the respective manufacturers. Hence for laptops as well as smartphones, the battery control possibilities also depend on the specific device. Our application uses the concept of limiting the maximum SOC and expands it by adaptively doing so as well as by adaptively setting the start time of the charging process based on the usage pattern. Both concepts reduce the overall average SOC. Lowering the target SOC avoids the disadvantageous, high voltages while delaying the charging process only reduces the time spent at the high voltages. The typically more distinct regularity of smartphone usage patterns compared to the ones of laptops facilitates an adaptive implementation on smartphones.

In the case of smartphones, the application *Battery Doctor* [23] claims to prolong battery life by a three-stage charging method. As the source code of this application is not publicly available, it is unclear whether the application's developers control the charging current, which however seems unlikely as Android does not provide access to charging control functionalities on unrooted devices. It seems that the application mainly encourages the user to develop a battery-friendly charging behavior by notifying the user on, e.g., when to unplug the phone.

4.2.3 Smartphone usage predictors

As already mentioned, we suggest adaptively delaying the point in time when the SOC is charged to its target value to lower the average SOC. Hence, we need to estimate the unplug time of the phone by either evaluating the alarm clock time or predicting the unplug time, based on statistics of the previous user behavior to adjust the starting time of the charging process. The assumption that most people charge their phones overnight has been confirmed by [112] and [45]. Users that mainly charge overnight have a longer average plug duration than users that also charge during the day, which means that keeping one's phone plugged overnight [112] leads to an unnecessary high average SOC. In [45] it is shown that in 77 % of the cases the smartphone is plugged-in for longer than 30 min after the full charge level has been reached. Therefore, the charging start time can be delayed to decrease the average SOC.

Besides, predicting the SOC drain between two charging sessions helps to adjust the cut-off SOC (or voltage) when charging. Often different power sources, such as USB and AC, go along with different plug durations. The usage frequency of these different sources varies among users [74]. Also, the start of charge and end of charge level depends on patterns determined by the individual use [74]. According to [45], the average lowest SOC level before recharging determined among multiple users is at 30 %. Accordingly, a great number of users

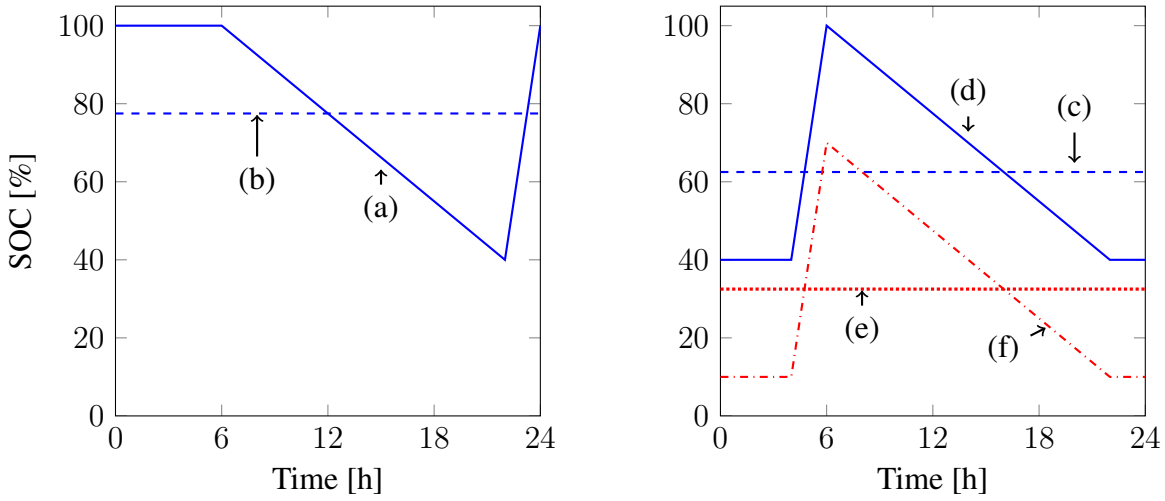

Figure 4.2: Comparison of charging schedules with and without smart charging. Curve (a) is the conventional charging scheme, curve (d) shifts the charging in time, and curve (f) additionally has a lower maximum target SOC. Curves (b), (c), and (e) are the respective average SOCs.

could discharge their phones to a lower SOC while still having enough energy left in their batteries before the next recharge.

Several predictors of future battery levels have been presented in the literature [74, 112]. We need to estimate times of unplugging events and energy consumption until the next plug event. This requires similar methods as the ones on predicting the battery level that are presented in the literature.

4.3 Aging-aware charging

In the following, we explain our aging aware charging concept and discuss challenges and design options when realizing our approach on different target platforms.

4.3.1 Aging mitigation by delayed charging

As stated before, one of the factors that increase the battery aging is a high average SOC. By lowering the average SOC of a smartphone battery, its degradation can be decreased. This is done by shifting the start of the charging process in time and by adaptively reducing the maximum SOC. Figure 4.2 illustrates this charging scheme. The left graph shows a typical profile (a), where the SOC stays at $100\,\%$ overnight with an average SOC of $77.5\,\%$ (b). In the right graph, our proposed optimizations are applied. The average SOC is lowered to $62.5\,\%$ (c) by delaying the charging process to be done in the morning (d). In the lower graph on the right, the average SOC is further reduced to $32.5\,\%$ (e) by lowering the charging target SOC (f).

The delay of the charging process is either set manually by the user, gathered automatically by reading the alarm clock, or predicted from the user's statistical usage pattern. Similarly, the target SOC can be either selected by the user or can be learned by the system based on

the average daily usage including a safety margin. As a wrong assumption on the unplug time causes great inconvenience for the user, i.e., the battery is still uncharged when unplugged, we suggest to immediately charge to a medium SOC and delay the charging only after this medium SOC has been reached (see Section 4.3.4), which however results in a less efficient aging mitigation.

An obvious objection towards this scheme is that charging overnight with a reduced charging current might also have an improving effect on battery degradation. Hence the question arises which of the two schemes should be used. First of all, no definitive answer can be provided as this question needs further investigation in future work. There already exists a patent [100] for charge rate reduction which argues that a reduced charging current has a positive impact on the battery lifespan in terms of reducing the capacity fading. Unfortunately, no measurement or simulation results are provided. However, one has to keep in mind that the charging of the smartphone is likely to have an impact on the temperature of the smartphone, which has a strong effect on battery aging. Therefore it cannot be said without further discussion, whether a reduced charging current has a better effect than a delayed one. We revisit this question in Section 4.6 where we discuss advances made in the meantime.

In the following, we describe two realization options of the proposed system: A software implementation in terms of a smartphone application and a dedicated charging device. We then introduce an algorithm that relies either on values manually entered by the user or uses the alarm clock and predictors to calculate delay and target SOC.

4.3.2 Smart charger Android application

The above-described solution can be implemented either directly on the smartphone or an external charging device. To later understand the drawbacks of the direct implementation, we first need to explain the dependencies of the Android OS and the smartphone hardware with its respective drivers.

Figure 4.3 shows the abstraction layers of the hardware and the software. On the hardware layer, three main components are involved in charging the smartphone battery. The power Integrated Circuit (IC) manages power sources and the power distribution to the system. Among other tasks, it is responsible for voltage regulation, voltage scaling, power source selection, and charging functions. The charger controls the charging process of the battery and one of its tasks is to ensure a safe charging process. The fuel gauge monitors the battery and provides SOC, SOH, state of connection, capacity, and voltage readings to the system.

On the software level, the application has a registered broadcast receiver for the power connector state. A broadcast receiver receives a notification if a system or application event occurs, i.e., when a charger is connected or disconnected. If the application is notified about a plug event and the desired charging time is in the future, the charging has to be disabled. Hereby, the virtual file system *sysfs* is used to exchange information between the power management chip and the user space, i.e., writing to the corresponding *sysfs* file can enable or disable the charging process.

Due to different power-ICs with different drivers, not all smartphone models provide the same charging control functionalities. At the time of writing, the *sysfs* charging control varies.

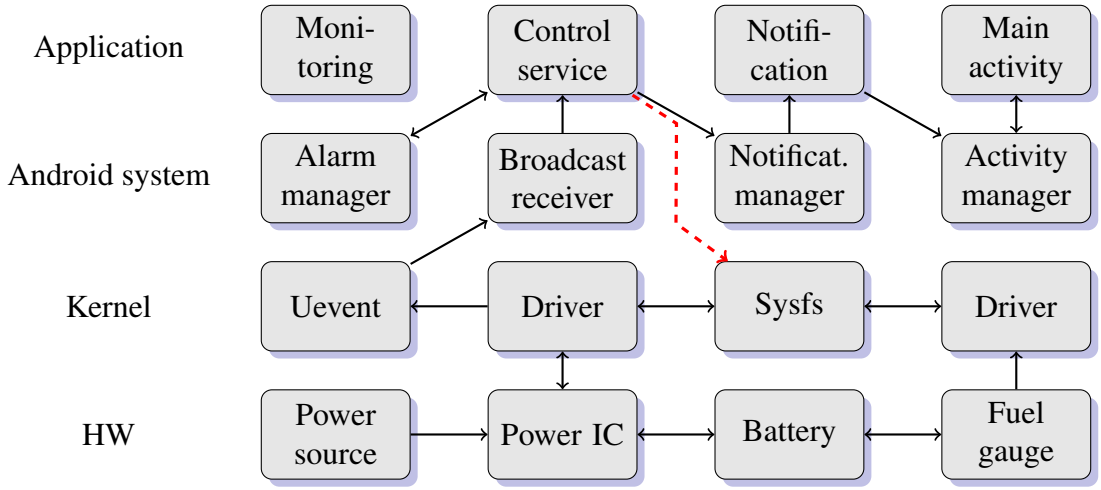

Figure 4.3: System abstraction layers in Android

For example, for the Nexus 4 phone, a switch variable enables or disables charging, whereas, in the Nexus 5 phone, a parameter is provided to reduce the charging current.

As the *sysfs* is located in the kernel space and no standardized Application Programming Interface (API) is provided by the Android system, it is currently not possible to write a universal application that works for all Android smartphones. When writing an application for a specific smartphone, root access is required to access the *sysfs* interface. However, a solution that can be used for almost all current smartphones is to implement our smart charging scheme into the charger device. Such smart charger hardware is described next.

4.3.3 Smart charger hardware

As explained above, no standardized implementation from the smart charger as a pure Android application is currently possible. Therefore, we develop a second solution that is based on hardware and hence works independently of the smartphone model. The attractiveness of this hardware solution arises from its independence of the smartphone power IC and a less profound intervention in the OS. A switch is inserted in the supply lines of the USB cable used for charging to interrupt the current supply if needed. The switch is controlled by a microcontroller which also is used as a USB host controller to receive SOC data and the alarm clock information from the smartphone.

4.3.4 Alarm clock based charging delay

The battery health-aware charging algorithm can be implemented either on the external microcontroller or directly on the smartphone. To reduce the average SOC, we adjust two parameters: We adaptively delay the start time of the charging process and we lower the target SOC S_{tar}. Algorithm 2 determines the reserve amount of charge S_{med}, target SOC S_{tar} and the unplug time t_{up}. These are then used to manage the charging scheme.

Algorithm 2 Smart charging

Require: mode

1: **if** mode == manual **then**
2: S_{med} = GetReserveChargeFromSettings()
3: S_{tar} = GetTargetSocFromSettings()
4: t_{up} = GetUnplugTimeFromSettings()
5: **else**
6: **if** mode == alarm **then**
7: t_{up} = GetUnplugTimeFromAlarmTime()
8: **else**
9: t_{up} = GetUnplugTimeFromPredictor()
10: **end if**
11: S_{med} = SetReserveChargeToConstantValue()
12: S_{tar} = GetTargetSocFromPredictor()
13: **end if**
14: EnableCharging(S_{med})
15: DisableCharging(t_{up} - T_{chg})
16: EnableCharging(S_{tar})

The *mode* variable allows switching between three operation scenarios: *manual*, *alarm*, and *predictor*. If *mode* is set to *manual* the target SOC S_{tar}, reserve amount of charge S_{med} and unplug time t_{up} are set manually by the user in the preferences settings menu. To retrieve this data, we determine three functions:

- `GetReserveChargeFromSettings()`
  Gets the manually set value for the reserve amount of charge S_{med}.
- `GetTargetSocFromSettings()`
  Gets the manually set value for the target SOC S_{tar}.
- `GetUnplugTimeFromSettings()`
  Gets the manually set value for the unplug time t_{up}.

Alternatively, the unplug time is set to either the value of the alarm clock if it is set or else it is predicted based on unplugging statistics as indicated by the *mode* variable being set to *alarm* or *predictor*, respectively.

- `GetUnplugTimeFromAlarmTime()`
  In case the alarm clock is set, the unplug time t_{up} is determined from its set value. We use the alarm clock application that comes pre-installed with Android and is used by most users.
- `GetUnplugTimeFromPredictor()`
  In case no alarm clock is set, a predictor is used to determine the unplug time t_{up}.

The reserve amount of charge and the target SOC are obtained in the same way for both modes *alarm* and *predictor*.

- `GetTargetSocFromPredictor()`
  Another predictor determines the target SOC S_{tar}.

- `SetReserveChargeToConstantValue()`
  The medium SOC S_{med} is set to a predefined, preferably low value.

Once the smartphone is plugged-in, it charges to the medium SOC S_{med} to have a safety margin in case the smartphone is unplugged earlier than expected. After charging to the reserve SOC S_{med}, charging is disabled until the charging time is reached. The charging time is derived from the difference between the determined unplug time and the estimated duration: $(t_{\mathrm{up}} - T_{\mathrm{chg}})$. The charge duration T_{chg} describes the time it takes to charge the phone to the target SOC S_{tar}. For the sake of simplicity of presentation, in our implementation, we set this duration to a constant value because the variation among phones is small. Nevertheless, this duration could also be estimated from previous charging cycles which might be included in future versions. Two functions control the charging:

- `EnableCharging(`S`)`
  This function charges the battery until a certain SOC S value has been reached.

- `DisableCharging(`t`)`
  This function disables the charging until a given time t.

4.4 Plug duration model

Three predictors that model the plug duration have been developed and will be compared in the following: An SMA predictor, an EMA predictor, and a probabilistic predictor.

As discussed in Section 4.2, the best results in lowering the average battery SOC, and hence the battery aging, are expected when delaying the night time charging. Previous studies [112] as well as our sample data in Figures 4.4a and 4.4b show that plug durations tend to be longer when the plug event occurs at night time.

As expected, the charging behavior varies among users, see Figure 4.5. The x-axis shows the charging duration rounded to full hours. The number of events per a certain duration is counted. User 2 has many short charges. Both users have an increased number of samples for charge durations of 8 h to 9 h which is likely to be the charging overnight. Due to the differences among users, adaptive predictors are of advantage.

4.4.1 Simple moving average predictor

If the manual mode is not active, two predictors take action. In case the alarm clock is not available, a first predictor estimates the time the phone will be unplugged from the power source (AC, USB). To further lower the SOC, a second predictor computes a target SOC S_{tar} below 100%. A moving average can be used for a simple implementation. However, more elaborate models exist in literature.

To predict the duration the phone usually remains plugged T_{plg}, we sort the last plug durations $T_{m,n}$ into multiple bins n according to the plug time. We use one bin per hour of the day,

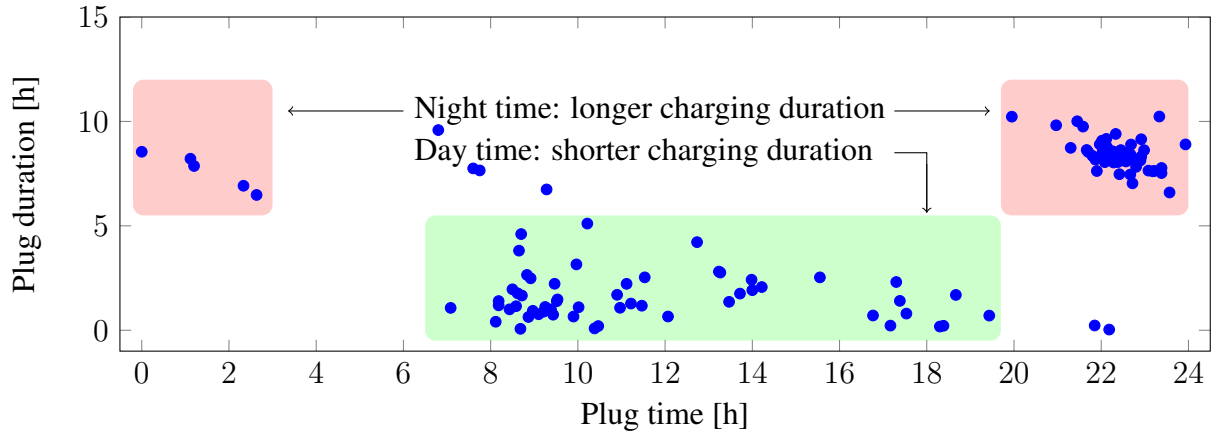

(a) User 1

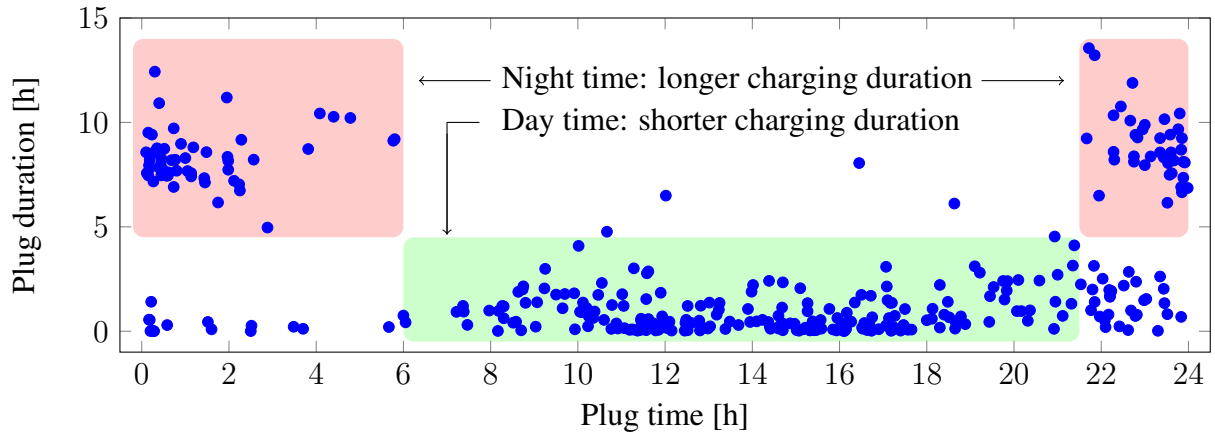

(b) User 2

Figure 4.4: Plug duration vs. plug time for User 1 and 2. If plugged during the day the charging durations tend to be shorter. Longer charging durations occur when plugged at night times.

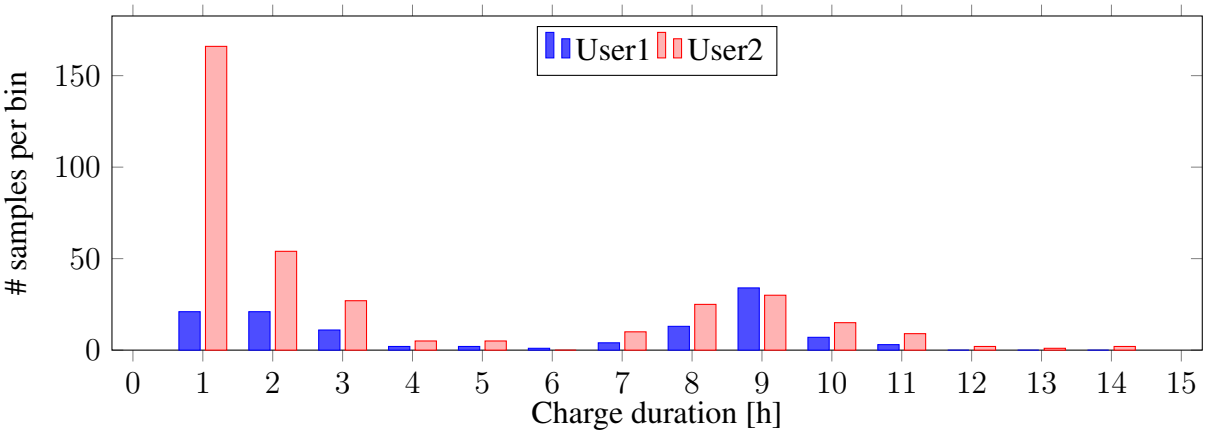

Figure 4.5: Number of charging events for given charge duration

hence the total number of bins is $N_{\text{bins}} = 24$. Once a plug event is detected, the moving average in bin n over the last $N_{\text{PE}} = 5$ events (the number compromises between smoothing over the last numbers and forgetting the past fast enough when the user's behavior changes) is calculated by

$$\overline{T_{\text{plug,n}}} = \frac{1}{N_{\text{PE}}} \sum_{m=N_{\text{E,n}}-(N_{\text{PE}}-1)}^{N_{\text{E,n}}} T_{m,n}, \tag{4.1}$$

where $N_{\text{E,n}}$ is the total number of entries into one specific bin and $T_{m,n}$ is the stored duration in bin n and counter m.

The time when charging should be enabled t_{start} is determined by

$$t_{\text{start}} = t_{\text{now}} + \overline{T_{\text{plg}}} - T_{\text{chg}} - T_{\text{buf}}, \tag{4.2}$$

where T_{chg} is the duration it takes to charge the battery to the target SOC S_{tar} and T_{buf} is an additional safety time to account for possible wrong predictions.

We need a second predictor that determines the target SOC S_{tar} for our evaluation. It uses the same number of bins $n = 0...23$ and calculates the moving average over the last $N_{\text{SOC}} = 5$ events in the respective bin n:

$$\Delta S_n = \frac{1}{N_{\text{SOC}}} \sum_{m=N_{\text{E,n}}-(N_{\text{SOC}}-1)}^{N_{\text{E,n}}} \Delta S_{m,n}, \tag{4.3}$$

where $\Delta S = S(t_{\text{upprev}}) - S(t_{\text{plg}})$ with $S(t_{\text{upprev}})$ being the SOC when the phone was previously unplugged and $S(t_{\text{plg}})$ being the SOC when the phone was plugged. The target SOC S_{tar} is then calculated by

$$S_{\text{tar}} = \Delta S_n + S_{\text{buf}}, \tag{4.4}$$

with S_{buf} being a safety margin to account for longer usage. Also, note that the bin n_{S} is determined by the time the phone was last unplugged t_{upprev} instead of using the plug time t_{plg} as for the plug duration T_{plg}. Algorithm 3 shows the sequence of calculations. If a plug event occurs, first the history of ΔS values is updated in the respective bin (Algorithm 3, line 2).

Next, the unplug time t_{up} and the target SOC S_{tar} are predicted (Algorithm 3, lines 3 and 4) based on the current hour. When the phone is unplugged, the plug duration is stored in the respective bin (Algorithm 3, line 7).

4.4.2 Exponential smoothing

As a comparison, we use exponential smoothing. We simply replace Equation 4.1 and calculate the EMA recursively by the previous plug durations. We start with the plug duration and the counter $m = 1$: $T_{\text{plug,1,1}}$. The estimated plug durations are then:

$$T_{\text{plug},n,1} = T_{1,n}, \quad \text{for } m = 1 \tag{4.5}$$

$$T_{\text{plug},n,m} = \alpha T_{m,n} + (1-\alpha) T_{\text{plug},n,m-1}, \quad \text{for } m > 1, \tag{4.6}$$

where the smoothing factor α is set to 0.2 in our example.

Algorithm 3 Predictor

1: **if** PlugEvent **then**
2: $\mathcal{H}_S \leftarrow$ UpdateSocHistory (ΔS_{now})
3: CalculateUnplugTime($\mathcal{H}_P$)
4: CalculateTargetSoc($\mathcal{H}_S$)
5: **end if**
6: **if** UnplugEvent **then**
7: $\mathcal{H}_P \leftarrow$ UpdatePlugDurationHistory(T_{now})
8: **end if**

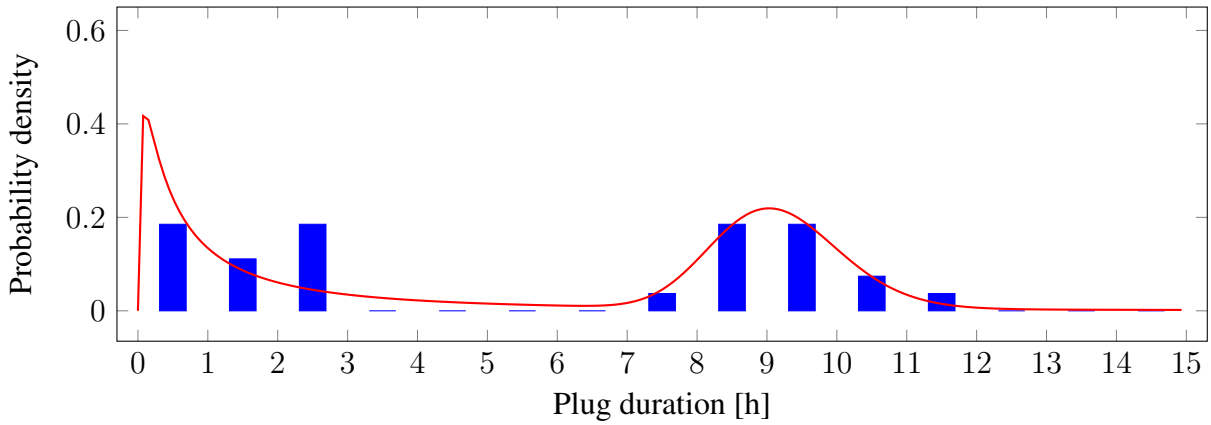

Figure 4.6: Fitting a bimodal log-normal probability density function to the statistical data

4.4.3 Probabilistic predictor

Our third predictor fits the data to log-normal distributions, similar to the one suggested by [36] for stay durations at a given location. Given a certain plug time t_{plg}, we can fit the conditional probability density function $f(T_{\text{plg}}|t_{\text{plg}})$ to the statistical data. We use discrete hourly bins $t_{\text{plg}} = 0...23$. As can be seen from Figure 4.5, the plug duration is either very short or lies in the range of 8 h to 9 h. Furthermore, the duration cannot take negative values. Hence, we model the probability density function of the charging delay as a bimodal log-normal distribution. We fit the data to a mixture of log-normal functions:

$$\begin{aligned} f(T_{\text{plg}}|t_{\text{plg}}) = &\frac{w_{\text{plug}}}{T_{\text{plg}}\xi_1\sqrt{2\pi}} \exp\left(-\frac{(\ln T_{\text{plg}} - \mu_1)^2}{2\xi_1^2}\right) \\ &+ \frac{1 - w_{\text{plug}}}{T_{\text{plg}}\xi_2\sqrt{2\pi}} \exp\left(-\frac{(\ln T_{\text{plg}} - \mu_2)^2}{2\xi_2^2}\right), \end{aligned} \tag{4.7}$$

where T_{plg} is the plug duration, ξ_1 and ξ_2 are the variances of the log-normal functions, μ_1 and μ_2 are the mean values of the two functions and w_{plug} is a weight applied to the two probability density functions. The data is fitted using a maximum likelihood estimator. Figure 4.6 gives an example of a resulting curve compared to the measured data.

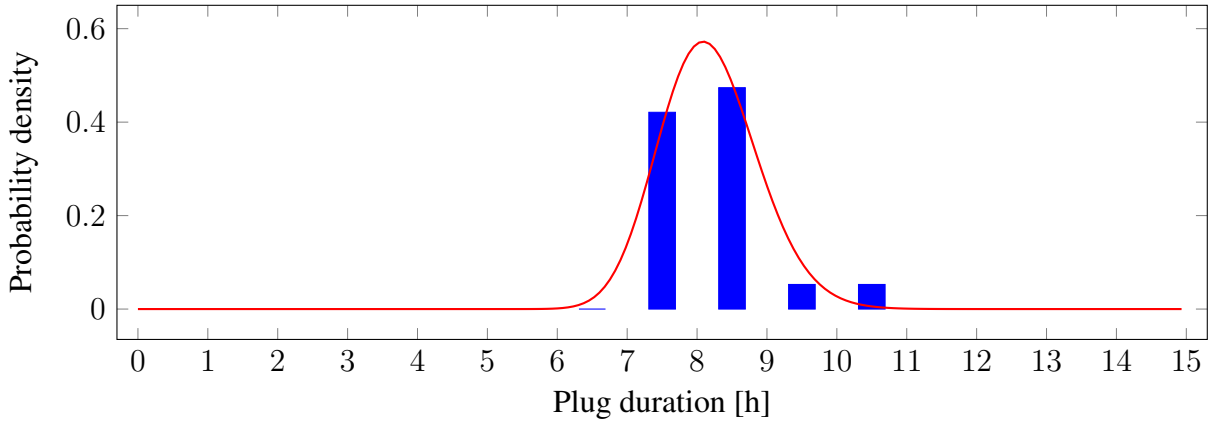

Figure 4.7: Statistical data fitted to a unimodal log-normal function

Apart from the additional information that is provided by the mixture of log-normal distributions, such as variance, expected value, and the respective weights, we can also determine a value that gives us a prediction on the duration.

One drawback of this predictor, which fits the statistical data to a probability density function, is that in case the sample size is very low, fitting is impossible or very inaccurate. Hence, our implementation deals with the following cases. If no samples are available, the delay is set to zero, and charging starts immediately. If there are only one or two data samples, the mean value of theses samples is calculated. In the case of three samples or if the bimodal predictor fails to fit the data and degrades, a unimodal predictor is used:

$$f(T_{\text{plg}}|t_{\text{plg}}) = \frac{1}{T_{\text{plg}}\xi\sqrt{2\pi}} \exp\left(-\frac{(\ln T_{\text{plg}} - \mu)^2}{2\xi^2}\right). \tag{4.8}$$

Figure 4.7 shows data fitted to a unimodal log-normal function. For four samples and more, the bimodal log-normal predictor is used.

4.5 Evaluation

In this section, we show the amount of battery aging that can be mitigated by delaying the charging and lowering the target SOC. We first evaluate our smart charger application, which delays charging based on the alarm clock, in a real user test. We then compare the results of an optimal predictor to the ones achieved by the predictor that determines its decisions on statistical usage patterns.

4.5.1 Smartphone application evaluation

Our first experiment shows how charging is delayed merely based on the alarm clock in a real usage scenario. A user runs our smart charger application on his smartphone for two weeks and the charging is delayed according to his alarm clock settings. As can be seen in Figure 4.8,

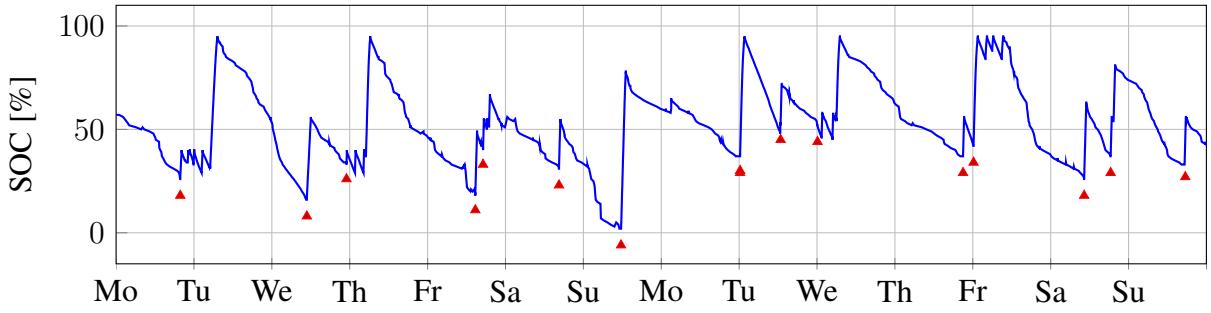

Figure 4.8: Battery profile for a user that runs the smart charger application. Charging is delayed according to a set alarm. The red triangles indicate the plug times.

the target SOC is adjusted according to user preferences on the maximum SOC in the morning and minimum SOC in the evening and a linear interpolation when charged during the day. Therefore, the SOC usually varies between 95 % and 50 %. The estimated cycle life for this usage is 6.6 years. When comparing Tuesday and Thursday in week 1 to Wednesday in week 2, one can see that the minimum SOC was set from 50 % to 40 % during the test period. The profile does not have long periods of being at a high SOC and starts discharging shortly after being unplugged (the only exception is the second Friday when no alarm was set). It can be seen that having reached the target value when charging the smartphone triggers drawing a rather high discharge current, with a gradient that is even higher than the discharge current while in use. We assume that this is due to some background processes remaining active in the assumption that the phone is powered by AC since it is plugged-in even though charging is disabled. Currently, we counteract by frequently recharging to the target value. However, a better solution would be to schedule the background processes differently.

4.5.2 Smart charging with optimal predictor

Next, we would like to quantify the separate as well as joint effects on the aging of shifting the charging process in time and adjusting the target SOC. Towards this, we derive the battery aging for the unmanaged curve and compare it with three scenarios: Delaying the charging, lowering the target SOC and the combination of both. We first calculate the aging for the three scenarios by optimally delaying the charging with an optimal predictor. In Section 4.5.3, we determine the aging for the same three scenarios but instead of optimal adjustments, we simulate the use of a predictor instead. We collect real user data using the Android application Battery Log [67] for a duration of two weeks. The average SOCs per profile vary between 54.4 % and 78.5 %. The accumulated hours spent at 100 % SOC during the recording period are between 16 h and 120 h.

Using these profiles, we simulate a smart charging behavior and determine the corresponding amount of battery aging using the aging model from [104] implemented in MATLAB. The MATLAB model takes the SOC profile and temperature data as an input. The model provides a bound on the cycle life and real aging is likely to be even faster than our numbers suggest as has been explained in Section 4.2. We use an optimal predictor, therefore the battery reaches full

Profiles	**1**	**2**	**3**	**4**	**5**	**6**	**7**	**8**	**9**
Original	2.6	2.5	3.3	4.2	3.7	3.1	5.6	3.3	4.6
Optimal predictor for									
Delay charge time	3.4	3.6	6.0	5.2	4.3	5.1	6.3	3.8	5.2
$S_{\text{tar}} = 90\%$	3.8	3.6	4.8	6.0	5.4	4.6	8.1	4.8	6.7
Delay and S_{tar}	4.8	4.9	7.6	7.2	6.1	6.7	8.9	5.7	7.5
SMA predictor for									
Delay charge time	3.2	3.0	5.2	4.3	4.7	3.8	6.2	4.0	6.0
S_{tar}	3.3	3.4	3.7	6.7	5.8	4.1	7.1	3.7	5.9
Delay and S_{tar}	4.4	4.4	5.8	7.2	6.7	6.4	7.9	4.5	8.3

Table 4.1: Estimated cycle life in years for recorded user data. We use an optimal predictor and SMA prediction of delayed charging, lowered target SOC, and a combination of both.

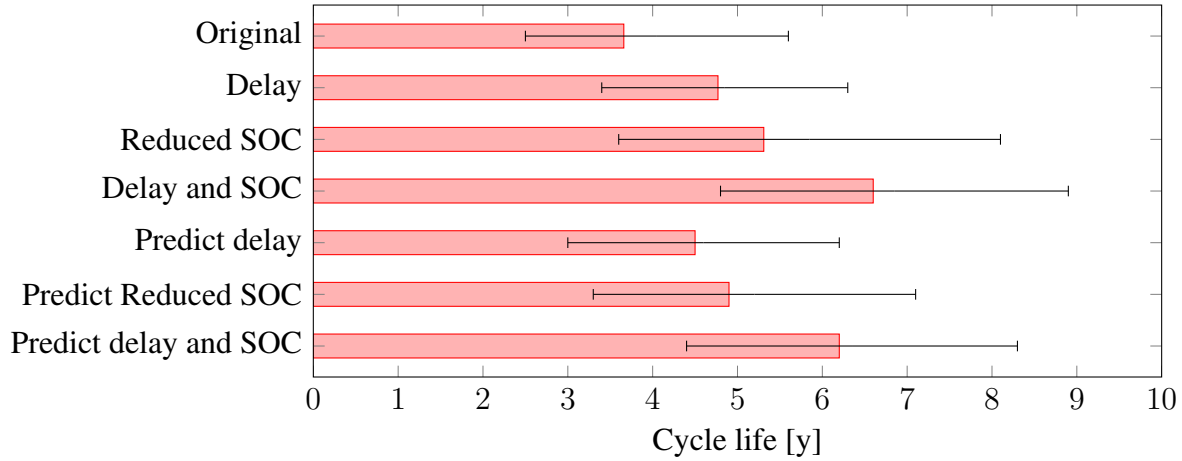

Figure 4.9: Lifetime comparison. Average cycle life estimation over 9 users from Table 4.1 and range from minimum to maximum estimation.

charge precisely at the moment when it is unplugged. To not leave the user with no charge in case he unexpectedly has to unplug the phone earlier, the battery is charged to an SOC of $50\,\%$ immediately when plugged. After that, charging is delayed.

As can be seen in Table 4.1 and Figure 4.9, considering the original unmanaged profile, most batteries last for about three to four years, with some exception that would last up to almost six years for normal charging behavior. If the batteries would be charged smartly, the expected cycle life would have an average above six years. Hence, delaying the charge time increases the cycle life, i.e., the duration until the battery capacity has faded to $80\,\%$ of its initial value, by factor 1.1 (profiles 7 and 9) to 1.8 (profile 3). The average of all profiles is 1.3.

Next, we lower the target SOC to a fixed value of $90\,\%$. The effect on aging mitigation lies within a similar range as delaying the charging start time. The battery cycle life is increased by a factor of 1.5 on average for our examples.

It should be noted that sometimes simulations of lowering the target SOC result in a full drain of the battery before the plug event in the recorded data set. Also lowering the target SOC

potentially effects the user behavior, e.g., the user might decide to plug-in his phone earlier. This kind of psychological effect can of course not be captured in the simulation. Delaying the charging process usually does not result in similarly negative simulation effects.

A combination of both, delay of the charging process and lower target SOC, yields the most benefit. Here, the achieved increase in lifetime has a factor of 1.6 up to 2.2 compared to the battery cycle life without any SOC management. The average is 1.8. Figure 4.10 (a)-(d) shows the recorded and simulated battery profiles for User 4.

4.5.3 Smart charging with predictor

Now the same comparison as in the previous section is done for the SMA predictor that estimates the delay time and the target SOC. The predictor shows good results performing only a little worse than the results of the optimal predictor, see Table 4.1. On average, the improvement factor, which is the predicted cycle life divided by the original cycle life, is decreased by 0.1 for each of the three prediction combinations (predict delay, predict target SOC, joint prediction). For the joint SMA prediction of delayed charging and decreased target SOC, the gain of lifetime over the original cycle life yields factor 1.7, while a factor of 1.8 was achieved with the optimal predictor results.

A problem that occurs when using a predictor is that the battery is sometimes drained down to $0\,\%$ of SOC due to a wrong prediction of the charging delay or wrong prediction of the target SOC and remains at its empty state for some time. This lowers the average SOC and therefore increases the cycle life, however, it is not the desired behavior as the smartphone cannot be used during this time. Such happenings can partly be seen from the data provided in Table 4.1 in case the predicted cycle life for the delay predictor is larger than the simulated cycle life. Making the user recharge during the day is not a desired behavior of the predictor but infrequent occasions may be considered acceptable in terms of battery aging.

Further, it should be noted that the predicted target SOC is not allowed to be below $70\,\%$ and hence lies within the range of $70\,\%$ to $100\,\%$. Therefore in some cases, the target SOC predictor may perform better than the fixed value simulation because the predicted target SOC may be lower than the one fixed at $90\,\%$. In Figure 4.10 (e)-(f), the charge plots for User 4 are shown. To sum up, even the relatively simple SMA predictor helps to reduce aging. However, further means of improvement are the optimized choice of bin size and buffer terms. Also, the SOC predictor should be replaced by more elaborate suggestions from the literature that incorporate further data. Alternatives for the plug duration predictor are discussed in the following.

As explained earlier, a major drawback of the use of the predictor is that in case of the wrong prediction and earlier unplug time, the user will be left with an empty battery. We suggest two measures to deal with this drawback. Firstly, when plugged-in, the phone should immediately charge to a medium SOC to provide a reserve amount of charge in case of an earlier unplug time at the cost of slightly less efficient aging mitigation. Secondly, the predicted unplug time should be displayed in a user interface to provide the user the opportunity to immediately charge the phone or to manually set an earlier unplug time.

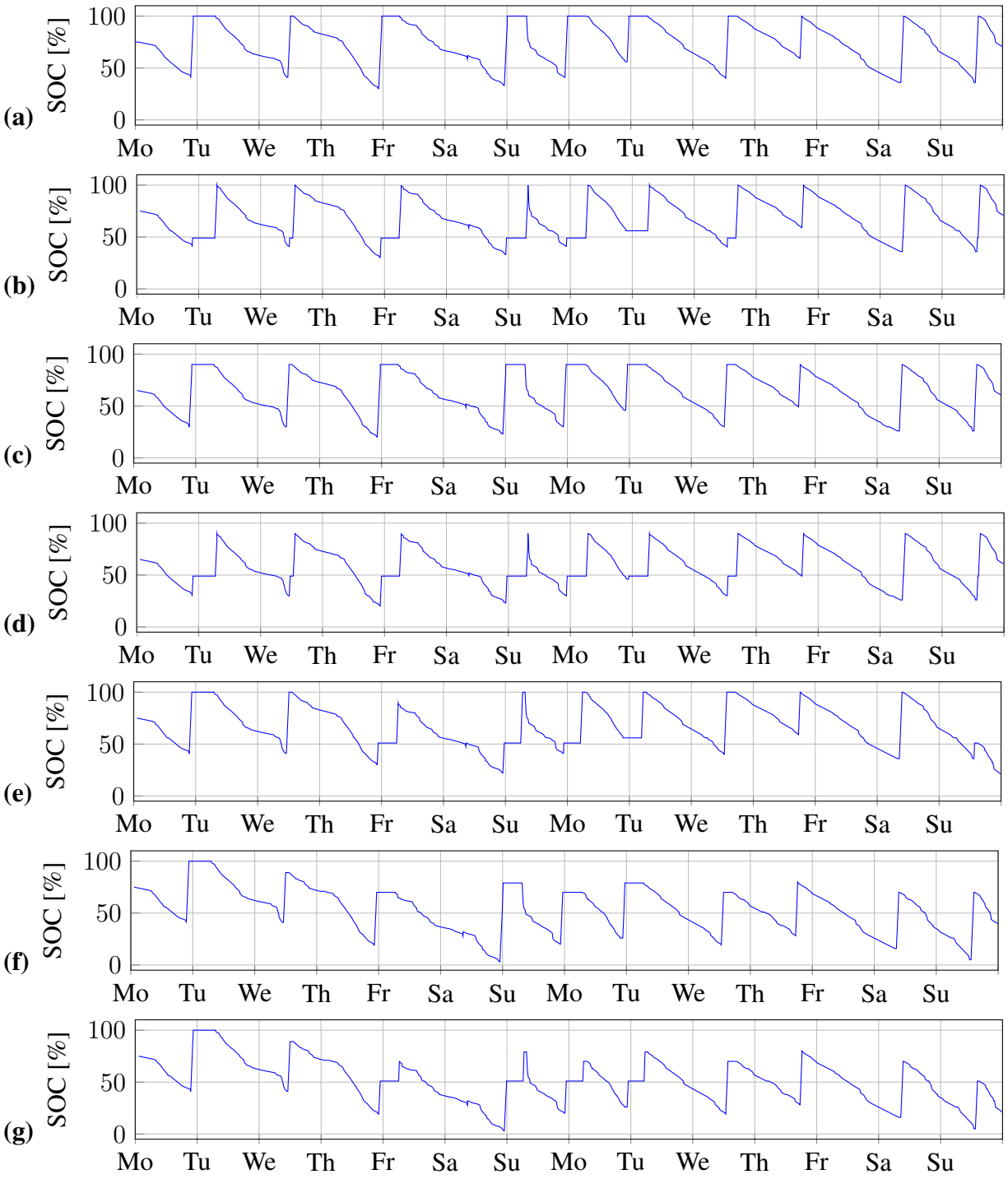

Figure 4.10: Charging plot of User 4 with recorded data (a), an optimal predictor for delayed charging (b), lowered target SOC $S_{\text{tar}} = 90\%$ (c), and a combination of both (d). As well as SMA prediction of delayed charging (e), predicted lowered S_{tar} (f), and a combination of both (g).

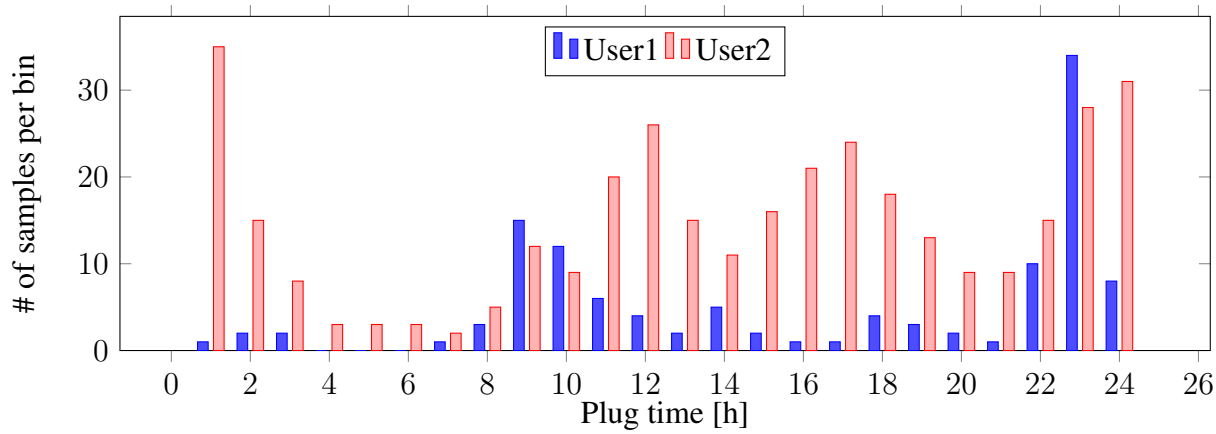

Figure 4.11: Sample sizes per plug time bin for the two data sets. The two users favor different plug times.

4.5.4 Comparison of predictors

In Section 4.4, we discuss three predictors for estimating the plug duration: An SMA predictor, an EMA predictor, and a probabilistic predictor. For evaluating these predictors, we use two data sets of two different users that contain data for several weeks. In future work, further evaluation with bigger data sets containing more users is planned.

As can be seen from Figure 4.11, the two users show distinct patterns. The number of samples per bin (plug times rounded to hours of the day) varies. All three predictors have difficulties with outliers, independent of the data set (User 1 or User 2), see Figures 4.12a and 4.12b. The peaks of increased error are either real outliers or represent the first entry within a bin for which no previous knowledge can be used.

A comparison of the predictors is done by calculating the mean squared error per sample and computing the average of all errors. The results are shown in Figure 4.13. It can be seen that the EMA predictor is slightly better than the one using an SMA predictor. The probabilistic predictor is more accurate for both data sets.

Figure 4.14 shows a comparison of mean squared errors within a single bin. Outliers occur also at later points in time and all three predictors have similar difficulties in dealing with them.

In summary, the advantage of the probabilistic predictor is that it is more accurate. However, the SMA predictor and the EMA predictor are easier to implement. Using a probabilistic predictor can bring the efficiency of aging mitigation from the previous experiment even closer to their optimum.

4.6 Discussion and open issues towards intelligent charging

Having presented the use case of the smart charger, in the following, we discuss further measures for the intelligent charging of mobile devices in general. Since the openly available solu-

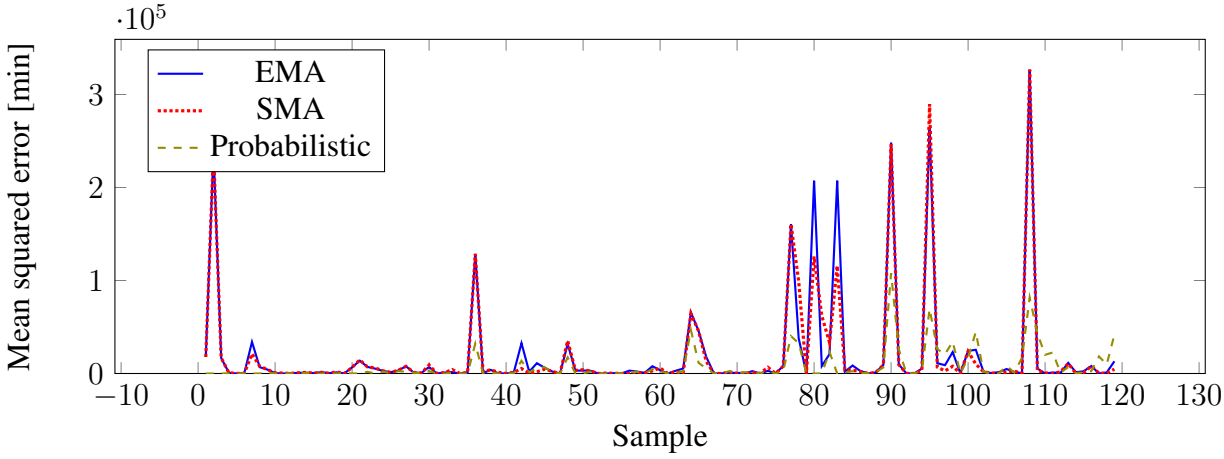

(a) User 1

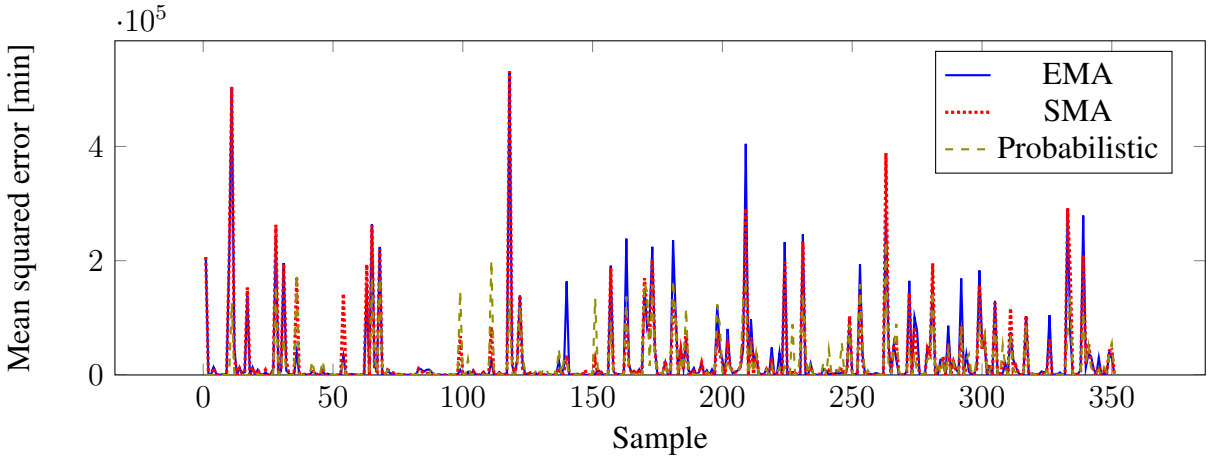

(b) User 2

Figure 4.12: Mean squared error per sample for User 1 and 2. The outliers are likely to represent empty bins. All predictors have similar difficulties with outliers.

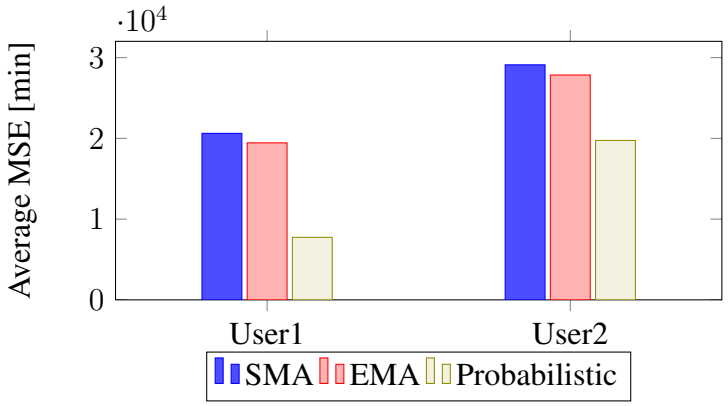

Figure 4.13: Comparison of the mean squared error over all samples using the SMA predictor, the EMA, and the probabilistic predictor.

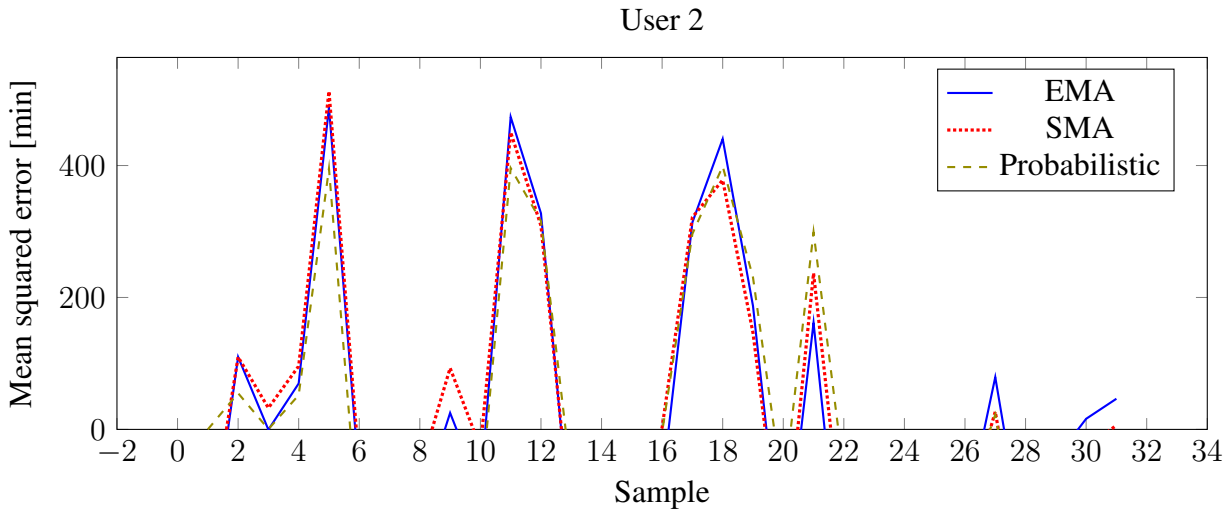

Figure 4.14: Comparison of errors within a single bin. Outliers occur also at later points in time and all three predictors have difficulties.

tions do not make full use of the potential strategies, we show the open issues in implementation as well as open research questions. We extend our discussion to not only include smartphones but also tablets and laptops.

The following text and figures contain excerpts from an early version of [120], which are quoted mostly verbatim. Adjustments have been made to ensure good readability and layout of the full thesis. ©2020 IEEE. Excerpts, with permission, from [120]. It is enhanced by perspectives from [83], which are rephrased cited separately.

Several works have dealt with health-aware charging [14, 26, 59, 83, 121]. However, commercial solutions are not mature and further improvement of intelligent chargers that mitigate battery aging is needed. First, we propose further extensions to the smart charger presented in this chapter and outline the properties of an intelligent charging protocol. Then, we discuss hardware extensions to under-dimensioned charge adapters. It had been found that the small form factor of laptop chargers leads to insufficient power supply when connected to a charger. Peak power demands cannot be met in high load conditions and the battery is used instead. This results in increased aging. A possible solution is to use a hybrid energy storage consisting of a battery with a capacitor, where the capacitor is used to meet additional load demands during charging situations where the charger cannot fulfill the overall demand. Finally, we discuss open issues and give suggestions on how to proceed with the development of intelligent chargers.

4.6.1 Intelligent charging protocol

We have seen in this chapter that many users charge their phones overnight. What makes sense from the user perspective, however significantly increases the time a battery spends at high charge level, thereby increasing battery aging. Intelligent chargers should avoid such situations by adjusting the charging protocol and delaying the time until the battery reaches full charge without compromising on the usage comfort.

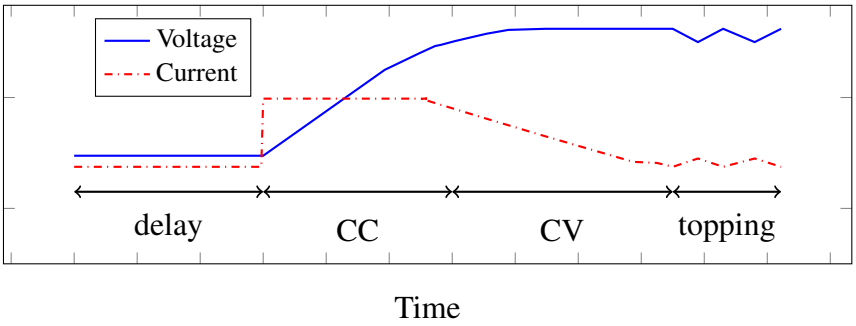

Figure 4.15: The intelligent charging protocol includes delay times, adjusts the charge current during the CC charging, and adapts the length of the voltage relaxation phase during the CV charging phase.

Present chargers follow the so-called CC-CV protocol as shown in Figure 4.15. First, the device is charged with Constant Current (CC) to a certain threshold voltage, then the voltage is kept constant during the Constant Voltage (CV) phase, where the current is slowly reduced until full charge is reached. If the device remains plugged after a full charge is reached, the self-discharge is compensated by occasionally topping charge.

The goal of an intelligent charger is to mitigate battery aging during the charging process. The charging protocol could be modified not only by delayed charging as shown in this chapter but also in combination with reduced charging current [14, 26] and voltage relaxation periods [59] as has been shown in the literature. Compared to the traditional charging protocol, in an optimized protocol, the CC and CV phases are still present, but their duration and timing need to be varied. To the best of our knowledge, so far a joint optimization of delay length, charge current, charge duration and voltage relaxation phase length has not been discussed in the literature.

Cycle life gains reported for the above-mentioned works are up to $46.2\,\%$ [14] for optimal charging current and delay, and adjusted voltage relaxation, on average $36\,\%$ percent [59]. If the charge delay is combined with adjusted SOC the cycle life could almost be doubled as has been shown in this chapter. These gains are significant and given the huge environmental impact that could be achieved, we need to equip mobile devices with intelligent chargers.

The potential for positive environmental impact but also economic benefits for consumers is immense. In 2018, the number of smartphones sold to end-users worldwide has reached 1.55 billion [51], all of them equipped with a Li-Ion battery. The smartphone user prevalence worldwide is expected to reach $37\,\%$ in 2019 and will further grow in the next years [41]. All these smartphones are used for a relatively short time. The average replacement lifespan for smartphones in the US is estimated to be 2.9 years for consumers and 2.57 years for enterprise [32]. These discarded phones will ultimately be disposed of.

Design challenges

To implement an intelligent charging protocol, the unplug time and required SOC need to be known by the system. Modeling of the charge phase can be easily done by feature extraction

Figure 4.16: Possible charge delay implementation using remote-controlled switches

from data sheets [13]. Predictors can estimate such values or else the user provides such information when plugging-in the phone, laptop, or tablet. In the latter case, the user has full control but might opt for more conservative choices lacking the understanding of battery aging factors. The challenge is to develop accurate predictors that significantly improve aging while maintaining the usage comfort.

Different strategies to address the problem of too low SOC when unplugging the phone have been proposed in related works: Either the mobile device could be charged to a minimum SOC before the delay starts (as we propose in this chapter) or the delay is reduced and a minimum charging current is applied while maintaining a good quality of service, which is defined as the required SOC being reached at the time of unplugging [26]. Intelligent chargers should achieve good user acceptance while mitigating aging.

Designing such a protocol in theory and solving optimization problems is only part of the challenge. Common phone manufacturers and operating systems designers do not provide a sufficiently accessible and standardized interface to delay charge, change the charge current, and target SOC. Also, a wide range of different charger chips has been built into phones, all with different interfaces. Remotely controlled power outlets are a possible implementation, see Figure 4.16, with the advantage of being independent of the phone type.

The required length of charge delays can be determined by predictors or by reading set alarm clocks, in particular, if the user charges overnight. The gains in the lifetime from introducing charge delays and lower charging SOC have been shown in Figure 4.9. Notably, all measures significantly improve cycle life, and also the predictors are close to ideal performance.

Existing solutions and apps

Solutions for battery health-aware charging range from mere battery health monitoring apps to joint hardware and software solutions.

Existing apps show remaining charge capacity and cycle count [137] or even remind users through alarms to unplug their phones, thereby avoiding charge topping once the full charge has been reached [164]. However as discussed above, intelligent chargers should consist of more, namely lower SOC, delayed charging, appropriate voltage relaxation time, and adjusted charge time.

For Android devices, an app exists that encourages the user to charge to lower SOCs [33]. As it is not possible to stop charging in Android from user or kernel space, the user is alarmed by the app to unplug the phone once the desired charge level is reached. While some people might be willing to take this extra effort, the common user most likely prefers more comfort.

Some manufacturers realize that a growing number of users cares about the sustainability of their devices. For example, *Apple* announced to include battery cycle life-enhancing features into its new operating system release [3]. They claim to learn from past charging routines and delay the last $20\,\%$ of charge to complete charging just in time when the user unplugs the phone. We could observe that a similar strategy is implemented in some Sony phones. In case the user deviates from past routines, he/she will be left with $80\,\%$ SOC which should be sufficient almost always. Yet, this strategy does not exploit the full potential of intelligent charging. In particular, new phones most likely have a higher headroom than $20\,\%$ and adjustments of charge current and voltage relaxation periods are not mentioned.

Additional to charge delays and lower target SOC, the charge rate could be reduced. High charging currents are even more detrimental than high discharge currents and boost charging has a particularly negative impact [79]. Manufacturers hold patents for adaptive charge rate methods [97]. However, we could not find any such approaches being promoted by manufacturers at the moment.

A promising approach towards health-aware charging comes from the startup company *Qnovo*. They sell joint hardware and software solutions to manufacturers [125] that implement EIS on mobile platforms to measure battery health in real-time. Based on the results they claim to adjust the charging parameters. However, they do not give any details on which kind of parameters are adjusted, let alone their algorithm. Concluding from one of their patents, the adjustment of charging current and voltage relaxation times is part of the method [96]. This seems to be a promising direction towards intelligent chargers.

Based on these examples, we find that intelligent charging requires access to the charger chip, which is usually not available to independent developers. In particular, no app solutions that work for all devices of the same operating system are feasible at the moment. Hence, customers need to rely on manufacturers to provide intelligent charging. Even though we observe some promising approaches, the current version of intelligent chargers is not mature, and better and faster solutions need to be found. Not only customer awareness needs to be raised but also standardized charging interfaces need to be provided to app developers. To become independent of manufacturers, dedicated devices for intelligent charging need to be developed that at least adapt target SOC and delays such as proposed in this chapter.

4.6.2 Under-dimensioned chargers

Not only the charging protocol shows deficits, but also the charger capacity often does not sufficiently satisfy the peak power demands of the device [83]. With laptops having become more lightweight, also laptop chargers have decreased in size. The disadvantage of such chargers is that their power capability is also reduced. The common laptop usage happens in the office and at home. Hence, laptops are mostly used while they are plugged-in to an AC-outlet. The reduced power of chargers leads to an additional current drain from the battery, thereby increasing its aging.

Table 4.2: Power gap between consumers and adapter power [83]

Model	**T530-2359-A44**		**MacBook Pro 2013**	
Component	Specification	Power	Specification	Power
CPU	i7-3610QM	45 W	i7-3840QM	45 W
LCD	15.4"	W 6 W	15.4"	6.2 W
VGA	NVS5400M	35 W	GT650M	45 W
HDD	7200rpm	5.5 W	7200rpm	5.5 W
RAM	DDR3 8G	2.5 W	DDR3 8G	2.5 W
Total design power		94 W		104 W
Adapter		90 W		85 W
Gap		4 W		19 W

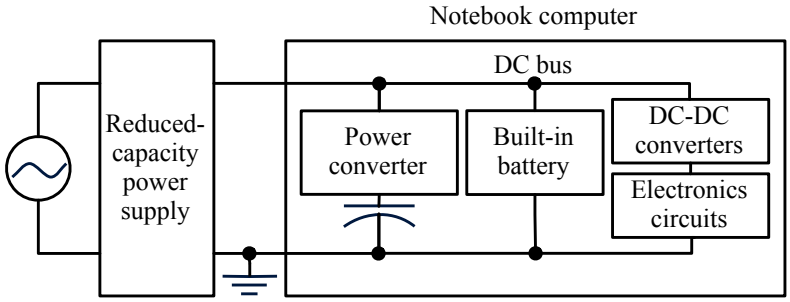

Figure 4.17: Hybrid charger with supercapacitor [83].

A comparison [83] of total design power and charger power for two laptop computers is shown in Table 4.2. A power gap exists for all models. When the device is operated while plugged to a power supply, the battery is exposed to detrimental additional discharge currents at peak loads as the charger does not provide enough power. The reduced capacity power supply is incapable to satisfy the peak power requirement and battery aging progresses, which is unexpected by the common user.

As a remedy, a hybrid energy storage consisting of a supercapacitor and a battery can be used [83]. The supercapacitor, which has a much better cycle life, supplies the additional energy while connected to a power supply and the battery can rest, see Figure 4.17. Experimental results confirmed that benchmark performance increased when using the reduced capacity power supply in combination with the supercapacitor. The hybrid energy storage in this scenario is also very cost-effective as the capacitor needs to be of small size and comes at low cost, while a battery replacement is very expensive in relation as shown in Figure 4.18. As such a supercapacitor buffer reduces aging by up to 69 % [83], it helps to significantly delay the battery replacement which is the reason for the high cost savings.

This hybrid energy storage solution has particular importance during the top-up charging phase, while the previously discussed intelligent charging strategies have focused on the CC and CV phase of the charging protocol.

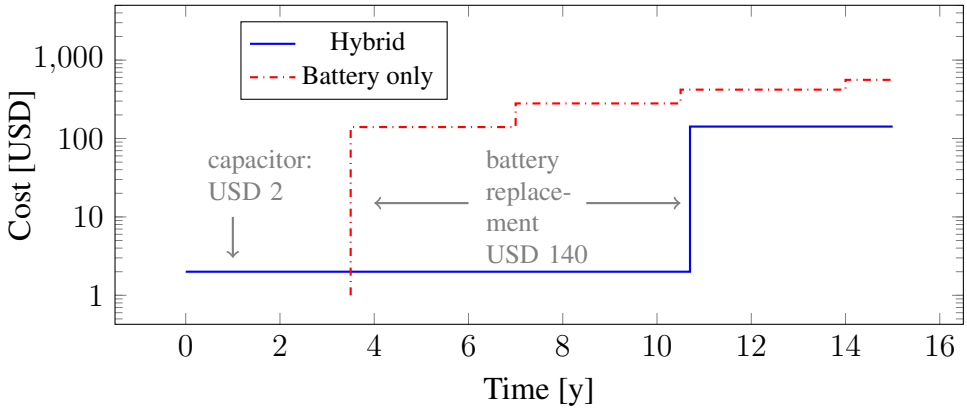

Figure 4.18: A small capacitor costs USD 2 and significantly extends the cycle life while each battery replacement costs USD 140 [83].

Additionally, when operated unplugged, the supercapacitor can be used for peak shaving and in conjunction with the rate capacity effect will result in longer runtime for the device as the Li-Ion battery will be exposed to lower current rates and therefore delivers more energy. Co-optimization with thermal management strategies can further improve cycle life while a trade-off with runtime is required as higher fan speeds result in higher power consumption. Using the right thermal strategy, cycle life is improved [159]. When the supercapacitor performs peak shaving then more output power is available due to the rate capacity effect and also the temperature of the battery increases less because the ohmic resistance of the battery is proportional to the square of the discharge current. The challenge is to find the right trade-off between fan speed and battery degradation. With lower fan speed more tasks can finish but higher battery degradation occurs. While with high fan speed, system performance will be lower but the aging is less.

The advantage of supercapacitors is their lower aging rate. Of course, hybrid energy storages could also be built from multiple battery cells and joint charge and discharge strategies. Such charging control strategies for heterogeneous battery cells should be based on the available charging current, available charge time, cell temperatures, aging constraints, and other contextual information [46].

4.6.3 Open issues

While we have discussed only two use cases, we believe that a lot of potential for innovation exists and commercial solutions are not yet mature in this domain.

First of all, the implementability of intelligent charging strategies remains a big issue due to the high variability of operating systems, charger chips, and missing common interfaces. This could be solved if phone and operating system manufacturers would agree on standardized interfaces to control charging. Current efforts have been negligible and do not have broad visibility.

Implementation of intelligent charging without the help of manufacturers is possible but more cumbersome as additional hardware is required which is less user friendly. Also, alarms

and notifications to encourage battery health-friendly behavior are mostly considered inconvenient. User acceptance itself is a crucial point for better battery health. Intelligent chargers need to maintain convenient usability. Users need to contribute by either manually providing plug times and required SOC levels. Otherwise, predictors can be applied. Raised user awareness would also increase the pressure on manufacturers as the demand for sustainable battery health-friendly devices would grow.

Furthermore, prediction of charging opportunities based on user location, such as proposed in [126], and estimated future energy consumption may also help to lower the SOC swing and to further reduce battery sizes.

Finally, the charging protocol design needs to be refined. The appropriate length of CC and CV phases as well as the amount of charge current and required voltage relaxation times may depend on the specific battery. More experimentally verified research that does not only rely on models is required. Such information could also be provided by battery manufacturers, however, usually is not extensively included in datasheets. Online measurement and according adjustments are an alternative but this requires costly additional hardware to be built into every device. Furthermore, the necessity and impact on battery degradation of fast charging need to be further explored. Fast charging may be of less importance to users if they know that it degrades battery health. Finally, the joint optimization of charge current, charge delay, and voltage relaxation periods needs to be investigated. Such parameters might change with the age of the battery, which also remains an open question.

4.7 Concluding remarks

The concept of an intelligent smartphone battery charger has been presented. The charger makes use of typical smartphone usage profiles, i.e., most smartphones are charged overnight. The charger delays charging and hence lowers the time spent at a high SOC, which is one of the factors that increase battery degradation. We presented Smart^2 a context-aware charging device that determines the possible charging delay by either manually applied settings, reading an alarm, or using a predictor. Simulation of the battery aging showed, that the battery cycle life could be extended by a factor of 1.8 on average when delaying charging and lowering the target SOC. A probabilistic predictor for plug duration estimation shows the most accurate results compared to an SMA and an EMA predictor.

Further, the necessity of intelligent chargers to increase the cycle life of our mobile devices has been highlighted. Current charging strategies of mobile devices bear a huge potential for significantly extending the useful life of devices. Existing strategies such as adaptive charge current, charge delays, and adaptive voltage relaxation times have been discussed. Previous studies reveal the great potential of these strategies in significantly increasing cycle life, while their availability in present commercially available devices is negligible. Also, the potential of hybrid energy storages during plug times to shave power peaks and save the battery from detrimental cycling has been discussed. Using supercapacitors to overcome the power cap stemming from undersized charge adapters, financial longterm costs can be reduced significantly.

However, several open issues remain. Particularly manufacturers are in charge to provide intelligent charging capabilities and to open interfaces for longer cycle life and higher sustain-

ability of products. For example, charge delays and adaptive charge current should be integrated into all devices. Besides, providing access to the charging interface in the user or kernel space would help developers to integrate more intelligent charging solutions. With this in mind, we encourage more research on optimal charging strategies. Ideally, for any battery, the interdependence of charge delays, charging current, and voltage relaxation periods should be provided in the datasheet. Finally, the customer awareness of battery health-aware charging is required to raise demand for battery health improvements in their mobile devices.

5

Cost/privacy co-optimization in smart energy grids

The smart energy grid features real-time monitoring of electricity usage such that it can control the generation and distribution of electricity as well as utilize dynamic pricing in response to the demands. For this purpose, smart metering systems continuously monitor the electricity usage of customers and report it back to the UP. This raises privacy concerns regarding the undesired exposure of human activity and the time of use of home appliances. PV and residential EES have proven to be effective in mitigating privacy concerns. However, this comes at several costs: Installation of PV and EES, their subsequent aging, and the possibly increased electricity cost. We quantify the trade-off between privacy exposure and financial costs by formulating a stochastic dynamic programming problem. Our analysis shows that i) there is a quantifiable trade-off between the financial cost and privacy leakage, ii) proper control of the system is crucial for both metrics, iii) a strategy solely focusing on privacy results in high financial costs, and iv) that for a typical residential setting, the costs for a trade-off solution lie in the range of USD 600-1700. As the load flattening has a peak shaving effect desirable for UPs, increasing privacy is mutually beneficial for both, customers and UPs.

Chapter outline: Chapter 5 is organized as follows. Section 5.1 motivates the problem of privacy leakage in smart energy systems. A brief overview of related works is presented and the contributions of the chapter are summarized. A motivational example and problem formulation are shown in Section 5.2. System modeling and controller derivation are presented in Sections 5.3 and 5.4, respectively. Simulation results are discussed in Section 5.5. The chapter concludes in Section 5.6.

The following text and figures are quoted mostly verbatim from [123]. Small adjustments have been made to ensure good readability and layout of the full thesis.

5.1 Introduction

Smart grids promise more efficient, reliable, and sustainable electricity generation and distribution thanks to the use of information and communication technologies. Dynamic energy pricing motivates the users to shift loads and perform demand-side management increasing the energy efficiency of the grid. All this is enabled by the use of smart meters, which continuously monitor the load and communicate the data to the UP. The UP can then set electricity prices to encourage customers to voluntarily shift the load out of the peak hours. At the grid-scale, the avoidance of peak loads increases load predictability and reduces the need for costly fossil-fuel reserve generators, which enhances energy efficiency and reduces the carbon dioxide emission.

5.1.1 Motivation and related works

The load profiles gathered by smart meters convey private information [102, 106]. While conventional electricity meters only record the accumulated electricity usage over a month, smart meters allow the UP to access real-time and fine-grained usage data. In the worst case, if accessed by an unauthorized third party, the data can be used to extract information on residential activities. For example, Non-Intrusive Load Monitoring (NILM) could be used to identify individual appliances and respective usage profiles [57].

Prior works

Prior works have aimed at reducing privacy leakage by using battery storage to modify and hide the usage pattern of certain appliances and human activities [53, 73, 90, 161]. Other works propose distributed load shifting [93]. Also, the impact of additional renewable energies on the privacy leakage rate has been investigated [53]. Generally, the proposed algorithms either flatten [73, 161] or randomize the load [93]. Interestingly, these works overlooked an important advantage of load flattening: Its peak shaving effect is very much desirable for the UP's demand-side management by increasing the predictability of grid power and hence reducing reserve power. Thus, load flattening is mutually beneficial for customers as well as UPs.

While the effectiveness of the approaches in privacy protection has been well studied, there has been limited research on the **cost** of privacy enhancement. There have been approaches to reduce battery energy losses [73], electricity cost of a dynamic pricing policy [161], and maintenance cost in terms of battery cycle life [73, 161]. However, the latter is one of the most important factors and has not been considered properly, mainly due to the complexity of the battery aging models. Previous work calculates the battery degradation based on cycle counting [161], which is very inaccurate unless very simplistic battery usage profiles are assumed. Other works consider the effect of DOD on battery aging, but neglect other important factors such as average SOC and C-rate [73], where C-rate is defined as the battery current relative to the battery capacity. However, it is widely known that the battery aging not only depends on the number of charge/discharge cycles or DOD but also on several other factors such as average SOC, temperature, and C-rate. As such works intend to develop sophisticated battery management policies resulting in complex battery usage profiles, cycle life estimation will be inaccurate without considering such factors, and proper analysis of the relationship between the privacy

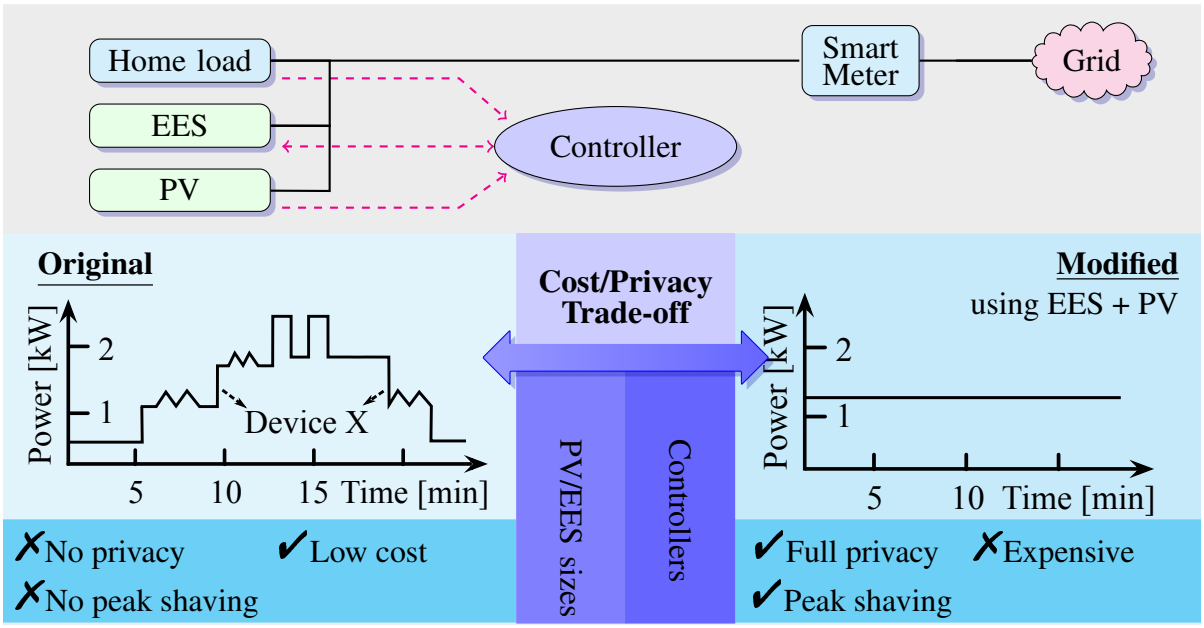

Figure 5.1: The original profile seen at the smart meter can be modified through a water filling strategy using EES and PV to increase privacy at an increased cost. We propose a cost/privacy trade-off.

enhancement and entailing costs cannot be made. Today, battery costs are significant and they have to be properly estimated to evaluate the cost of privacy protection.

The trade-off between privacy and cost

The general setup is shown in Figure 5.1: An EES and PV jointly modify the power profile such that less residential activity information can be extracted. The power generated by the PV could be either used directly to satisfy any household appliances or it could be stored in the EES for later use. Similarly, electricity could be drawn from the grid, stored in the EES, and consumed at a later point in time. An example strategy for privacy protection would be the *water filling* policy [73], which completely flattens the load profile and leaks no privacy information, see Figure 5.1. This particular strategy has the additional advantage of also being beneficial for the UP's demand-side management through its peak shaving effect, a synergy that should be exploited. On the other hand, costs arise from PV and EES installation and maintenance and possibly increased electricity bills. For example, larger EES sizes provide more flexibility for privacy protection but come at a higher installation cost. Larger PV sizes in general provide financial benefit by reducing the use of electricity from the grid, but their usefulness in protecting privacy should be carefully evaluated as, if too large, they might saturate the EES and reduce its capability of flattening out the load profile. Apart from those sizes, EES degradation depends very much on the usage pattern, i.e., the chosen control actions. In general, higher EES usage increases the aging rate.

5.1.2 Contributions

In this chapter, we, perform a novel, comprehensive analysis of the trade-off between the privacy enhancement with concurrent peak shaving and the associated financial overhead. To the best of our knowledge, this is the first work to present a control strategy that not only minimizes the privacy leakage and performs peak shaving but also minimizes the financial cost with realistic battery aging models. To jointly consider the reduction of privacy leakage and financial costs, we synthesize an optimal controller for a given EES and PV setup. We model a whole residential system as a Markov Decision Process (MDP), formulate an average reward maximization problem, and derive the optimal controller using a relative value iteration algorithm.

The **contributions** of this chapter are summarized as follows.

- We propose a control strategy for a system consisting of EES and PV that minimizes both financial cost, i.e., the sum of battery and PV depreciation and grid electricity costs, as well as the privacy enhancement, that simultaneously results in peak shaving.
- We *quantify* the trade-off of privacy enhancement with peak shaving and financial overhead under privacy and financial cost optimal control strategies. Using our framework, we identify the Pareto-optimal solutions.
- We achieve increased accuracy in our solution and analysis by using an elaborate battery model in our framework that is more precise compared to models in previous works and considers SOC, C-rate, and temperature.
- We identify balanced strategies that trade-off privacy and financial cost. Towards this, we show that, while full privacy can be achieved at acceptable but non-negligible costs, a controlled cost/privacy trade-off based on our methodology reduces these costs by more than half.
- Due to the correlation of privacy enhancement and peak shaving, which mutually benefit consumers and UP, we propose cost splitting of trade-off-strategies, potentially creating a new business model.

5.2 Motivational example and problem statement

Several algorithms exist for extracting privacy information from an electricity usage trace. Among them, NILM algorithms are capable of identifying when individual appliances are turned on and off [142], and of distinguishing different instances of light bulbs using cluster analysis [165]. This sort of information could be exploited by malicious attackers to find times in which the residents are routinely out of the house or to undesirably disclose the behaviors of the residents.

Motivational example

One possibility for full privacy protection would be a *water filling* strategy such as the one shown in Figure 5.1 using EES and PV. The EES is used in a way to hide the residential load

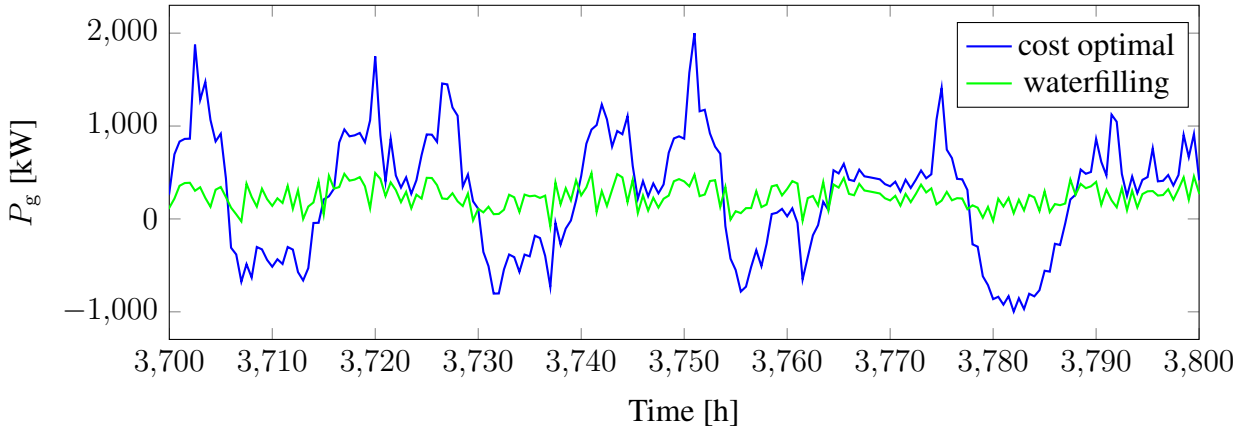

Figure 5.2: Grid power of privacy-focused water filling $w_p = 1$ vs. grid cost-focused strategy $w_g = 1$. The mutual information for the privacy and grid cost-focused strategy is 10.733 and 11.28, respectively. Data: EES 3 and PV 1, June 4-10, 2015.

completely such that the power usage seen from the grid is almost constant and maintained around a target line. On the downside, such a strategy would extensively use the EES and not optimize towards time-of-use prices resulting in accelerated EES degradation in addition to increased electricity cost. In Figure 5.2, we show two grid power profiles of a home equipped with PV and EES resulting from a financial cost-focused strategy and a privacy-focused strategy. In our results, we find that the total system cost of privacy leakage reduction and peak shaving sums up to around USD 1300 to 1600 per year, while a conventional, financial cost-optimal set-up reduces the electricity bill and costs around USD 600 per year. This high discrepancy, which is dominated by battery aging costs, confirms the need for an improved cost analysis in particular by using a more accurate battery aging model compared to the ones in previous works [73, 161]. In reality, a resident who wants a certain degree of privacy protection would desire a policy that balances cost and privacy. Our optimization objective, therefore, is to minimize privacy leakage, battery degradation, and grid cost at the same time. A bilateral profit originates from load profile flattening also being known as peak shaving, which benefits the UPs' demand-side management and motivates cost splitting among the involved parties.

Problem statement

We propose to solve this multi-objective optimization problem by formulating a single-objective weighted sum problem. The weighted objective consists of the cost associated with buying and selling electricity to and from the grid λ_g, the battery degradation cost λ_h, and the privacy cost λ_p, here determined by the deviation of the grid power from the average household load power. We want to find the EES current $I_{EES}(t)$ that minimizes the sum of the aforementioned costs over the total lifetime of the system:

$$\min_{I_{EES}} \lim_{T\to\infty} \sum_{t=0}^{T} w_g\lambda_g(t, I_{EES}) + w_h\lambda_h(t, I_{EES}) + w_p\lambda_p(t, I_{EES}), \tag{5.1}$$

with w_g, w_h, and w_p being the associated weights. We need a decision at each time instance t and reformulate the objective:

$$\forall t : \min_{I_\mathrm{EES}} w_\mathrm{g}\lambda_\mathrm{g}(t, I_\mathrm{EES}) + w_\mathrm{h}\lambda_\mathrm{h}(t, I_\mathrm{EES}) + w_\mathrm{p}\lambda_\mathrm{p}(t, I_\mathrm{EES}) \tag{5.2}$$

5.3 System models

In this section, we present the models required in the MDP optimization framework: An elaborate battery cycle life model, which is crucial for correctly assessing the financial cost, a stochastic residential load model, a PV power generation model, a dynamic energy pricing policy, and a privacy metric.

5.3.1 Battery cycle life and associated cost

We model the Li-Ion battery behavior according to the equivalent circuit model and respective parameterization in [24] and derive its cycle life degradation in terms of an empirically fitted severity factor map using the Suri et al. model [140]. The model has been summarized in Chapter 2.2.3. The severity factor ζ_funct describes the amount of damage done to a battery by its current SOC, the applied C-rate, and the temperature as shown in Figure 2.2. This cycle life model is particularly developed for control applications as the computational effort is comparably low and no iterative dependencies exist. The model is derived for Li-Ion batteries, which are commonly used in hybrid electric vehicles but also stationary storages. The framework can be easily adapted to other cell chemistries by using a similar data fitting approach as in [15].

We use the severity factor ζ_funct for the controller design and determine the actual financial loss due to EES degradation. Assuming that a new storage is purchased at some cost of Λ_EES in USD and that an EES that has reached its EOL $\varepsilon_\%$ (in percent), i.e., when 80% of the initial capacity is left, is worth USD 0.00, we calculate the cost in USD depending on the capacity loss in percent $Q_\text{loss,\%}$:

$$\Lambda_\text{SOH} = \frac{1}{1-\varepsilon_\%}\Lambda_\mathrm{EES} Q_\text{loss,\%} \tag{5.3}$$

5.3.2 Residential load model

We use the publicly available *UMass Smart* Home Data Set* [147] to model a residential load. The data set monitors several appliances in a home with three residents. The accumulated load power of Home A in 2014 is used for model training and to show the effectiveness of the method, other data than the training data is used for the evaluation, i.e., Home A data from 2015. Most times, the residential load data is in the range of 0 kW to 2 kW. Rarely, higher values occur, and in a preprocessing step, these data points are removed to reduce the state space of our model and simulation time. We use six equally spaced power states whose probabilities are shown in Figure 5.3. We compute the transition probability matrix M_Ld from the transition histogram for Home A in 2014.

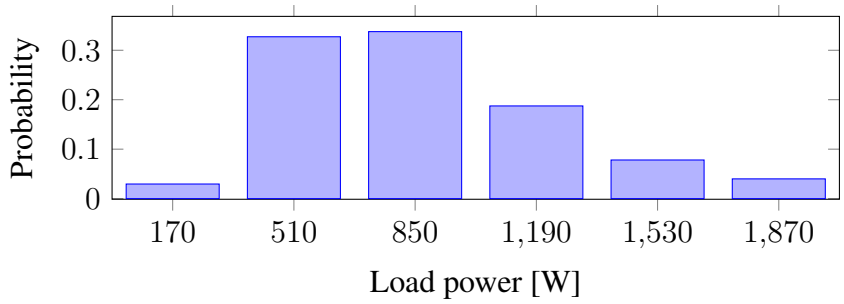

Figure 5.3: Load probability distribution

5.3.3 PV power generation model and PV cost

The PV power generation depends on the location and orientation of the PV cells as well as the solar irradiance, which varies according to the cloud cover. If more clouds occlude the sky, the irradiance is less, and therefore less PV power is produced. The *UMass Smart* Home Data Set* [147], we used for the load model, also contains cloud cover data. Similar to the load transition probabilities, we calculate the cloud cover transition probability matrix. We use the model from [40] to derive the solar irradiance from the cloud cover. The model requires the latitude and longitude associated with the cloud cover data. Due to data protection, the exact location is not conveyed in the data set, but the rough location is known to be in Western Massachusetts [6]. As any location within that region suits our purposes, we choose the latitude 42.45° and longitude -73.2458333° of Pittsfield. The solar irradiance is then integrated into a PV model [134]. We choose the dominant PV characteristics, however, refining of the model might be possible by considering further factors, such as series-parallel connections of panels, shading, bypass diodes, and hardware choice of microinverters.

PV cost

Additionally to the gain from PV power selling (Section 5.3.4), the costs of installation and degradation of the PV need to be considered. We assume a cost of USD/W 1.37 in 2011 [44]. Then, the overall installation cost, that considers also other factors such as the inverter, sums up to USD/W 3.43 for rooftop use. The PV degradation rate can be estimated by $0.8\,\%$ per year [70]. The EOL is reached when the PV has degraded by $80\,\%$. We assume a linear degradation over the resulting lifetime of 25 years.

5.3.4 Dynamic energy pricing

Modern grid energy price policies vary the prices depending on the time of the day. We use the pricing schemes offered by the Los Angeles Department of Water and Power [94] on weekdays in June 2017. The prices are in USD per kW h.

$$\Lambda_{\text{USD}}(t) = \begin{cases} \text{USD } 0.13967 & \text{for 00:00 - 09:59, 20:00 - 23:59} \\ \text{USD } 0.16411 & \text{for 10:00 - 12:59, 17:00 - 19:59} \\ \text{USD } 0.24328 & \text{for 13:00 - 16:59} \end{cases} \tag{5.4}$$

Selling energy comes at a gain of USD 0.145 per kW h [94].

5.3.5 Mutual information

We need a metric to quantify privacy exposure and use mutual information as in many prior works [53,90]. Mutual information $\mathcal{I}_{\mathrm{MI}}(\mathcal{X};\mathcal{Y})$ is an information-theoretic quantification metric that describes the amount of information that one random variable $\mathcal{X} = \{x_1, x_2, ..., x_n\}$ contains about another random variable $\mathcal{Y} = \{y_1, y_2, ..., y_n\}$. It is defined as

$$\begin{aligned}\mathcal{I}_{\mathrm{MI}}(\mathcal{X};\mathcal{Y}) &= H(\mathcal{X}) + H(\mathcal{Y}) - H(\mathcal{X},\mathcal{Y}) \\ &= \sum_{x\in\mathcal{X}}\sum_{y\in\mathcal{Y}} p(x,y)\log_2\frac{p(x,y)}{p(x)p(y)}.\end{aligned} \tag{5.5}$$

The average amount of information contained in one random variable is expressed by its entropy, $H(\mathcal{X})$ and $H(\mathcal{Y})$, and $H(\mathcal{X},\mathcal{Y})$ denotes the joint entropy. Mutual information can also be expressed in terms of the joint probability mass function $p(x,y)$ and the probability mass functions $p(x)$ and $p(y)$. In our problem setup, the two random variables are the original residential grid power consumption and the new grid power draw after the original residential load profile has been modified using EES and PV. We use mutual information to evaluate and compare the performance of our control strategies.

5.4 Financial cost and privacy optimization

To solve the optimization problem stated in Section 5.2, we formulate an MDP average reward maximization problem based on the component models from the previous section. The goal is to minimize the weighted sum of electricity cost, battery depreciation cost, and privacy exposure. We provide the Transition Probability Matrix (TPM), Transition Reward Matrix (TRM), and synthesize a controller.

5.4.1 States, actions and reward

An MDP enhances Markov chains by actions and rewards. The latter ones motivate state transitions as the goal is to maximize the reward. Actions and random variables influence the transitions between states. Additionally, the states are influenced by random variables. In our problem, a state $b \in \mathcal{B}$ is defined by the tuple (u, z, l, S) consisting of the present *cloud cover* $u \in U$ at a given *time-of-day* $z \in \mathcal{Z}$, resulting in a certain PV power, the *load power* $l \in L$, and the EES *SOC* $S \in \mathcal{S}$. A change in any of the four variables results in a state transition. Changes in time-of-day are deterministic as the next time-of-day state depends on the previous one. The action $a \in \mathcal{A}$, that should be determined, is the charge or discharge current applied to the EES. A non-zero EES current will automatically result in a state change. The reward $R(b,b')$ for transitioning from one state b to another state b' takes values in $r \in R$. The overall reward is the weighted sum of privacy leakage, the EES aging cost, and the cost from buying or selling electricity to or from the grid. It also depends on the time-of-day z due to the time-of-use pricing scheme.

5.4.2 Transition probability matrix

The TPM contains the probability for a transition from state b to state b' if action a is taken. Assuming that the cloud cover and load are independent processes, we can simply multiply the respective probabilities:

$$\Pr_a(b, b') = \Pr_u(u_b, u'_b)\Pr_z(z_b, z'_b)\Pr_l(l_b, l'_b)\Pr_{S,a}(S_b, S'_b) \tag{5.6}$$

The sequence of states should be aligned with time. Hence, the probability of moving from one time-of-day to the subsequent one is $\Pr_z(z_b, z'_b) = 1$, while all other transitions of z have probability 0. Contrary to the probabilities of cloud cover state transition $\Pr_u(u_b, u'_b)$ and load power transitions $\Pr_l(l_b, l'_b)$, the SOC transition probabilities $\Pr_{S,a}(S_b, S'_b)$ depend on the action a. The SOC change is largely deterministic, but the accuracy of runtime estimation of SOC is known to be limited, and hence, we probabilistically model the transition. We assume that the probability of the actual SOC is uniformly distributed around the estimate S_b from $S_b - S_u/2$ to $S_b + S_u/2$, where S_u is the SOC granularity. As a result, the probability of the actual SOC after Δt would be uniformly distributed in a window of length S_u around $S_b + \iota_C(a)\Delta t/3600$ where $\iota_C(a)$ is the C-rate corresponding to a. We omit the exact equation for $\Pr_{S,a}(S_b, S'_b)$ due to space constraints.

5.4.3 Transition reward matrix

The objective of the problem is to find a policy $\pi(b)$ that defines an action a to be taken when in state b. The average reward over an infinite time window should be maximized:

$$\lim_{T_\mathrm{O}\to\infty} \mathrm{E}\big[\sum_{t=0}^{T_\mathrm{O}} R_a(b_t)\big], \tag{5.7}$$

where $R_a(b_t)$ is the instantaneous reward for state b_t at time t, and a is the action to be taken when in b_t. In our work, the instantaneous reward $R_a(b, b')$ when transitioning from state b to b' is the weighted sum of the inverse normalized costs for battery depreciation $\lambda_{\mathrm{h,norm}}$, grid-related expenses from buying or selling electricity $\lambda_{\mathrm{g,norm}}$ and action a induced privacy leakage $\lambda_{\mathrm{p,norm}}$:

$$\begin{aligned} R_a(b, b') =& w_\mathrm{g}(1 - \lambda_{\mathrm{g,norm}}(b, b')) + w_\mathrm{h}(1 - \lambda_{\mathrm{h,norm}}(b, b')) \\ &+ w_\mathrm{p}(1 - \lambda_{\mathrm{p,norm}}(b, b')), \end{aligned} \tag{5.8}$$

where the w_g, w_h, and w_p are the respective weights. Due to normalization, we let the sum of the weights equal 1.

5.4.4 Battery aging, grid and privacy cost

Let us now see how the individual costs are calculated. The health or *cycle life* cost is determined by the severity factor for the given SOC S_b, the C-rate stemming from action a, and the temperature θ_EES. Assuming a perfect cooling, the latter is constant.

$$\lambda_\mathrm{h}(b, b') = f(S_b, a) = \zeta_{\mathrm{funct}}(S_b, \iota_C(a), \theta_\mathrm{EES}) \tag{5.9}$$

Table 5.1: Maximum and minimum costs

j	$\lambda_{\mathbf{j},\max}$	
h	$\zeta_{\text{funct}}(1, \iota_{C,\max}, \theta_{\text{EES}})$	100% SOC, highest possible C-rate
g	$P_{\text{g,max}}\Delta t\Lambda_{\text{USD,peak}}$	maximum grid power $P_{\text{g,max}}$ at peak hours
p	$\lvert P_{\text{g,max}} - P_{\text{target}}\rvert$.	maximum grid power
j	$\lambda_{\mathbf{j},\min}$	
h	$\zeta_{\text{funct}}(0, 0, \theta_{\text{EES}})$	0% SOC, zero discharge current
g	$-P_{\text{g,max}}\Delta t\Lambda_{\text{USD,peak}}$	maximum grid selling of PV and EES power
p	$\lambda_{\text{p,max}} = 0$.	no diversion from target value

The *grid cost* is determined by the amount of power drawn from the grid P_{g}, which can easily be derived from the required load power, the cloud cover dependent PV generation, and the EES power using the following relation: $P_{\text{EES}} = P_{\text{load}} - P_{\text{PV}} - P_{\text{g}}$. The grid electricity cost at a particular time-of-day is applied for period Δt.

$$\lambda_{\text{g}}(b, b') = f(a, u, z, l) = P_{\text{g}}(a, u, l)\Delta t\Lambda_{\text{USD}}(z) \tag{5.10}$$

Finally, we model the *privacy cost* as the diversion of the grid power P_{g} from a defined target value P_{target}. From an information-theoretic perspective, such flattening of the power profile effectively reduces mutual information and simultaneously achieves peak shaving.

$$\lambda_{\text{p}}(b, b') = f(a, u, z, l) = \lvert P_{\text{g}}(a, u, l, z) - P_{\text{target}}\rvert \tag{5.11}$$

The target value P_{target} equals the average load power reduced by the average PV generation. The average load power can be estimated from past values, i.e., the average load over a year. Even though the PV generation is subject to high seasonal as well as daily variations, in a real system, the PV generation for a particular day can be estimated from weather forecasts. We synthesize different controllers for discretized levels of PV generation. The above costs are normalized using the maximum and minimum cost from Table 5.1:

$$\lambda_{j,\text{norm}}(b, b') = \frac{\lambda_j(b, b') - \lambda_{j,\min}}{\lvert\lambda_{j,\max} - \lambda_{j,\min}\rvert}, \quad j \in \{g, h, p\} \tag{5.12}$$

5.4.5 Solution

The solution of the MDP is a policy that defines an action a for each state that maximizes the long term expected reward. The *MDPToolbox* from [20], which is used to solve our optimization problem in MATLAB, implements a relative value iteration algorithm to find the controller which maximizes the long term average reward. The interested reader may refer to [124] to get more information on the algorithm.

5.5 Simulation results

In this section, we provide the simulation and evaluation results of the controllers derived above. The evaluation is done on a custom developed simulator in MATLAB. Additionally to the models, we consider converter efficiencies for connecting EES and PV to the grid. We compare

Table 5.2: Parametrization for EES and PV sizes

parameter	**EES1**	**EES2**	**EES3**
nominal size	6.75 kW h	13.5 kW h	27 kW h
purchase cost	USD 5k	USD 8k	USD 15.4k
$P_{\mathrm{ESS,min}}$,$P_{\mathrm{ESS,max}}$	$\pm$2.3 kW	$\pm$4.59 kW	$\pm$9.18 kW
$P_{\mathrm{g,max}}$	4.3 kW	6.59 kW	11.18 kW
# actions a	51	126	251

parameter	**PV1**	**PV2**	**PV3**
$P_{\mathrm{PV,out}}$	1 kW	3 kW	5 kW
purchase cost	USD 3430	USD 10290	USD 17150

three EES and three PV sizes, as shown in Table 5.2, and vary the weights of the cost function. The sizes of EES 2 and EES 3 are the two smallest commercially available Tesla Powerwall storages [143]. EES 1 has half the capacity of EES 2. The sampling time $\Delta t = 1800\,\mathrm{s}$ is the same as the one used in the load data set and is also typical for smart meters. The number of discrete states for EES SOC $\mathcal{S}$, cloud cover U and load power L is 21, 9, and 6, respectively. The number of discrete actions, i.e., the number of discrete EES current levels, depends on the EES size and is 51, 126, and 251 for EES 1, EES 2, and EES 3, respectively. The EES is maintained at θ_{EES} =25 °C, the initial SOC is $S_{\mathrm{init}} = 0.5$, and the EOL $\varepsilon = 0.8$. We find that the grid power target level P_{target} should vary depending on the predicted PV power generation on a particular day. It changes based on the weather prediction and has a discretization granularity of $0.25\,\mathrm{kW}$ steps. The predictor does not need to be perfect as the error could easily be compensated.

5.5.1 Privacy-cost trade-off

We are interested in the Pareto-optimal settings in terms of EES size, PV size, and weights. Figure 5.4 shows the financial cost versus privacy leakage, which is equivalent to the degree of peak shaving. Different data points within a data group, defined by PV and EES size combinations, denote results for different weight values. As expected, higher weights for a particular reward come with better performance for the reward, but a worse one for other rewards. Strategies with high grid weight generally show lower cost but higher privacy leakage. Strategies with high privacy weight generally result in higher cost but lower privacy leakage. However, the gain in one domain is not always linear with the loss in another domain and hence a DSE approach is applied to ensure the best quality of control achieved at the lowest financial cost. The Pareto-front is depicted as a dashed line. We can observe a trade-off relationship between the financial cost and privacy leakage. The spread of mutual information may seem small at first glance. But the grid power profiles of this seemingly low difference differ very much. As shown in Figure 5.2, the grid power profile for a privacy-optimal strategy, $w_{\mathrm{p}} = 1$, with mutual information 10.733 is relatively flat, while the profile for a grid cost-optimal strategy, $w_{\mathrm{g}} = 1$, with mutual information 11.28 has much higher variation. The controllers synthesized with a particular combination of weight values, namely the ones whose results are part of the Pareto-front, perform better even

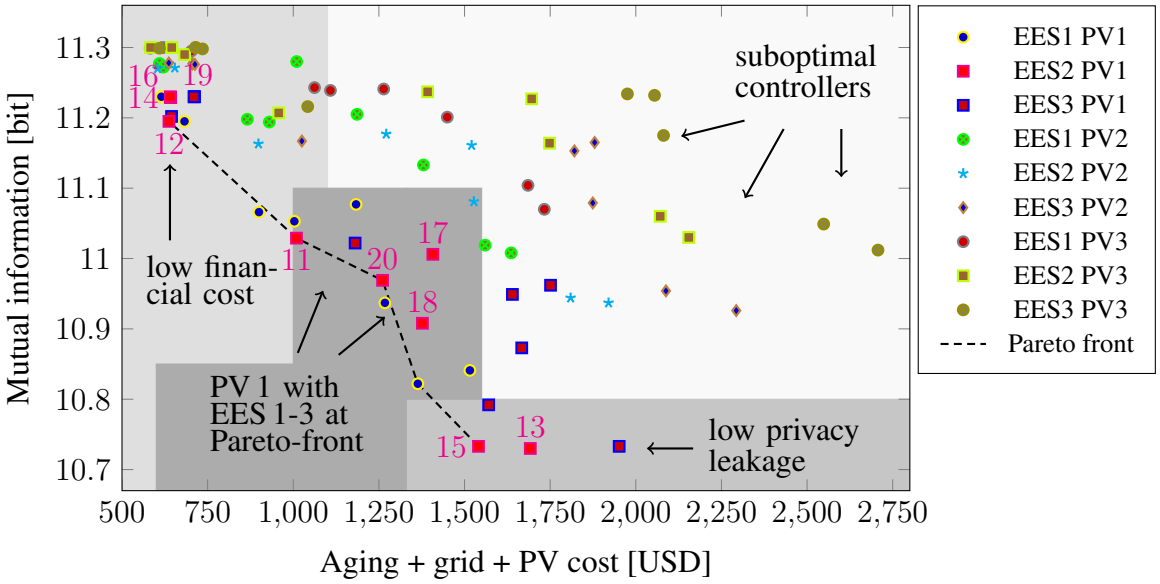

Figure 5.4: DSE: Trade-off between privacy (low mutual information) and the total cost of ownership for EES and PV combinations and different strategies. The selected node labels link to the indices in Table 5.3.

though the EES and PV sizes are the same. This shows the significance of our approach: **The quality of control is crucial** in achieving these Pareto-fronts.

5.5.2 Dimensioning of PV

In Figures 5.4 and 5.6, we can study the impact of varying PV and EES sizes on mutual information and financial cost. We find that all points at the Pareto-front use the smallest PV size, PV 1. Larger PV sizes do not reduce the mutual information as the EES loses flexibility in storing grid power to flatten the grid profile. From the information-theoretic perspective on the similarity of two random processes, more mutual information exists between a profile selling PV power to the grid and the original profile than a flatter profile and the original profile. In future work, instead of either storing or selling the PV power, a third option could be to not use excess PV power. From Figure 5.4, we also observe that no clear impact of PV sizes on the financial cost is visible. With larger PV sizes, more energy can be sold to the grid, but the cost of purchasing the PV is also higher.

5.5.3 Dimensioning of electrical energy storage and quantification of costs

We find that, if the best control is performed, all EES and PV sizes achieve good financial costs while larger EESs result in better (lower) mutual information values as more energy can be stored and hence, a flattening of the grid power is easier to achieve. We find that combinations of PV 1 with EES 1 and EES 2 achieve good trade-offs when an appropriate controller is used. The annual costs for the Pareto results of PV 1 with EES 2, as shown in Table 5.3, are about USD 600 (data point 12) for a financial cost-focused strategy, and USD 1700 (data point 13)

Table 5.3: DSE selected results - PV 1, EES 2

idx	EES [kWh]	PV [kW]	w_{g}	w_{h}	w_{p}	Financial Cost [USD]	mutual Info
11	13.5	1	$\frac{1}{3}$	$\frac{1}{3}$	$\frac{1}{3}$	1009.30	11.029
12	13.5	1	1	0	0	637.05	11.195
13	13.5	1	0	0	1	1692.00	10.730
14	13.5	1	0	1	0	641.72	11.229
15	13.5	1	0.5	0	0.5	1540.70	10.733
16	13.5	1	0.5	0.5	0	641.72	11.229
17	13.5	1	0	0.5	0.5	1407.60	11.006
18	13.5	1	0.4	0.2	0.4	1377.00	10.908
19	13.5	1	0.4	0.4	0.2	641.10	11.230
20	13.5	1	0.2	0.4	0.4	1260.70	10.969

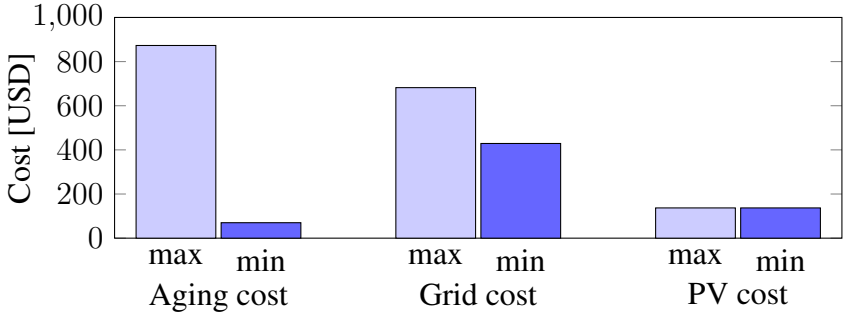

Figure 5.5: Cost breakdown EES 2, PV 1: Aging cost varies most.

for a privacy-focused strategy. The costs of trade-off strategies naturally lie in between. For example, the more balanced scheme of data point 11 results in much lower costs of USD 1000. Note that the cost for the smallest EES 1 is lowest for a purely aging-focused strategy if PV 1 and PV 2 are installed. This means that the EES cost cannot be compensated by grid gains. For all other cases, the lowest total cost occurs for a grid price-focused strategy.

Let us now analyze the contribution of the grid, PV, and aging cost to the overall financial cost. Figure 5.5 shows a cost breakdown for EES 2 and PV 1. As expected, the PV cost is the same for all controllers as it only depends on the PV size. The EES aging cost strongly depends on the respective controller, where the high aging cost comes with a reduction in mutual information and higher grid cost. The accumulated grid cost from buying and selling to the grid varies less in comparison to the EES aging cost. Given the high impact of aging on the overall cost, it may be tempting to assign a high battery health weight to w_{h}. However, purely battery health optimal strategies, $w_{\mathrm{h}} = 1$, are not advisable for real employment as they result in keeping the EES at a low SOC without charging or discharging. Adding some aging-awareness will however result in increased cycle life and hence minimal long-term financial losses.

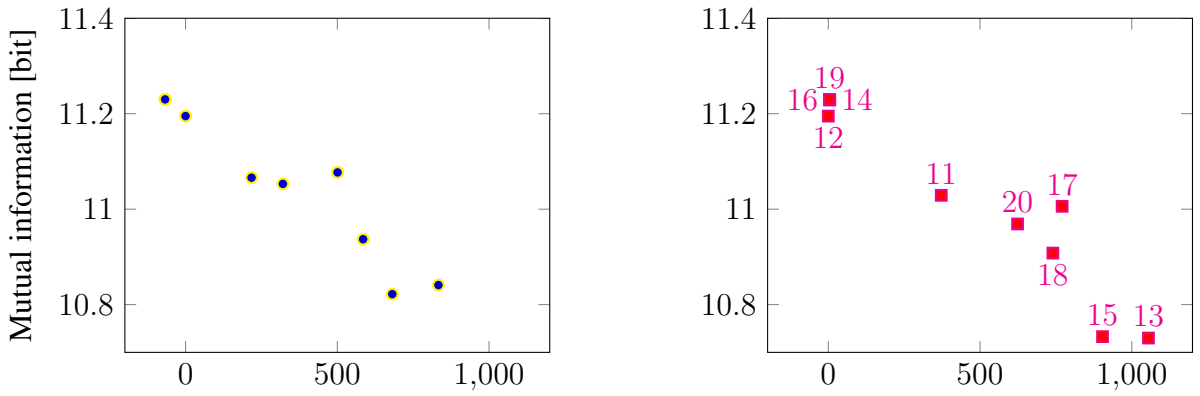

(a) Overhead EES 1, PV 1 in USD

(b) Overhead EES 2, PV 1 in USD

Figure 5.6: Cost overhead: total ownership cost reduced by grid strategy cost. Max. privacy for existing EES and PV costs a) USD 750 and b) USD 900. The node labels in (b) link to the indices in Table 5.3.

5.5.4 Cost overhead for existing installations

Assuming that several owners of already existing EES and PV systems may desire to switch from a purely grid optimal strategy to a strategy that improves their privacy, the cost overhead for EES 1 and EES 2 with PV 1 is shown in Figure 5.6. The cost overhead is determined by the total cost of ownership (aging + grid + PV cost) reduced by the cost that arises for a grid cost-optimal strategy ($w_{\mathrm{g}} = 1$). Note that in a few cases, the aging optimal strategy may be cheaper than the grid optimal strategy resulting in a negative cost overhead. However, a purely aging-focused strategy would mean not to use the EES which can be considered as being poorly dimensioned EES and PV combinations and the respective data points may be ignored. Again, the trade-offs between privacy and financial cost are achieved by selecting appropriate controllers.

5.5.5 Cost splitting

Another interesting analysis our framework provides is whether UPs could come up with a specialized contract to encourage load flattening for users with EES and PV. This is beneficial for the UPs in that they could better provision and manage the electricity grid, and also for the users whose privacy is preserved. However, as indicated by our results, the high battery aging costs result in high costs of flattening. Nevertheless, load flattening could be subsidized by the UP by providing lower rates. Consider the example in Table 5.3: The yearly EES, grid and PV costs for a flat profile are approximately USD 1692, USD 682, and USD 137, respectively (data point 13). On the other hand, a financial cost-focused strategy entails EES, grid and PV costs of USD 70, USD 430, and again USD 137, respectively (data point 12). Hence, the cost of flattening the profile entails an additional aging cost of USD 1055 from the consumer side. This value is much larger compared to the grid cost, which makes it impractical for the UP to come up with a reasonable full compensation scheme. However, in the future, when the battery price

is expected to drop continuously, the UP could introduce specialized contracts, which motivate the consumers to perform load shaving and concurrently protect their privacy.

5.6 Concluding remarks

Privacy leakage is a serious concern of smart metering systems and discourages some users from taking advantage of them. However, the installation of EES and renewable energy sources can improve privacy while preserving the benefits of smart grids. We present a framework, which allows us to investigate the privacy-cost trade-off. It is based on accurate system models, and hence, provides the most realistic estimations so far. We show how EES and PV size, and also the weights of the cost function impact the privacy leakage, grid cost, and aging cost. As for designing the controller, sensitive data such as PV location and load power histograms are required, future work should also investigate the controller performance under more generic assumptions and the applicability of machine learning. While finding the Pareto-optimal points, we observe that i) proper control of the system is crucial for performance, ii) a strategy solely focusing on privacy results in high financial costs, iii) significant privacy enhancement for a three-residents home comes at acceptable but not negligible cost, and iv) when the user increases privacy, the UP benefits from peak shaving and should partially compensate costs.

Further research in this field should investigate the visibility of certain devices. With NILM algorithms, single devices can be determined from the power signal, where some information might be more critical than others. Evaluation of the EES charge/discharge strategy to determine the number and category of detected devices, as well as the occupancy and number of present persons, is left for future work.

6

Battery health-aware multi-scale design and management

The number of battery-powered applications ranging from mobile phones and laptops to electric vehicles and stationary energy storages is constantly growing. Prolonging the device lifetimes by mitigating battery aging is imperative from both environmental and economical perspectives. In this chapter, we introduce the holistic view of multi-scale battery health management along with a framework for designing battery health-aware systems and operational strategies. Battery health management is performed on multiple abstraction levels: cell-, module-, device- and system-level. Our modular framework allows rapid analysis of health management techniques at these abstraction levels. On the cell-level, we propose battery healthy operational limits. On the module-level, component choices and corresponding control strategies are proposed, e.g., active cell balancing and thermal management systems. By leveraging application-specific usage patterns, we introduce cycle life-improving operating strategies on the device-level. Finally, on the system-level, we suggest intelligent algorithms that trade-off the overall battery degradation with system performance and cost. We show the impact of individual as well as cross-scale battery health management techniques on cycle life in extensive case studies.

Chapter outline: We provide an overview of the multiple levels on which battery health management is performed in Section 6.1. Next, we introduce a selection of techniques and strategies in Section 6.2, that is suitable for battery aging mitigation and are applicable for a wide range of applications. Further, we introduce a framework that can be used for the evaluation of such strategies. Then, in Section 6.3, we revisit the EV pack scenario from Chapter 3 and discuss health management strategies on several levels and also cross-scale observations. Finally, we conclude this chapter in Section 6.4.

6.1 Introduction

Many devices that we surround ourselves with are powered by batteries. These range from low-power devices such as smartphones, tablets, and laptops to high-power applications such as EVs, PHEVs, and stationary EESs. Run time is one of the biggest concerns in all of these devices. We have reached a state where a depleted smartphone battery can leave us in a state of big helplessness. An aspect that is not so visible as it creeps in slowly over time, is battery aging, that comes in the form of capacity and power fading. Even though battery aging happens at a relatively slow speed, it is nevertheless highly undesired from multiple points of view. The device with an aged battery often becomes unusable and instead of just replacing the battery which itself is annoying, we often see ourselves forced to replace the whole device. This has a serious impact on the environment and also results in a huge financial overhead. Therefore, mitigating battery aging is an important aspect considered not only from the electrochemical perspective but also from the circuit designers and system-level algorithm developers.

Battery health management focuses on mitigating the aging process of the battery and it can be classified into different abstraction levels such as cell-level, module-level, device-level, and system-level. Multiple health management techniques have been proposed at each abstraction level as summarized below.

1. **Cell-Level:** On the cell-level, setting limits for the operational parameters such as minimum and maximum operating cell voltage and maximum charge or discharge current play an important role in minimizing battery degradation and premature damage.

2. **Module-Level:** On module-level, where multiple cells are connected in series to obtain high voltage, for example in the case of EVs, the aging of each cell varies due to manufacturing and operating temperature differences. Here, techniques such as active cell balancing that equalizes the charge levels of individual cells based on their aging rate and aging-aware thermal management minimize battery degradation and improve their useful life.

3. **Device-Level:** By leveraging the application-specific usage patterns, many health management techniques have been proposed on the device-level abstraction layer. Typically, these techniques have a trade-off in terms of battery health improvement and the performance or usability of the device itself.

4. **System-Level:** Finally, in an environment consisting of multiple battery-powered devices or energy sources, aging mitigation can be achieved by intelligently controlling the interaction between the individual devices. This can be achieved by formulating multi-objective optimization problems to satisfy the requirements of the individual devices.

While several health management techniques have been proposed in the literature so far, no analysis of the interactions of different health management techniques proposed at multiple abstraction levels has been conducted to the best of our knowledge. Existing approaches only show the improvement in the battery life obtained with a particular health management solution. However, the improvement in battery lifetime achieved by the combination of health management techniques from multiple abstraction levels has not been sufficiently studied in the

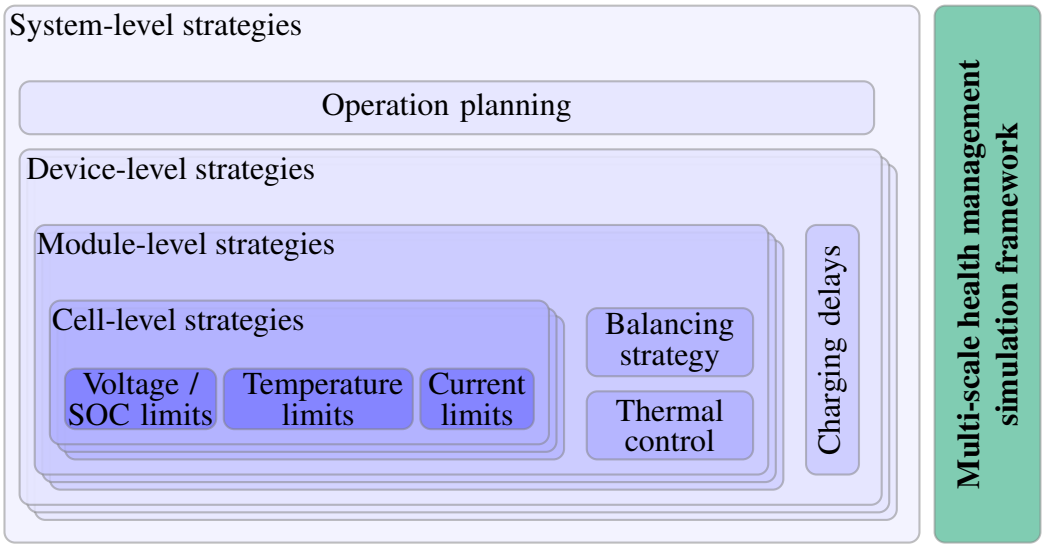

Figure 6.1: Concept of the multi-scale health management framework

literature so far. For instance, it is not possible to calculate what will be the impact of limiting the charging/discharging currents at the cell-level to the battery health-aware active cell balancing strategies on the module-level. Towards this, we propose a lightweight framework for rapid development and evaluation of health management strategies and system components.

Multi-scale battery health management

In this chapter, we perform a detailed analysis of the benefits of different battery health management techniques proposed at multiple abstraction levels as explained earlier. We introduce a novel perspective of battery aging mitigation *multi-scale battery health management*, that combines the individual health management approaches proposed at different abstraction levels. Towards this, we propose a modular simulation framework that enables rapid analysis of different aging mitigation techniques. Figure 6.1 provides an overview of our proposed multi-scale health management framework highlighting the different health management approaches proposed at each level. While battery aging is considered a relatively slow process, happening over a long period, our proposed framework is capable of rapidly estimating the gain achieved in terms of the number of charge/discharge cycles considering the control circuit components, management strategies, and external environmental impacts. Moreover, using our proposed simulation framework, we can accurately calculate the combined benefits of different health management techniques proposed at each abstraction level. The modular design of the framework allows flexible updates of any particular block such as new battery aging models or new health management strategies proposed at any abstraction level. Such a framework enables a battery system designer to develop battery health-aware operating strategies, design control circuits (i.e., active cell balancing) that minimize the aging, and also to perform fast design space exploration for evaluating different kinds of system components (such as thermal management systems) that will improve the cycle life of the battery pack at a minimum overall system cost.

Our specific contributions in this chapter are organized as follows:

- We introduce the novel concept of multi-scale battery health management in Section 6.2. While existing approaches have only focused on a particular battery aging mitigation solution at any one of the abstraction levels explained earlier, our proposed multi-scale health management approach combines the individual aging mitigation techniques to further improve the lifetime of the battery.

- To evaluate the combined benefits of the individual health management techniques on battery lifetime, we develop a modular simulation framework that allows us to rapidly simulate the slow battery aging process. Our proposed framework enables us to combine the individual health management techniques at different abstraction levels and to evaluate the battery cycle life improvement achieved by all the health management techniques together. Moreover, the modular architecture of the framework allows us to flexibly update the individual blocks including the circuit components, models (battery and circuits), and operational strategies.

- Using our proposed simulation framework, we perform a multitude of case studies in Section 6.3 showing the benefits of individual health management techniques and the gain in the cycle time of the battery pack with the combination of the several aging mitigation techniques at each abstraction level.

6.2 Multi-scale health management techniques

In this section, we present health management techniques on each abstraction level that extend battery cycle life. Most of the presented techniques are already included in our framework. As discussed previously, the main factors contributing to battery aging are the average SOC, SOC swing, and cell temperature. As the SOC swing over time is related to C-rate, the battery charge and discharge current is also a useful control knob. Generally, low SOC swing or battery current, medium average SOC, and medium temperatures are most beneficial to the battery. All techniques presented in the following, aim at modifying the load profile and controlling the periphery in a way that achieves less detrimental SOC and temperature values over time while maintaining the usability of the device.

A multitude of design options both on software as well as on hardware level impacts the battery health, where battery health is measured in terms of charge and discharge cycles achieved until the EOL, i.e., $70\,\%$ or $80\,\%$ remaining from the initial capacity. A conceptional overview of the framework is shown in Figure 6.1. We group components and operation strategies into cell-level, module-level, battery device-level, and system-level. While techniques on the cell-level, aim at improving the operating conditions of single cells, strategies on the module-level need to consider additional system components such as a balancing architecture or the cooling system. Component choices and respective operation strategies need to be optimized towards the longevity of the battery pack. On the device-level, the load comes into consideration. Within battery-powered devices, such as EVs, smartphones, or laptops, internal loads such as CPUs, Electronic Control Units (ECUs), displays, etc. draw energy from the battery. Understanding their load pattern helps to find control parameters for health improving strategies, e.g., appropriate SOC levels. Similarly, on system-level, external components can interact with the battery

device, e.g., a PV whose generated energy is stored in a stationary storage. System-level optimization may also consider a group of battery-powered devices, e.g., multiple EVs forming a fleet. Load pattern optimization or battery scheduling has the potential to significantly improve the cycle life of the battery-powered device. Load estimation and prediction, e.g., using probabilistic methods, are required to develop operating strategies that adequately modify load patterns. But also user notifications and encouragement towards a health-aware device usage is an effective measure for extending the cycle life.

Towards the design of a lightweight battery health simulation framework, we introduce several abstractions that result in well-scaling simulation times and that can also be used with limited knowledge of the real usage data. Therefore, we discuss component models and the required level of detail of strategies in the following. Generally, as aging is a very slow process and load profiles are often not known in full detail, abstract high-level models are sufficient to estimate the expected cycle life. In the best case, data traces of current, voltage, and temperature are available for the expected usage scenario. If existent, they serve as input for the simulation. However, often such data traces are not available at design time. Therefore, the reduction of complex system behavior is desired. Such reductions and simplifications result in lower computational complexity and hence lesser simulation time.

6.2.1 Cell-level

We start by discussing the battery management aspects to be considered on the cell-level to protect the cell from increased health degradation.

Voltage and SOC limits

Generally, over-charging or under-discharging, and hence exceeding voltage limits, damages the battery [11]. Too high or low voltages can result in dangerous explosions. Upper and lower voltage limits for safe operation should therefore be obtained from respective datasheets. However, the system designer may deliberately choose to further narrow the operation range by tightening the SOC limits, which is equivalent to a tighter voltage range. As tighter SOC limits naturally result in lesser available capacity, the trade-off needs to be carefully decided. Some systems adaptively change the SOC limits to compensate for capacity fading once the battery ages and give the user the impression that no capacity fading occurs.

Current limits

Higher charging currents result in increased aging [128]. Hence, it is advisable to limit the charging current. The same holds for discharge currents. In particular, for applications with high C-rates, the maximum discharge current limit is higher compared to the maximum charge current limit. The reason is that in many applications, high load power peaks are of relatively short duration, while a high charging current would be constantly applied over a longer period, and hence it would have a greater impact on battery aging.

Temperature limits

Temperature limits for safe operation should be obtained from the respective battery datasheet. However, additional thermal adjustments may be achieved on the module-level through a thermal management system.

6.2.2 Module-level

On the module-level, we suggest two component choices with associated management for improved health management. Firstly, cell balancing systems not only equalize charge and extend the driving range but they also improve the cycle life of a battery pack. The impact of charge balancing on battery health as well as an SOH-aware operational scheme have been discussed in the literature and this thesis.

Secondly, cooling systems or heating systems for sub-zero degree scenarios help to keep the temperature of a battery in a less detrimental range. Management of the cooling systems should ensure the power efficiency of the cooling system while maintaining a suitable battery temperature. Further measures applicable to module-level are hybrid storages and reconfigurable systems with appropriate operational strategies. They are not discussed in detail within the scope of this work but they have been shown to have a positive impact on battery health.

Active cell balancing

Active cell balancing is commonly used to compensate for the capacity imbalance between series-connected cells. Charge transfers from higher capacity cells towards cells with lower capacity compensate for imbalanced battery aging and manufacturing variations and improve the pack runtime. Previous measurements have shown that compared to passive balancing, active SOC balancing narrows the capacity imbalance among cells in the long term and increases cycle life [136]. An approach that goes beyond mere charge balancing is to preserve the weakest cell as much as possible and get most of the required charge from stronger cells using existing cell balancing architectures as has been presented in Chapter 3.

While a broad variety of different cell balancing architectures exists [18, 107, 114], we choose a neighbor-only inductor based architecture from [86] for the scope of our framework. Despite focusing on the neighbor-only balancing architecture, it is noted that the framework also allows using custom models of other balancing architectures such as non-neighbor balancing as in [76] or reconfigurable systems as in [58].

Thermal management

With the temperature being one of the driving factors of increased battery aging, proper thermal management of battery packs is crucial. Towards this, airflow cooling or liquid cooling is applied in large high-power battery packs as they are used in EVs or stationary storages. The cooling system can be modeled by setting the average individual cell temperatures. We will derive our modeling approach, which is based on currently available studies, in the following. However, we would like to point out that thermal modeling is an active area of research and more elaborate models can be applied in the future. Similar to [95], we assume that the air

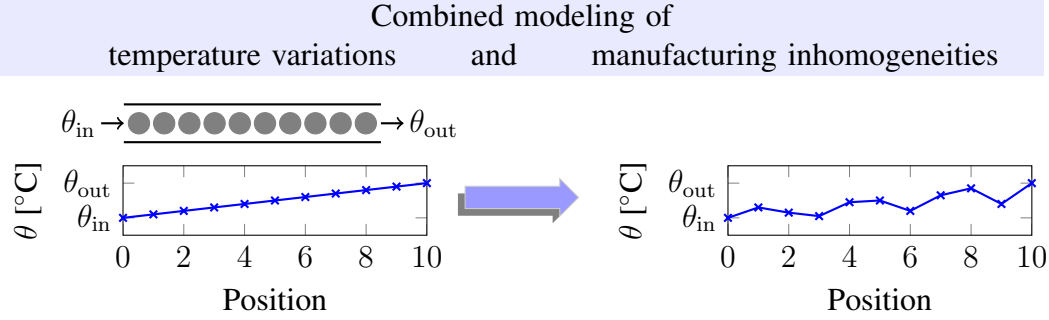

Figure 6.2: Joint modeling of temperature variations and manufacturing inhomogeneities

stream cools the cells such that all parallel cells experience the same temperature while series-connected cells have an increased cooling temperature compared to the inlet temperature. This is due to the heat exchange of cells with the flowing air. This scenario is shown in the left part of Figure 6.2 with inlet and outlet temperatures being denoted as θ_{in} and θ_{out} and assuming that the cell temperatures can be approximated by linear interpolation. The temperature gradient is then determined by

$$\Delta\theta = \theta_{\text{in}} - \theta_{\text{out}}. \tag{6.1}$$

Note that θ_{out} is assumed to equal the maximum temperature within the tube. For estimating the battery aging, we assume constant temperatures over time that level out short term self-heating of cells and temperature variations from short term thermal control. This is safe to assume if the gradient over time is small enough.

Manufacturing inhomogeneities are another effect that influences aging speed in addition to the temperature distribution. Even though it is known that temperature has an impact on aging speed, the observed cell behavior for a given temperature is commonly not identical. In modeling, we account for this observation by superposing a random distribution over the cell temperature.

$$\theta_{\text{cell}} = \text{rand}(\theta_{\text{in}}, \theta_{\text{out}}) \tag{6.2}$$

An example of random temperature distribution of cells within a tube is shown in Figure 6.2 on the right-hand side.

Jiang et al. [69] find that for some packs, an aging speed pattern in dependency of the cell location can be observed while for other packs such a correlation cannot be made. Campestrini et al. [17] observed that the capacity distribution correlated with the temperature gradients for the first half of the total number of cycles, while in the second half, the cell to cell variations from manufacturing inhomogeneities dominated the SOH evolution. Currently, cells are sorted according to their quality and similar cells are placed within a pack. However, this sorting process is costly and inhomogeneities can be compensated through, e.g., cell balancing architectures. A final answer to whether sorting or compensation is the financially and energy loss wise more efficient approach is beyond the scope of this thesis. Therefore, we keep both scenarios in mind. However, within the scope of this thesis, we assume that manufacturing inhomogeneities superimpose the cooling system effects and apply a random distribution of cell temperatures.

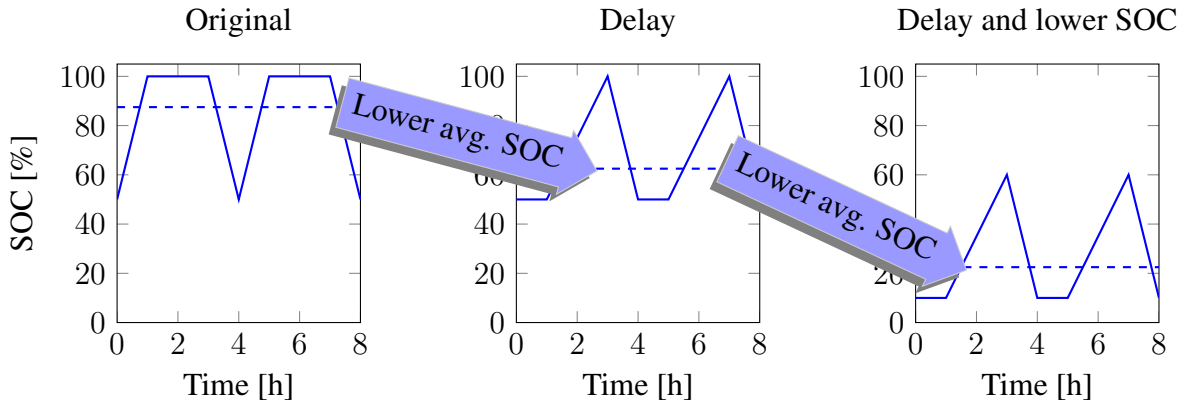

Figure 6.3: Charge delay and SOC reduction as a means to mitigate aging. Lower average SOC leads to lower aging speed.

6.2.3 Device-level

On the device-level, leveraging load patterns, that are influenced by the human user or internal energy consumers, facilitate health-friendly battery usage. The means of modification strongly depend on the application. Improved battery performance, however, often needs to be traded-off with usability or flexibility.

Often, battery devices are charged and remain plugged longer than required for a full charge. This results in an unnecessarily high SOC. For example, the smart charger in Chapter 4 targets the human behavior of charging smartphones overnight. Charging a smartphone overnight results in high SOC, which is kept at a high level over a long period, i.e., the whole night. This results in faster degradation of the battery. The concept of the smart charger is to delay the recharge of the smartphone depending on a set alarm clock or predictor. As a result, the average SOC is lowered and hence battery degradation is mitigated. Similarly, the charge of an EV could be delayed. Figure 6.3 shows how delaying the charging to be completed exactly at the unplug time lowers the average SOC. If also SOC levels are lowered on cell-level, such as proposed in Section 6.2.1, the average SOC decreases further as a result of cross-layer health management. The required charge can be estimated by exploiting usage patterns. For example, Chon et al. [29] predict the battery usage of smartphones based on the cell tower Identity (ID). Further, Falaki et al. [42] determine the expected energy drain based on idle periods and different types of busy periods. Using such predictions, the charge level can be lowered accordingly for battery health management. Such charge and discharge patterns cannot always be modified. However, if modifications are possible, significant SOH mitigation can be achieved.

Assuming that both unplug time t_{up} and charge duration T_{chg} can be determined, the advisable charge delay T_{del} of a device that is unplugged at time t_{plg} can be found by

$$T_{\mathrm{del}} = t_{\mathrm{up}} - t_{\mathrm{plg}} - T_{\mathrm{chg}}. \tag{6.3}$$

The plug time t_{plg} is equivalent to the current timestamp. The charge time can be estimated from current SOC, charge current, and expected drain during charging. The expected unplug time can either be determined by direct user input or by predictions based on the previous usage.

6.2.4 System-level

On the system-level, operational strategies that take into account the interplay of multiple generators, consumers, prosumers, and battery packs or subsets of the before-mentioned system components need to be found. Such a system could consist of, for example, a stationary battery storage along with a PV. Another example could be the management of a fleet of EVs. When designing a battery health-aware operation strategy, often the task is to find battery currents $i_n(t)$ at a time t for series-connected cells $n \in 1 \dots N_\mathrm{S}$ such that the overall battery SOH consisting of individual series-connected cell SOH levels $\kappa_n(t)$ is maximized:

$$\text{find } i_n(t) \text{ s.t.} \qquad \max \sum_{n=1}^{N_\mathrm{S}} \kappa_n(t) \quad \forall t \tag{6.4}$$

Sometimes, the reduction of SOH variances among packs is more meaningful:

$$\text{find } i_n(t) \text{ s.t.} \qquad \min \sum_{n=1}^{N_\mathrm{S}-1} \left(\kappa_n(t) - \kappa_{n+1}(t)\right)^2 \quad \forall t \tag{6.5}$$

Constraints need to be formulated according to the specific application. Solutions can be found by solving the optimization problem. Depending on the aging model and problem characteristics, finding a solution might not be trivial and heuristics are the preferable option.

The above objective functions can be applied if battery health is the primary objective. Often, however, battery health conflicts with other objectives, and therefore trade-offs need to be found. An example of such a trade-off has been presented in Chapter 5. In a smart energy scenario with stationary energy storage, PV, and a residential home load, the battery current should be found such that the grid electricity cost and battery aging are minimized while at the same time load flattening is achieved, which helps the residents to protect their privacy. In this particular example, we added models for PV, residential load traces, and time-of-use tariffs to the framework to evaluate the performance of various MDP policies found through relative value iteration concerning the time achieved until EOL is reached.

6.2.5 Cross-layer health management

Having discussed health management strategies on cell-, module-, device- and system level, cross-layer management strategies combine these single strategies to further improve the battery pack health. In the following, we discuss the implications and interdependencies when combining strategies on several levels. Generally, we expect the gains on all levels to sum up to result in even increased health gains. We limit our discussion to the techniques presented above. However, further dependencies might exist when introducing other techniques.

Cell- and module-level

On cell- and module level, the combination of adjusted SOC limits with an active cell balancing architecture and SOH-aware cell balancing algorithm is investigated. When lowering SOC target limits per predicted charge requirement, the individual cell limits can additionally be

adjusted such that weaker cells experience an even lower average SOC. The missing charge is later transferred by a healthier cell, which therefore is assigned a higher target SOC. Thereby, the weaker cell ages slower, and the pack aging is mitigated. However, if the SOC imbalance gets too large, the resulting voltage differences need to be considered for efficiency. Within the scope of this thesis, we consider these differences to be small enough to be approximated as negligible.

Cell- and device-level

On cell- and device-level a combination of lowered SOC limits and delayed charging is proposed. If the target SOC is lowered, the delay can be even extended. Towards this, the non-linearity resulting from the charging protocol needs to be considered. As has been discussed in Section 4.6, the insertion of voltage relaxation periods should be considered as well. The design of the optimal charge protocol is still an open question and should be targeted in future work. The combination of charge delays and lower target SOC has also been considered in Chapter 4 and additional gains in cycle life have been achieved.

Both, determination of target SOC as well as estimation of the charge delay require usage statistics as an input, namely the predicted plug duration and the charge consumption between plug events. Furthermore, both strategies lower the average SOC of the battery and hence mitigate aging. Potential but undesired overestimation of the feasible delay results in too low final SOC, which is beneficial in terms of aging mitigation but reduces user experience, and therefore predictors should be chosen with care. In summary, we observe a co-dependence between strategies on both layers.

Module- and device-level

On module- and device level, the interdependencies of cell balancing and charge delays is investigated. In general, charge equalization requires long times in the range of hours. Active cell balancing can be applied during charge or discharge. Depending on the state of SOC imbalance, the balancing might continue during the charge delay. If the imbalance is very high, voltage differences might need to be considered. Within the scope of this work, we assume an operating range where voltage differences can be neglected as explained above.

Cell-, module- and device-level

Finally, the strategies on cell-, module, and device-level are combined, namely, target SOC, SOH-aware cell balancing, and charge delays. The same limitations and co-dependencies as discussed above persist. We expect the gains to further grow as the gains on single levels add up.

6.2.6 Battery health management framework

In the following, we present a lightweight multi-scale simulation framework that can be used for battery health management design and optimization as a rapid evaluation of the cross-layer

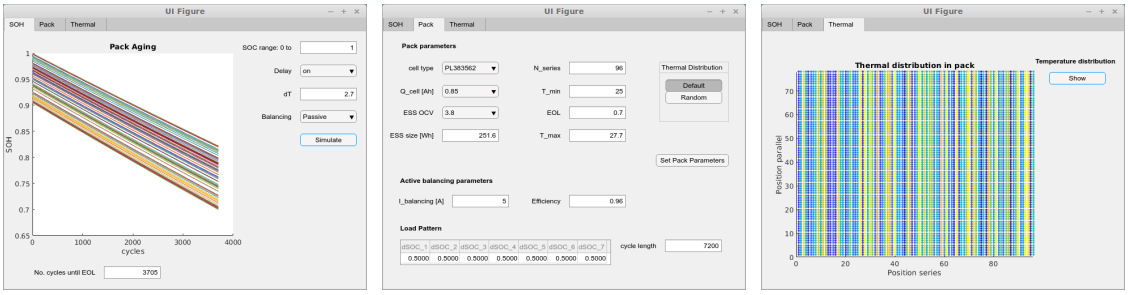

(a) Aging Simulation tab (b) Parameter settings (c) Thermal visualization

Figure 6.4: MATLAB framework

strategies is not possible with state-of-the-art tools. The proposed modular simulation framework enables the rapid analysis of different aging mitigation techniques. While battery aging develops over a long period, our framework rapidly estimates the number of charge/discharge cycles achieved considering the control circuit components, management strategies, and external environmental impacts. Moreover, the calculation of the combined benefits of health management techniques on each abstraction level can be performed. The modularity of the framework allows us to flexibly plug-in different models and blocks. Hence, updates of, e.g., aging models or operating strategies are easily integrated. We aim to enable the development of aging-mitigating operating strategies, the design of control circuits (i.e., active cell balancing), and the realization of fast design space exploration for evaluating different kinds of system components to improve the cycle life of the battery pack at a minimum overall system cost.

We implement the framework in MATLAB as shown in Figure 6.4. The aging tab (Figure 6.4a) allows us to set cut-off SOC limits, charge delays, and temperature gradients inside the pack. Further, an active balancing architecture may be enabled. The pack tab (Figure 6.4b) allows us to set the cell type, cell capacity, and cell OCV. Furthermore, the number of cells in series, inlet air temperature, and EOL can be set. EES size and maximum temperature are derived from the previous parameters. The thermal distribution among cells can either be randomly generated or else a fixed distribution can be loaded using the default button. This is useful if different strategies need to be compared with the same settings. In case active cell balancing is used, balancing current and efficiency need to be set. Besides, the DODs of the load pattern and cycle length are defined. In the thermal tab (Figure 6.4c), the thermal distribution is visualized for easier debugging.

Based on the described abstractions and models included, we present a lightweight, modular, and multi-scale simulation framework. It includes the effects of subsystem components and operation strategies. The framework not only allows the simulation of the effects of single components but also the interplay of health management techniques. Due to its modularity, the framework allows flexible updates of components and strategies. The results can be used for system-level design space explorations and cost calculations. Additionally, the evaluation of subsystem components and strategies is possible.

6.3 Results

In this section, we use our framework to evaluate the cross-layer effects of health management strategies. We revisit the EV pack health management use case from Chapter 3. We combine various health management techniques such as SOH-aware cell balancing as described in Chapter 3 as well as lower target SOC level and charge delays as introduced in the use case in Chapter 4. In the following, we investigate the combined effects of such techniques.

6.3.1 Experimental set-up

We consider a similar experimental set-up as in Section 3.6. The architecture of our battery pack is similar to the one of the Nissan Leaf 24 kW h battery pack which has 96 cells in series and 2 in parallel (96s2p). The pack comes with the active cell balancing architecture from Section 3.3. The simulation runs in MATLAB and we use the Millner aging model from Section 2.2.3 to calculate the battery health degradation. The cells connected in series vary in SOH and aging-speed, while cells in parallel are considered to be electrically indistinguishable. We assume the cells' initial SOHs to be uniformly distributed in the interval $[0.9, 1]$ and an aging-speed range of $[54.352, 55.264]$ ppmc. This is a resemblance of the temperature inhomogeneity in a pack and the cells' manufacturing variations. We model the aging speed inhomogeneities through a thermal difference of up to $2.7\,°\mathrm{C}$ and the temperature of the coolest cell being $\theta_{\min} = 25°\mathrm{C}$. We run a simulation where we charge and discharge the pack with a DOD of 0.5 and a cycle length of 2 h. The efficiency of a charge transfer is $96\,\%$. The EOL is reached when the SOH of the least healthy cell reaches 0.7.

We run experiments for the combination of maximum SOC limits (named target SOC in the following) on the cell-level, an SOH-aware cell balancing strategy as well as cooling system performance on the module-level and charge delays on device-level. We discuss the cross-layer health management aspects for the combination of (i) cell- and module-level, (ii) cell- and device-level, (iii) module- and device-level and, (iv) cell-, module- and device-level. Towards this, we present three experiments. In the first experiment, we investigate the impact of the length of the charge delay in combination with passive and SOH-aware cell balancing as well as high and low target SOC limits. The results are shown in Figure 6.5. The balancing current in this experiment is 7 A.

In a second experiment, we vary the performance of the cooling system. The cooling system is a highly critical part of battery health-aware system design because a pack without cooling would either soon reach dangerous temperatures, or the aging of cells would be highly inhomogeneous and as a result, the imbalance among cells would increase with the effect of reduced driving range and shorter cycle life. The cycle life relevant characteristics of cooling systems are the inlet temperature and the temperature gradient achieved. Intuitively, a cooling system that achieves lower gradients between inlet and outlet temperature results in higher financial costs. Therefore, a performance/cost trade-off is advisable. In the following, we use our framework to discuss the loss of cycle life and its dependence on the performance of the cooling system. At the same time, we investigate compensation mechanisms in terms of charge delays and lower SOC limits.

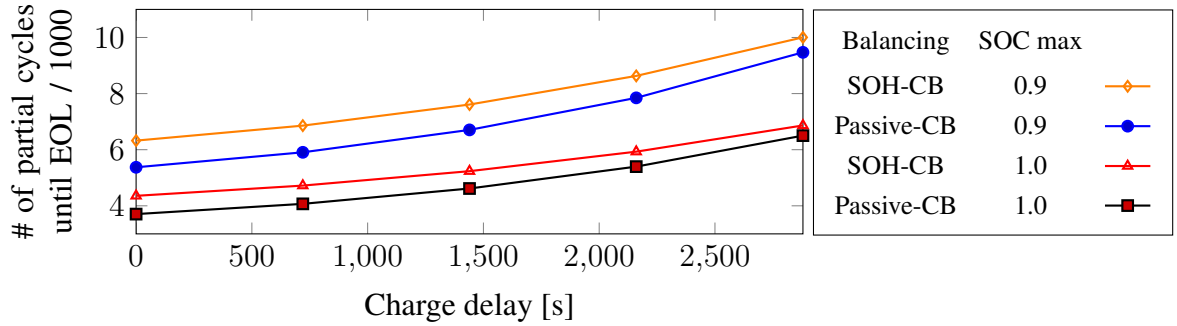

Figure 6.5: The cycle life increases with higher charging delays

As in the first experiment, we simulate cycles with a DOD of 0.5 and a cycle length of $2\,\mathrm{h}$. The cycles are interleaved with rest periods of $1\,\mathrm{h}$. Depending on whether these rest periods are inserted before or after charging, we say that delayed charging is *off* or *on*, respectively. Additionally, we vary the upper SOC limit. For practical considerations, having a charge buffer for spontaneous trips is desirable. We call $100\,\%$ target SOC *high* and $90\,\%$ *low* maximum SOC in the following. We assume a balancing current of $5\,\mathrm{A}$, which is available in state-of-the-art architectures. However, it should be noted that this current does not achieve the best possible results with SOH-aware cell balancing. The results are shown in Figure 6.6.

In the third experiment, we compare the potential for health gains of strategies on cell-, module-, and device-level. The goal is to determine whether differences in health gains of different strategies and levels exist. The results are shown in Figure 6.7.

6.3.2 Combination of cell- and module-level

We start by discussing the combined effects on cell- and module-level. On the cell-level, we adjust the target charge SOC-level and on the module-level, we apply different balancing strategies in the first experiment (Figure 6.5) and different cooling systems in the second experiment (Figure 6.6). As has been shown in Chapter 3, active balancing with an SOH-aware balancing strategy exceeds passive balancing approaches. Lowering the maximum SOC to $90\,\%$ improves the cycle life even further. As expected and as shown in Figure 6.6, increased cycle life comes with better cooling systems.

Generally, we find that the cooling system and respectively achieved temperature gradient has a strong impact on cycle life as aging is very sensitive to the cell temperature. SOH-aware cell balancing can be used to compensate for the temperature gradient and respective aging speed difference. Therefore, even cooling systems with poor temperature gradients can achieve reasonable cycle life if combined with other aging mitigation techniques. However, the cell balancing current needs to be large enough and as has been shown in Chapter 3, the balancing current of state-of-the-art architectures does not yield the best results.

We conclude that substantial improvements in cycle life can be made by applying such measures. The effectiveness of single measures varies. Nevertheless, the combination of all

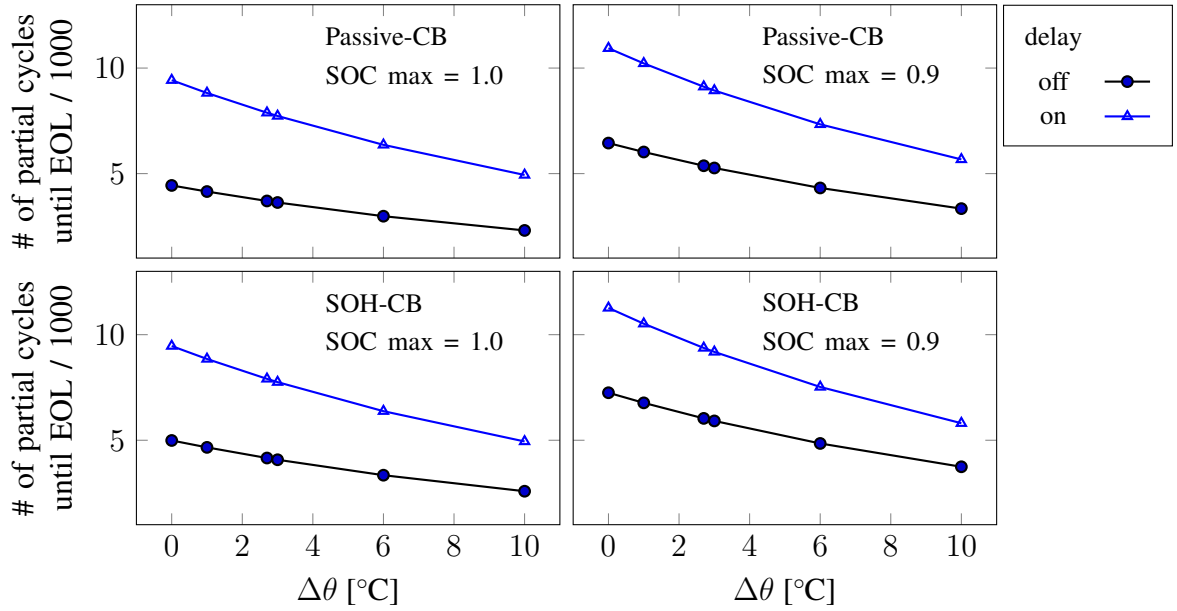

Figure 6.6: Cooling system-dependent temperature gradient and resulting cycle life

methods yields the best results. Economic considerations and predictability of load patterns help to decide the respective applicability of battery health measures.

6.3.3 Combination of cell- and device-level

Next, we discuss the combined effects of cell- and device-level strategies. On the cell-level, we adjust the target SOC levels and on the device-level, we alter the charge delays as shown in Figure 6.5. We find that charge delays have the potential to significantly mitigate battery aging. In many applications, load patterns incorporate a high amount of idle times. As the SOC-level during these idle times usually is of lesser importance to the user, it can be modified for health-awareness. This generally means to avoid very high (and also very low) SOC levels. Idle times at high SOC commonly occur when a device is charged and not immediately discharged after having reached the full charge level. By postponing the charging procedure to start just in time to reach the full charge state when idling is over and discharge starts, the average SOC is reduced and aging is mitigated. Analysis of typical usage profiles of a class of devices helps to identify such idle times. Most private-owned EVs park most of the time and hence a high potential for aging aware charging exists. As shown in Figure 6.5, the cycle life increases as the charging delay gets extended, which is as expected. We also observe that with lower maximum SOC on the cell-level, the cycle life can be significantly further improved.

6.3.4 Combination of module- and device-level

On the module- and device-level, we discuss the interplay of SOH-aware balancing strategies and cooling systems with charge delays. In Figure 6.5, we find that the gains achieved by sufficiently large charge delays outperform cell balancing strategies. However, both techniques can

be applied independently of each other. When combining cooling systems with charge delays (Figure 6.6), the high impact on improved cycle life with charge delays is very notable. We observe that gains achieved using lower SOC limits, charge delays and SOH-aware balancing are independent of the temperature difference achieved by the cooling system. The results support our claim that health management should be applied on multiple levels. Combinations of health management strategies on several levels yield the best results and should be preferred over single-level solutions.

In the future, other trade-off relationships should also be investigated. For example, the relation of the monetary investment for a better cooling system and the expected return in terms of lower battery depreciation costs could be researched.

6.3.5 Combination of cell-, module- and device level

We now investigate the combined effects of the cell-, module- and device-level strategies. We combine the previously presented aging mitigation methods and compare the achieved number of cycles until EOL with the respective conservative methods. Towards this, we extend the two previously discussed scenarios. We split the analysis into two parts. The first part in Figure 6.7 includes cooling systems and considers a limited amount of data for better readability. In Figure 6.8, we show a large number of data points to include the effects of variations in the individual control parameters. For example, a range of charge delays, target SOCs, and balancing currents. We consider two thermal systems, where the more power full one results in a temperature difference of $2.7\,^{\circ}\mathrm{C}$ between the coolest and hottest cell and the less effective but lower-cost cooling system achieves a temperature difference of $6\,^{\circ}\mathrm{C}$. Furthermore, active SOH-aware cell balancing is compared with passive cell balancing, maximum SOC levels can be lowered from $100\,\%$ to $90\,\%$ and an adaptive charging scheme, that delays charging until the trip starts, is compared with the scenario of no delay being applied.

In Figure 6.7, we plot the number of partial cycles achieved with aging mitigating measures as listed above versus the respective conservative approach. When we compare, e.g., charging delays with no delays, we do that for all combinations with other measures, i.e., passive balancing and SOH balancing, temperature gradients, and maximum SOC values. This is represented by multiple dots within one color cluster. The black line denotes the 45° line, where all dots above that line stand for improvement of cycle life achieved by the respective measure and higher distances between a point and the 45° line signify a higher gain in cycle life. The analysis in Figure 6.7 shows that all results lie above the 45° line. Hence, all aging mitigation measures considered are effective.

We have seen that applying aging mitigation measures comes at a cost. Such cost mostly is of either financial nature. Additionally, predictability of loads and user behavior potentially limits the applicability of aging mitigation measures such as target SOC limits and charge delays. Most battery-powered products, such as smartphones and EVs, are in very cost-sensitive markets, hence low financial cost can be critical for market success. On the other hand, for example in the EV market, longer guarantees on cycle-life can be a marketing advantage. Hence, most manufacturers need to trade-off the higher costs with the longer cycle life. For that, they need tools to easily estimate the expected lifetimes. In the future with a growing market share of EVs, the legislative body might even feel the need to regulate the negative environmental impact

Table 6.1: Multi-scale evaluation results from Figure 6.7

idx	$\mathbf{S}_{\mathrm{tar}}$	$\mathbf{T}_{\mathrm{del}}$ [s]	$\boldsymbol{\Delta\theta}$ [°C]	**balancing**	**# partial cycles** optimized	**# partial cycles** conservative
1	0.9		2.7	passive	9117	5373
2	0.9		6	passive	7334	4321
3	1		2.7	passive	7884	3705
4	1		6	passive	6363	2983
5	0.9		2.7	SOH-CB	9372	6035
6	0.9		6	SOH-CB	7524	4848
7	1		2.7	SOH-CB	7908	4158
8	1		6	SOH-CB	6377	3344
9	0.9	0		passive	5373	4321
10	0.9	3600		passive	9117	7334
11	1	0		passive	3705	2983
12	1	3600		passive	7884	6363
13	0.9	0		SOH-CB	6035	4848
14	0.9	3600		SOH-CB	9372	7524
15	1	0		SOH-CB	4158	3344
16	1	3600		SOH-CB	7908	6377
17	0.9	0	2.7		6035	5373
18	0.9	0	6		4848	4321
19	0.9	3600	2.7		9372	9117
20	0.9	3600	6		7524	7334
21	1	0	2.7		4158	3705
22	1	0	6		3344	2983
23	1	3600	2.7		7908	7884
24	1	3600	6		6377	6363
25		0	2.7	passive	5373	3705
26		0	6	passive	4321	2983
27		3600	2.7	passive	9117	7884
28		3600	6	passive	7334	6363
29		0	2.7	SOH-CB	6035	4158
30		0	6	SOH-CB	4848	3344
31		3600	2.7	SOH-CB	9372	7908
32		3600	6	SOH-CB	7524	6377

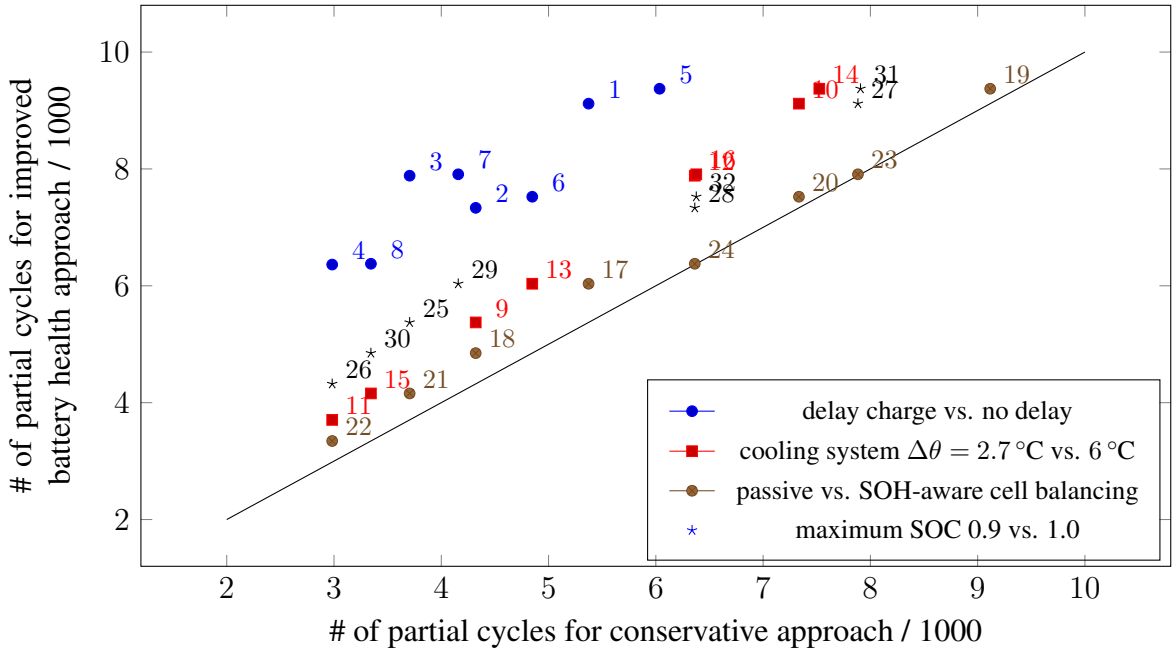

Figure 6.7: Multi-scale health management results. All aging mitigating measures are effective as the comparison results lie above the $45°$ line. The indices are resolved in Table 6.1.

of disposed unusable battery packs, by requiring manufacturers to publish estimated cycle lives of their vehicles for standardized cycles. Hence, estimating the cycle life at the design stage and implementing respective countermeasures to extend cycle life is required. From a global, environmental, and also longterm economic perspective, sustainable product design is needed.

We also see from Figure 6.7 and the detailed results in Table 6.1 that some measures result in higher cycle life gains than others. For example, charge delays have a relatively higher impact on cycle life improvement than balancing strategies or temperature gradients. Nevertheless, we find that the maximum number of cycles can only be achieved with all measures in place and no single aging mitigation technique outperforms all other techniques. Also, the relative impact to some extent depends on the particular parameters and assumptions made. We tried to make realistic assumptions and scenarios and therefore believe that the displayed trends can be guidelines in aging management. A careful combination of techniques considering also the trade-off factors such as financial costs and loss in user flexibility will lead to well-designed battery health management systems.

We extend the study to include variations of charge delays (Figure 6.8a), different target SOCs (Figure 6.8b), and different balancing currents (Figure 6.8c). The baselines displayed on the x-axis are a delay of $0\,s$, 100% target SOC, and passive cell balancing, respectively. As expected, longer charge delays, lower target SOC, and higher balancing currents extend the cycle life. However, we also observe that not all aging mitigating measures are similarly effective both in terms of quantitative as well as in qualitative improvements over the respective conservative approach. The higher the distance from the $45°$-line, the higher the qualitative improvement. As can be observed from Figure 6.8d, lower target SOCs are highly effective in

increasing the cycle life. The effectiveness increases the more health management techniques are combined.

6.4 Concluding remarks

In this chapter, we have introduced our perspective of battery health management taking place at the cell-, module-, device- and system-level. Towards this, we have presented a framework for multi-scale battery health simulation. Both, component choices as well as operation strategies impact battery aging. Using our framework, we can analyze the impact of design choices of, e.g., the cooling systems or cell balancing architectures along with respective control strategies. Additionally, we investigated combinations of different aging mitigation measures and estimated combined effects. The framework can be used for different application domains, such as smartphones, EVs, and stationary storages. Due to the modularity of the framework, new battery models, strategies, and component models can be easily integrated.

We further discussed the results for component design and operational strategy evaluation. We found that the combination of as many health mitigation techniques as possible results in the highest cycle life. However, some techniques come at increased costs and others require high predictability of load patterns as well as user behavior. If the inaccuracy of such predictions is high, the user experience suffers. Furthermore, a manufacturer can now trade-off the costs for sorting cells with the costs of cell balancing architectures. Sorting cells results in high-quality packs with high-performance cells while running a battery health-aware balancing algorithm on a balancing architecture compensates for such imbalances. Using the SOH-aware balancing strategy allows manufacturers to also use cells of lower quality in EV packs without endangering the warranty conditions that guarantee a certain useful life of a pack if sufficiently dimensioned. The safety margin of capacity over-dimensioning, if not removed, can at least be lowered leading to better utilization of available resources. It is also possible that in the future, EV manufacturers need to provide information about estimated cycle life for standardized usage cycles similar to carbon emission or (fine) particulate matter information for petrol engines or diesel engines. In such a scenario, analysis from frameworks such as ours helps to identify reasonable ways for extended cycle life.

We evaluated cross-level strategies and made the following observations. Lower target SOC on cell-level results in lower delay length on device level. Besides, usage pattern prediction is required for both, cell- and device-level. Health extending measures on one level can compensate for health degradation from components of lower performance on other levels. The combination of measures on cell-, module- and device-level results in the most effective health management. System-level trade-offs, e.g., financial cost comparisons of components and respective effectiveness on aging mitigation, is left for future work.

In summary, further advances in battery health management are expected in the future and the cross-scale effects and integration of multiple strategies need to be further investigated.

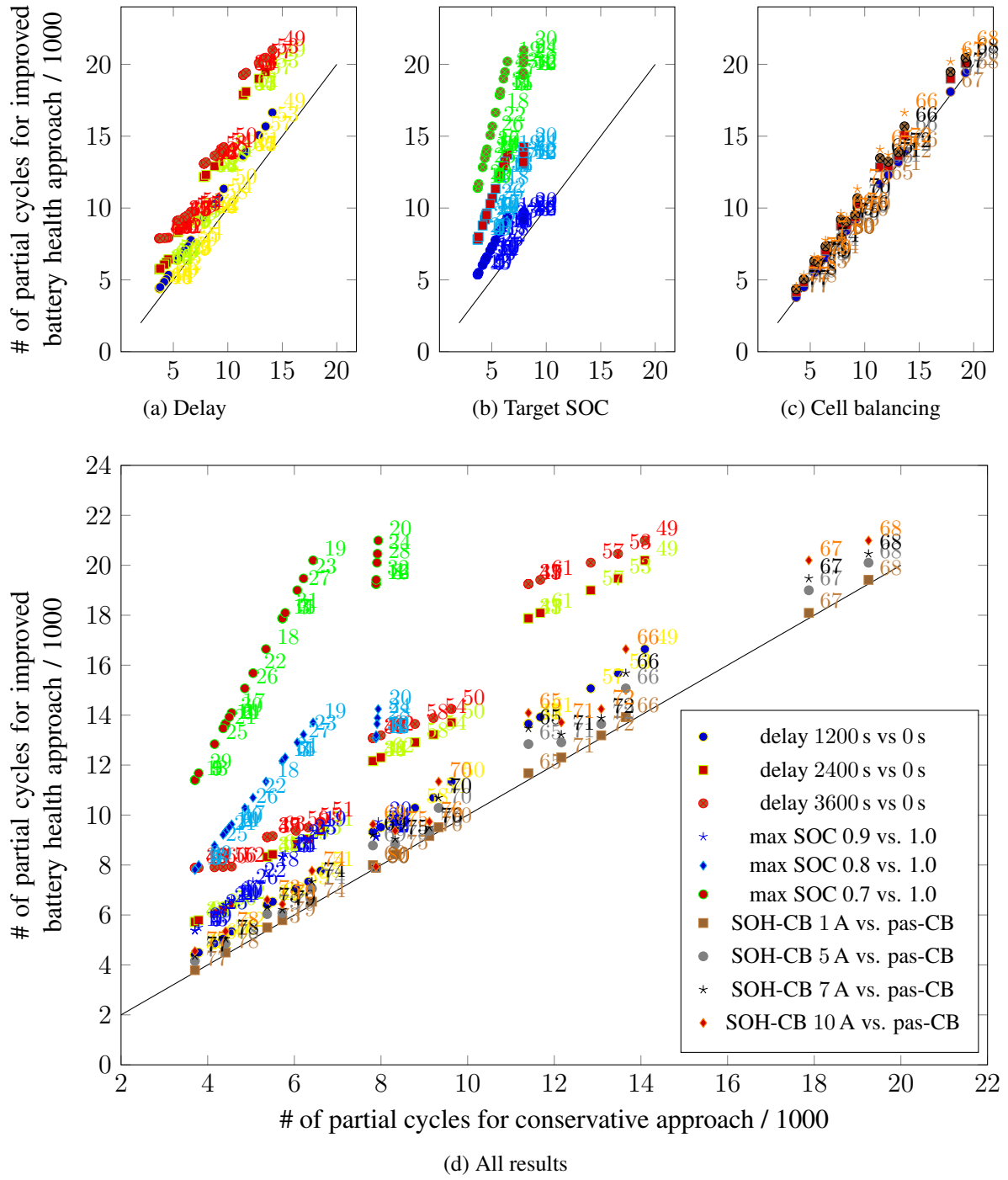

(a) Delay (b) Target SOC (c) Cell balancing

(d) All results

Figure 6.8: Multi-scale health management results. (a) Varying delays, (b) varying target SOC, (c) varying balancing current for SOH-aware cell balancing, (d) all results in one plot. All aging mitigating measures are effective as the comparison results lie above the 45° line. The indices are resolved in Tables 6.2, 6.3, and 6.4.

Table 6.2: Multi-scale evaluation results from Figure 6.8 for target SOC variations

idx	$\mathbf{T}_{\mathrm{del}}$ [s]	$\mathbf{I}_{\mathrm{B,max}}$ [A]	bal	# cyc $\mathbf{S}_{\mathrm{tar}} = 1$	# cyc $\mathbf{S}_{\mathrm{tar}} = 0.9$	# cyc $\mathbf{S}_{\mathrm{tar}} = 0.8$	# cyc $\mathbf{S}_{\mathrm{tar}} = 0.7$
1	0	10	0	3705	5373	7813	11403
2	1200	10	0	4413	6407	9330	13651
3	2400	10	0	5723	8326	12162	17875
4	3600	10	0	7884	9117	13083	19253
5	0	7	0	3705	5373	7813	11403
6	1200	7	0	4413	6407	9330	13651
7	2400	7	0	5723	8326	12162	17875
8	3600	7	0	7884	9117	13083	19253
9	0	5	0	3705	5373	7813	11403
10	1200	5	0	4413	6407	9330	13651
11	2400	5	0	5723	8326	12162	17875
12	3600	5	0	7884	9117	13083	19253
13	0	1	0	3705	5373	7813	11403
14	1200	1	0	4413	6407	9330	13651
15	2400	1	0	5723	8326	12162	17875
16	3600	1	0	7884	9117	13083	19253
17	0	10	1	4552	6610	9628	14090
18	1200	10	1	5344	7770	11340	16645
19	2400	10	1	6432	9368	13708	20198
20	3600	10	1	7936	9736	14245	20990
21	0	7	1	4356	6324	9209	13471
22	1200	7	1	5046	7333	10695	15682
23	2400	7	1	6211	9043	13225	19472
24	3600	7	1	7919	9502	13885	20460
25	0	5	1	4158	6035	8784	12841
26	1200	5	1	4856	7055	10285	15070
27	2400	5	1	6067	8831	12911	18999
28	3600	5	1	7908	9372	13647	20102
29	0	1	1	3791	5499	7997	11676
30	1200	1	1	4497	6531	9513	13922
31	2400	1	1	5789	8424	12307	18093
32	3600	1	1	7888	9161	13192	19417

Table 6.3: Multi-scale evaluation results from Figure 6.8 for charge delay variations

idx	$\mathbf{S}_{\mathrm{tar}}$	$\mathbf{I}_{\mathrm{B,max}}$ [A]	bal	# cyc del 0 s	# cyc del 1200 s	# cyc del 2400 s	# cyc del 3600 s
33	0.7	10	0	11403	13651	17875	19253
34	0.8	10	0	7813	9330	12162	13083
35	0.9	10	0	5373	6407	8326	9117
36	1	10	0	3705	4413	5723	7884
37	0.7	7	0	11403	13651	17875	19253
38	0.8	7	0	7813	9330	12162	13083
39	0.9	7	0	5373	6407	8326	9117
40	1	7	0	3705	4413	5723	7884
41	0.7	5	0	11403	13651	17875	19253
42	0.8	5	0	7813	9330	12162	13083
43	0.9	5	0	5373	6407	8326	9117
44	1	5	0	3705	4413	5723	7884
45	0.7	1	0	11403	13651	17875	19253
46	0.8	1	0	7813	9330	12162	13083
47	0.9	1	0	5373	6407	8326	9117
48	1	1	0	3705	4413	5723	7884
49	0.7	10	1	14090	16645	20198	20990
50	0.8	10	1	9628	11340	13708	14245
51	0.9	10	1	6610	7770	9368	9736
52	1	10	1	4552	5344	6432	7936
53	0.7	7	1	13471	15682	19472	20460
54	0.8	7	1	9209	10695	13225	13885
55	0.9	7	1	6324	7333	9043	9502
56	1	7	1	4356	5046	6211	7919
57	0.7	5	1	12841	15070	18999	20102
58	0.8	5	1	8784	10285	12911	13647
59	0.9	5	1	6035	7055	8831	9372
60	1	5	1	4158	4856	6067	7908
61	0.7	1	1	11676	13922	18093	19417
62	0.8	1	1	7997	9513	12307	13192
63	0.9	1	1	5499	6531	8424	9161
64	1	1	1	3791	4497	5789	7888

Table 6.4: Multi-scale evaluation results from Figure 6.8 for SOH-aware balancing current variations

idx	$\mathbf{S}_{\mathrm{tar}}$	$\mathbf{T}_{\mathrm{del}}$ [s]	# cyc pas	# cyc SOHCB 1 A	# cyc SOHCB 5 A	# cyc SOHCB 7 A	# cyc SOHCB 10 A
65	0.7	0	11403	11676	12841	13471	14090
66	0.7	1200	13651	13922	15070	15682	16645
67	0.7	2400	17875	18093	18999	19472	20198
68	0.7	3600	19253	19417	20102	20460	20990
69	0.8	0	7813	7997	8784	9209	9628
70	0.8	1200	9330	9513	10285	10695	11340
71	0.8	2400	12162	12307	12911	13225	13708
72	0.8	3600	13083	13192	13647	13885	14245
73	0.9	0	5373	5499	6035	6324	6610
74	0.9	1200	6407	6531	7055	7333	7770
75	0.9	2400	8326	8424	8831	9043	9368
76	0.9	3600	9117	9161	9372	9502	9736
77	1	0	3705	3791	4158	4356	4552
78	1	1200	4413	4497	4856	5046	5344
79	1	2400	5723	5789	6067	6211	6432
80	1	3600	7884	7888	7908	7919	7936

7 Concluding remarks

Battery health management takes place on several levels: The cell-, module-, device- and system-level. Its application areas range from small devices such as smartphones to devices with large battery packs such as EVs or stationary EESs. Mitigation of battery aging is beneficial in financial as well as environmental terms. In this thesis, we have presented three use cases that mitigate battery aging. In the first use case, an SOH-aware cell balancing scheme was introduced, that mitigated aging by putting less stress on already weaker cells. In the second use case, a smart charging scheme was discussed, that delayed the charging of smartphones based on alarms and past usage to lower the average SOC, thereby mitigating the aging. In the third use case, a system consisting of PV and EES within a residential home with smart meters was discussed. Smart meters potentially leak the privacy of a user, while an EES can be used to occlude the load profile, thereby protecting privacy. A trade-off control strategy was discussed, that not only protects privacy but also lowers financial costs for time-of-use prices, and that additionally mitigates the aging. As the battery nowadays is often the weak point in a battery-powered device, increasing its cycle life also improves the longevity of the whole device. Still many open questions and opportunities for further advances in health management exist.

7.1 Summary

The main research goal of this thesis was to design and investigate approaches for multi-scale battery health management from the perspective of the system-level designer. Towards this, three case studies for battery health management on different levels have been presented.

The main issue on module-level is the imbalance of cell capacities. Cell balancing architectures and respective strategies address this issue by balancing the SOC levels. This already positively impacts the overall cycle life. However, balancing architectures can be used to further improve the cycle life and pack SOH. We have developed an SOH-aware cell balancing strategy

that reduces stress on the least healthy cells and instead lets the healthier cells degrade faster. We found that using this strategy, the EOL of a pack can be significantly delayed. Furthermore, the architectural components should be chosen carefully, such as to provide a sufficiently high balancing current to get the most beneficial SOH equalization at a reasonable cost. Also, temperature management and the pre-selection and positioning of cells with varying SOH levels impact the performance of the algorithm. We have shown that our SOH-aware cell balancing strategy can improve cycle life by up to $23\,\%$.

The charge pattern is a very effective control parameter to mitigate aging on the device-level. With the example of a smart charger for smartphones, we demonstrate how delayed charging reduces the average SOC and results in improved cycle life. Furthermore, by adapting the maximum charge level on the cell-level to the expected required charge amount, the average SOC can be further reduced and cycle life is extended. Towards this, we compare various usage predictors and evaluate their performance. A probabilistic predictor shows the best performance. The cycle life could be extended by a factor of up to 1.8 times.

Finally, we have investigated the health management in a system-level scenario consisting of a stationary, residential EES, a rooftop-mounted PV, and a home equipped with smart meters. The optimization goal does not only cover aging-related degradation cost of the EES but also time-of-use dependent energy prices and privacy leakage through smart metering systems. A suitable controller that solves this multi-objective optimization problem is presented and the Pareto-results of the cost/privacy co-optimization are calculated. The evaluation shows that proper control is crucial for such systems and that a trade-off between cost and privacy exists. However, the privacy reduction approach, namely water-filling, has an additional beneficial effect for the UP in terms of peak shaving and resulting easier demand-side management which should be considered in the cost distribution among UPs and EES owners.

We then presented the holistic perspective of multi-scale health management. We discussed health management techniques on cell-, module-, device- and system-level. On the cell-level, the operation ranges are set such that usability is ensured at the least possible aging rate. Next, on module-level, interdependencies of cell conditions may result in increased aging or limitations in available capacity. Strategies on this level try to overcome such limitations and increase the available capacity in the middle and long term. On the device-level, usage patterns and user behavior are investigated and the health management system tries to compensate detrimental behavior while trying not to degrade the user experience. Finally, on the system-level, the interplay of multiple devices of the same or different types is researched and optimized control strategies are developed such that aging is mitigated in addition to the further system objectives.

The use cases of multi-scale battery health management presented in this thesis have in common that they adjust cell-level operational limits to mitigate battery aging. In the SOH-aware cell balancing scenario in Chapter 3, we leveraged the balancing architecture provided in an EV battery pack on module-level to reduce stress on less healthy cells. Next, in Chapter 4, we used device-level usage information on a smartphone, such as alarms and predictors, to delay charge and lower target SOC limits. Thereby, the average SOC was reduced and hence, the aging was mitigated. Finally, in Chapter 5, we considered a set-up of a PV and an EES in a residential home with smart metering systems. Smart meters potentially leak private information due to their fine-grained data recording if an outside attacker compromises the system. A water-filling strategy using the EES and PV can protect privacy. We derived a control strategy

for the EES and presented a strategy that co-optimizes time-of-use electricity prices, battery aging, and privacy. Aging mitigation is achieved through lower charge/discharge currents.

We observe, that significant aging mitigation is achieved by adaptively adjusting operational limits on cell-level at cycle runtime. Towards this, module-level infrastructure, e.g., cell balancing architectures, device-level usage information, i.e., by using predictors can be leveraged. Similarly, system-level optimization should be adjusted to use strategies that co-optimize aging. The developed strategies make use of the headroom in operational limits and battery usage as the battery is rarely fully depleted before being recharged. We also observe that components on the module-level can help to compensate effects on other levels. For example, the detrimental effect of under-dimensioned chargers on the device-level can be compensated by a hybrid energy storage and respective battery health-aware operational strategies. Similarly, the SOH imbalance on the cell-level can be compensated by using a cell balancing architecture, while the increase in SOH imbalance can be mitigated with respective strategies.

Summing up, we have shown how system-level battery health management operates on multiple scales. Our case studies show the feasibility and capability of health management on multiple levels and its significant impact on improving cycle life. The presented battery health management techniques resulted in significant aging mitigation. We hope that in the future, further integration of strategies can achieve even improved results.

7.2 Future work

The proposed multi-scale design and management approaches for battery health optimization can be further investigated, improved, and extended. Some promising directions for further research are summarized in the following.

Further integration of levels

Many advances have been made on individual levels of battery health management. However, the integration of multiple levels and the resulting effectiveness is yet to be investigated. Further analysis of cross-layer strategies would be of interest. But also the further investigation of intelligent exploitation of user behavior or usage patterns is needed. The current perspective in battery management system design that mainly focuses on runtime extension should be shifted towards co-optimization with aging mitigation strategies. This can be motivated by financial gains for the consumer and in some scenarios even related parties, e.g., electricity providers. But also the environmental perspective must be highlighted. The increasing prevalence of batteries leads to a massive increase of highly toxic waste without having sufficient recycling infrastructure in place. Battery health management cannot solve this problem but it can contribute to a deceleration.

Improved online SOH estimators

Online SOH estimation for health management systems is beneficial as adaptive algorithms can react to changes in health conditions. Of course, strategies such as the smart charger for average SOC reduction will also work without knowing the current SOH, but on the other hand,

approaches such as the SOH-aware cell balancing rely on sufficiently accurate SOH estimators. Advances in the domain of online SOH estimation will therefore positively impact the capabilities of health management.

Improved SOH modeling

For evaluation of the effectiveness of health management strategies, reliable SOH models are required. A comparison of existing models concerning accuracy and sensitivity towards aging factors would help to better interpret the results and to account for inaccuracies of individual models. Also, openly available aging data for different kinds of electrode materials would be helpful to fit these models. With current models, a qualitative assessment of aging mitigation strategies can be done. But in terms of quantification, the models show some discrepancies. Hence further research and a common database of aging data from multiple manufacturers would be helpful.

SOH inhomogeneities

Cells inside a battery pack show inequalities in capacity and health. These inhomogeneities stem from manufacturing variations and temperature distribution within the pack. However, the individual impact of these two sources is not yet clear. A better understanding of the sources of inhomogeneities could help to find more sophisticated placements of cells inside a pack such that stress factors could be distributed appropriately considering the individual health of a cell.

Investigation of further prediction approaches

Especially on higher levels of the multi-scale health management scheme, predictors of user behavior and load patterns are used to manage the battery health. Improving these predictors should therefore lead to better performance of the health management measures. One possibility would be to investigate the usability of machine learning approaches. In scenarios such as the smart charger, the user behavior concerning plug- and unplug times as well as charge consumption while the device is powered by the battery could be predicted by machine learning algorithms. Also in the cost/privacy co-optimization of residential storages in smart energy grids, machine learning approaches could be combined with the existing algorithms to make the system less dependent on external input and the impact on control performance should be investigated.

Impact of inaccuracies

The last point that is partially linked to the above-mentioned future work paths, is the investigation of the impact of inaccuracies. SOH estimation but also user behavior and load predictions expose a high degree of uncertainty. Therefore, probabilistic estimations should be developed and their impact on the accuracy of the health estimation should be estimated. Towards this, the possible reasons for inaccuracy and uncertainty need to be identified and quantified. Then, the impact of these probabilities on the overall aging mitigation should be simulated. Inaccuracies and uncertainties within the simulation model should be similarly considered. Research

questions would on the one hand be the robustness of health management strategies towards the inaccurate prediction of, e.g., user behavior or inaccurate SOH estimation. And, on the other hand, the quantification of the effectiveness of the approaches could be evaluated. Towards this, a broad study on battery aging data and user behavior data would be required.

Cross-layer investigations

While having addressed three use cases within the scope of this thesis and also some cross-layer strategies, further investigation of additional techniques and strategies are needed. In particular, on the system-level, a multitude of trade-offs exists. Such co-optimization problems can cover financial aspects but also joint management of multiple battery-powered devices as well as the alignment with further system objectives.

Batteries are increasingly used as power and energy source for more and more types of devices. Increased focus on battery health management is required from an economic perspective and to mitigate the negative environmental impact of prematurely disposed batteries and devices.

Bibliography

[1] D. Andre, C. Appel, T. Soczka-Guth, and D. U. Sauer. Advanced mathematical methods of SOC and SOH estimation for lithium-ion batteries. *Journal of Power Sources*, 224:20 – 27, 2013.

[2] M. André. The ARTEMIS European driving cycles for measuring car pollutant emissions. *Science of the Total Environment*, 334-335:73 – 84, 2004.

[3] Apple Inc. New features available with iOS 13. `https://www.apple.com/ios/ios-13-preview/features/`, 2019.

[4] S. Baek, M. Go, S. Lee, and H. Cha. Exploiting multi-cell battery for mobile devices: Design, management, and performance. In *Proceedings of the 15th ACM Conference on Embedded Network Sensor Systems (SenSys)*, pages 20:1–20:13, 2017.

[5] T. M. Bandhauer, S. Garimella, and T. F. Fuller. A critical review of thermal issues in lithium-ion batteries. *Journal of the Electrochemical Society*, 158(3):1–25, 2011.

[6] S. Barker, A. Mishra, D. Irwin, E. Cecchet, P. Shenoy, and J. Albrecht. Smart*: An open data set and tools for enabling research in sustainable homes. In *Proceedings of 2nd KDD Workshop on Data Mining Applications in Sustainability (SustKDD)*, 2012.

[7] A. Barré, B. Deguilhem, S. Grolleau, M. Gérard, F. Suard, and D. Riu. A review on lithium-ion battery ageing mechanisms and estimations for automotive applications. *Journal of Power Sources*, 241:680–689, 2013.

[8] S. Bashash, S. J. Moura, J. C. Forman, and H. K. Fathy. Plug-in hybrid electric vehicle charge pattern optimization for energy cost and battery longevity. *Journal of Power Sources*, 196(1):541 – 549, 2011.

[9] BBC business news. Samsung confirms battery faults as cause of Note 7 fires. `https://www.bbc.com/news/business-38714461`, 23 January 2017.

[10] M. Berecibar, I. Gandiaga, I. Villarreal, N. Omar, J. Van Mierlo, and P. Van den Bossche. Critical review of state of health estimation methods of li-ion batteries for real applications. *Renewable and Sustainable Energy Reviews*, 56:572 – 587, 2016.

[11] C. R. Birkl, M. R. Roberts, E. McTurk, P. G. Bruce, and D. A. Howey. Degradation diagnostics for lithium ion cells. *Journal of Power Sources*, 341:373 – 386, 2017.

[12] Bitkom. Number of smartphone users in Germany from January 2009 to 2018 (in millions). Statista - The Statistics Portal www.statista.com/statistics/461801/number-of-smartphone-users-in-germany/, 2018.

[13] A. Bocca, Y. Chen, A. Macii, and M. Poncino. Fundamental feature extraction of the battery charge phase from product data. In *Proceedings of the IEEE International Symposium on Circuits and Systems (ISCAS)*, pages 1–4, 2018.

[14] A. Bocca, A. Sassone, A. Macii, E. Macii, and M. Poncino. An aging-aware battery charge scheme for mobile devices exploiting plug-in time patterns. In *Proceedings of the 33rd IEEE International Conference on Computer Design (ICCD)*, pages 407–410, 2015.

[15] A. Bocca, A. Sassone, D. Shin, A. Macii, E. Macii, and M. Poncino. An equation-based battery cycle life model for various battery chemistries. In *Proceedings of IFIP/IEEE International Conference on Very Large Scale Integration (VLSI-SoC)*, pages 57–62, 2015.

[16] N. Bouchhima, M. Gossen, S. Schulte, and K. P. Birke. Lifetime of self-reconfigurable batteries compared with conventional batteries. *Journal of Energy Storage*, 15:400 – 407, 2018.

[17] C. Campestrini, P. Keil, S. F. Schuster, and A. Jossen. Ageing of lithium-ion battery modules with dissipative balancing compared with single-cell ageing. *Journal of Energy Storage*, 6:142 – 152, 2016.

[18] J. Cao, N. Schofield, and A. Emadi. Battery balancing methods: A comprehensive review. In *Proceedings of the IEEE Vehicle Power and Propulsion Conference (VPPC)*, pages 1–6, 2008.

[19] A. Carroll and G. Heiser. An analysis of power consumption in a smartphone. In *Proceedings of the USENIX annual technical conference*, volume 14, pages 21–21, 2010.

[20] I. Chades, G. Chapron, M. Cros, F. Garcia, and S. R. MDPtoolbox: a multi-platform toolbox to solve stochastic dynamic programming problems. *Ecography*, 37(9):916–920, 2014.

[21] W. Chang, A. Pröbstl, D. Goswami, M. Zamani, and S. Chakraborty. Reliable CPS design for mitigating semiconductor and battery aging in electric vehicles. In *Proceedings of the IEEE 3rd International Conference on Cyber-Physical Systems, Networks, and Applications (CPSNA)*, pages 37–42, 2015.

[22] ChargeHub. Electric vehicle charging guide. https://chargehub.com/en/electric-car-charging-guide.html, 2018.

[23] Cheetah Mobile Inc. Battery doctor (battery saver) 4.14. https://play.google.com, 2014.

[24] M. Chen and G. A. Rincon-Mora. Accurate electrical battery model capable of predicting runtime and IV performance. *IEEE Transactions on Energy Conversion*, 21(2):504–511, 2006.

[25] X. Chen, W. Shen, T. T. Vo, Z. Cao, and A. Kapoor. An overview of lithium-ion batteries for electric vehicles. In *Proceedings of the 10th International Power Energy Conference (IPEC)*, pages 230–235, 2012.

[26] Y. Chen, A. Bocca, A. Macii, E. Macii, and M. Poncino. A li-ion battery charge protocol with optimal aging-quality of service trade-off. In *Proceedings of the International Symposium on Low Power Electronics and Design (ISLPED)*, pages 40–45. ACM, 2016.

[27] Z. Chen, C. C. Mi, Y. Fu, J. Xu, and X. Gong. Online battery state of health estimation based on genetic algorithm for electric and hybrid vehicle applications. *Journal of Power Sources*, 240:184 – 192, 2013.

[28] S. S. Choi and H. S. Lim. Factors that affect cycle-life and possible degradation mechanisms of a li-ion cell based on $LiCoO_2$. *Journal of Power Sources*, 111(1):130–136, 2002.

[29] Y. Chon, W. Ryu, and H. Cha. Predicting smartphone battery usage using cell tower ID monitoring. *Pervasive and Mobile Computing*, 13:99–110, 2014.

[30] T. Cui, S. Chen, Y. Wang, Q. Zhu, S. Nazarian, and M. Pedram. Optimal co-scheduling of HVAC control and battery management for energy-efficient buildings considering state-of-health degradation. In *Proceedings of the 21st Asia and South Pacific Design Automation Conference (ASP-DAC)*, pages 775–780, 2016.

[31] H. Dai, G. Zhao, M. Lin, J. Wu, and G. Zheng. A novel estimation method for the state of health of lithium-ion battery using prior knowledge-based neural network and Markov chain. *IEEE Transactions on Industrial Electronics*, 66(10):7706–7716, 2019.

[32] Daniel Research Group. Average lifespan (replacement cycle length) of smartphones in the United States from 2013 to 2023 (in years). Statista - The Statistics Portal `www.statista.com/statistics/619788/average-smartphone-life/`, 2019.

[33] Digibites. AccuBattery. `https://www.accubatteryapp.com`, 2016 – 2019.

[34] E. Din, C. Schaef, K. Moffat, and J. T. Stauth. A scalable active battery management system with embedded real-time electrochemical impedance spectroscopy. *IEEE Transactions on Power Electronics*, 32(7):5688–5698, 2017.

[35] A. Dinger, R. Martin, X. Mosquet, M. Rabl, D. Rizoulis, M. Russo, and G. Sticher. Batteries for electric cars: Challenges, opportunities, and the outlook to 2020. *The Boston Consulting Group*, 2010.

[36] T. M. T. Do and D. Gatica-Perez. Contextual conditional models for smartphone-based human mobility prediction. In *Proceedings of the ACM conference on ubiquitous computing (UbiComp)*, pages 163–172, 2012.

[37] M. Dubarry, N. Vuillaume, and B. Y. Liaw. Origins and accommodation of cell variations in Li-ion battery pack modeling. *International Journal of Energy Research*, 34(2):216–231, 2010.

[38] M. Ecker, J. B. Gerschler, J. Vogel, S. Käbitz, F. Hust, P. Dechent, and D. U. Sauer. Development of a lifetime prediction model for lithium-ion batteries based on extended accelerated aging test data. *Journal of Power Sources*, 215:248–257, 2012.

[39] A. Eddahech, O. Briat, N. Bertrand, J.-Y. Delétage, and J.-M. Vinassa. Behavior and state-of-health monitoring of li-ion batteries using impedance spectroscopy and recurrent neural networks. *International Journal of Electrical Power & Energy Systems*, 42(1):487 – 494, 2012.

[40] J. Ehnberg and M. Bollen. Simulation of global solar radiation based on cloud observations. *ISES Solar Energy*, 78(2):157 – 162, 2005.

[41] eMarketer. Smartphone user penetration as percentage of total global population from 2014 to 2021. Statista - The Statistics Portal `www.statista.com/statistics/203734/global-smartphone-penetration-per-capita-since-2005/`, 2017.

[42] H. Falaki, R. Mahajan, S. Kandula, D. Lymberopoulos, R. Govindan, and D. Estrin. Diversity in smartphone usage. In *Proceedings of the 8th international conference on Mobile systems, applications, and services (MobiSys)*, pages 179–194, 2010.

[43] A. Farmann, W. Waag, A. Marongiu, and D. U. Sauer. Critical review of on-board capacity estimation techniques for lithium-ion batteries in electric and hybrid electric vehicles. *Journal of Power Sources*, 281:114 – 130, 2015.

[44] D. Feldman, G. Barbose, R. Margolis, R. Wiser, N. Darghouth, and A. Goodrich. Photovoltaic (PV) pricing trends: historical, recent, and near-term projections. Technical report, National Renewable Energy Laboratory (NREL) and Lawrence Berkeley National Laboratory (LBNL), 2012.

[45] D. Ferreira, A. K. Dey, and V. Kostakos. Understanding human-smartphone concerns: A study of battery life. In K. : Lyons, J. Hightower, and E. M. Huang, editors, *Pervasive Computing*, volume 6696, pages 19–33, Springer, Berlin, Heidelberg, 2011.

[46] A. J. Ferrese, P. Hu, S. E. Hodges, R. Chandra, J. L. Meinershagen, N. A. B. Priyantha, A. Badam, T. Moscibroda, and J. Dutra. Heterogeneous battery cell charging. US Patent App. 14/626,600, 2016.

[47] M. Fleckenstein, O. Bohlen, M. A. Roscher, and B. Bäker. Current density and state of charge inhomogeneities in li-ion battery cells with LiFePO4 as cathode material due to temperature gradients. *Journal of Power Sources*, 196(10):4769 – 4778, 2011.

[48] B. Flipsen, J. Geraedts, A. Reinders, C. Bakker, I. Dafnomilis, and A. Gudadhe. Environmental sizing of smartphone batteries. In *Electronics Goes Green 2012+*, pages 1–9, 2012.

[49] T. Franke, I. Neumann, F. Bühler, P. Cocron, and J. F. Krems. Experiencing range in an electric vehicle: Understanding psychological barriers. *Applied Psychology*, 61(3):368–391, 2012.

[50] J. L. Gallardo, C. E. Romero, M. M. I. Milanes, and M. M. A. Guerrero. Battery equalization active methods. *Journal of Power Sources*, 246:934 – 949, 2014.

[51] Gartner. Number of smartphones sold to end users worldwide from 2007 to 2018 (in million units). Statista - The Statistics Portal `www.statista.com/statistics/263437/global-smartphone-sales-to-end-users-since-2007/`, 2019.

[52] M. Gholizadeh and F. R. Salmasi. Estimation of state of charge, unknown nonlinearities, and state of health of a lithium-ion battery based on a comprehensive unobservable model. *IEEE Transactions on Industrial Electronics*, 61(3):1335–1344, 2014.

[53] G. Giaconi, D. Gündüz, and H. V. Poor. Smart meter privacy with renewable energy and an energy storage device. *IEEE Transactions on Information Forensics and Security*, 13(1):129–142, 2018.

[54] S. Gibbs. Apple and Samsung fined for deliberately slowing down phones. The Guardian, 24 October 2018.

[55] Goldman Sachs. Projected split of the global lithium-ion battery market in 2020, by segment. Statista - The Statistics Portal `www.statista.com/statistics/309579/lithium-ion-battery-market-estimation/`, 2018.

[56] T. Guena and P. Leblanc. How depth of discharge affects the cycle life of lithium-metal-polymer batteries. In *Proceedings of the 28th International Telecommunications Energy Conference (INTELEC)*, pages 1–8, 2006.

[57] G. Hart. Nonintrusive appliance load monitoring. *Proceedings of the IEEE*, 80(12):1870–1891, 1992.

[58] L. He, Y. Gu, T. Zhu, C. Liu, and K. G. Shin. SHARE: SoH-aware reconfiguration to enhance deliverable capacity of large-scale battery packs. In *Proceedings of the ACM/IEEE 6th International Conference on Cyber-Physical Systems (ICCPS)*, pages 169–178, 2015.

[59] L. He, Y.-C. Tung, and K. G. Shin. iCharge: User-interactive charging of mobile devices. In *Proceedings of the 15th Annual International Conference on Mobile Systems, Applications, and Services (MobiSys)*, pages 413–426, 2017.

[60] Z. He, M. Gao, G. Ma, Y. Liu, and S. Chen. Online state-of-health estimation of lithium-ion batteries using dynamic bayesian networks. *Journal of Power Sources*, 267:576 – 583, 2014.

[61] A. Hoke, A. Brissette, K. Smith, A. Pratt, and D. Maksimovic. Accounting for lithium-ion battery degradation in electric vehicle charging optimization. *IEEE Journal of Emerging and Selected Topics in Power Electronics*, 2(3):691–700, 2014.

[62] J. Hong, S. Park, and N. Chang. Accurate remaining range estimation for electric vehicles. In *Proceedings of the 21st Asia and South Pacific Design Automation Conference (ASP-DAC)*, pages 781–786, 2016.

[63] D. A. Howey, P. D. Mitcheson, V. Yufit, G. J. Offer, and N. P. Brandon. Online measurement of battery impedance using motor controller excitation. *IEEE Transactions on Vehicular Technology*, 63(6):2557–2566, 2014.

[64] X. Hu, H. Yuan, C. Zou, Z. Li, and L. Zhang. Co-estimation of state of charge and state of health for lithium-ion batteries based on fractional-order calculus. *IEEE Transactions on Vehicular Technology*, 67(11):10319–10329, 2018.

[65] X. Hu, C. Zou, C. Zhang, and Y. Li. Technological developments in batteries: A survey of principal roles, types, and management needs. *IEEE Power and Energy Magazine*, 15(5):20–31, 2017.

[66] I. A. Hunt, Y. Zhao, Y. Patel, and G. J. Offer. Surface cooling causes accelerated degradation compared to tab cooling for lithium-ion pouch cells. *Journal of The Electrochemical Society*, 163(9):A1846–A1852, 2016.

[67] T.-R. Hwang. Battery log, version 2.0.3. `https://play.google.com`, 2013.

[68] IDC. n.d. Average selling price for smartphones worldwide in 2013 and 2017, by region (in U.S. dollars). Statista - The Statistics Portal `https://www.statista.com/statistics/283334/global-average-selling-price-smartphones/`, 2018.

[69] Y. Jiang, J. Jiang, C. Zhang, W. Zhang, Y. Gao, and Q. Guo. Recognition of battery aging variations for LiFePO4 batteries in 2nd use applications combining incremental capacity analysis and statistical approaches. *Journal of Power Sources*, 360:180 – 188, 2017.

[70] D. C. Jordan and S. R. Kurtz. Photovoltaic degradation rates – an analytical review. *Progress in photovoltaics: Research and Applications*, 21(1):12–29, 2013.

[71] W. Jung, C. Kang, C. Yoon, D. Kim, and H. Cha. DevScope: A nonintrusive and online power analysis tool for smartphone hardware components. In *Proceedings of the 8th IEEE/ACM/IFIP International Conference on Hardware/Software Codesign and System Synthesis (CODES+ISSS)*, pages 353–362, 2012.

[72] S. Kalnaus, S. Pannala, S. Allu, W. Elwasif, S. Simunovic, J. Billings, A. Bennett, A. Kumar, and J. Turner. CAEBAT OAS/VIBE - production release v.1.1. Technical report, Oak Ridge National Laboratory, 2015.

[73] G. Kalogridis, Z. Fan, and S. Basutkar. Affordable privacy for home smart meters. In *Proceedings of the IEEE Ninth International Symposium on Parallel and Distributed Processing with Applications Workshops (ISPAW)*, pages 77–84, 2011.

[74] J.-M. Kang, S.-S. Seo, and J.-K. Hong. Usage pattern analysis of smartphones. In *Proceedings of the 13th Asia-Pacific Network Operations and Management Symposium (APNOMS)*, pages 1–8, 2011.

[75] S. Karagiannopoulos, A. Rigas, N. Hatziargyriou, G. Hug, and A. Oudalov. Battery energy storage capacity fading and control strategies for deterministic and stochastic power profiles. In *Proceedings of the Power Systems Computation Conference (PSCC)*, pages 1–7, 2016.

[76] M. Kauer, S. Naranayaswami, S. Steinhorst, M. Lukasiewycz, S. Chakraborty, and L. Hedrich. Modular system-level architecture for concurrent cell balancing. In *Proceedings of the 50th Annual Design Automation Conference (DAC)*, pages 155:1–155:10, 2013.

[77] M. Kauer, S. Narayanaswamy, M. Lukasiewycz, S. Steinhorst, and S. Chakraborty. Inductor optimization for active cell balancing using geometric programming. In *Proceedings of the Design, Automation & Test in Europe Conference Exhibition (DATE)*, pages 281–284, 2015.

[78] P. Keil and A. Jossen. Aging of lithium-ion batteries in electric vehicles: Impact of regenerative braking. *World Electric Vehicle Journal*, 7(1):41–51, 2015.

[79] P. Keil and A. Jossen. Charging protocols for lithium-ion batteries and their impact on cycle life – an experimental study with different 18650 high-power cells. *Journal of Energy Storage*, 6:125 – 141, 2016.

[80] P. Keil and A. Jossen. Impact of dynamic driving loads and regenerative braking on the aging of lithium-ion batteries in electric vehicles. *Journal of The Electrochemical Society*, 164(13):A3081– A3092, 2017.

[81] G.-H. Kim, K. Smith, K.-J. Lee, S. Santhanagopalan, and A. Pesaran. Multi-domain modeling of lithium-ion batteries encompassing multi-physics in varied length scales. *Journal of the Electrochemical Society*, 158(8):A955–A969, 2011.

[82] I. S. Kim. A technique for estimating the state of health of lithium batteries through a dual-sliding-mode observer. *IEEE Transactions on Power Electronics*, 25(4):1013–1022, 2010.

[83] J. Kim, A. Pröbstl, S. Chakraborty, and N. Chang. Aging mitigation of power supply-connected batteries. In *Proceedings of the 2014 International Symposium on Low Power Electronics and Design (ISLPED)*, pages 233–238, 2014.

[84] V. Klass, M. Behm, and G. Lindbergh. A support vector machine-based state-of-health estimation method for lithium-ion batteries under electric vehicle operation. *Journal of Power Sources*, 270:262 – 272, 2014.

[85] KPMG. Lithium-ion battery pack costs worldwide between 2010 and 2018 (in U.S. dollars per kilowatt hour). Statista - The Statistics Portal `www.statista.com/statistics/883118/global-lithium-ion-battery-pack-costs/`, 2018.

[86] N. H. Kutkut. A modular nondissipative current diverter for EV battery charge equalization. In *Proceedings of the Thirteenth Annual Applied Power Electronics Conference and Exposition (APEC)*, volume 2, pages 686–690, 1998.

[87] J. Lee, Y. Chon, and H. Cha. Evaluating battery aging on mobile devices. In *Proceedings of the 52nd Annual Design Automation Conference (DAC)*, pages 135:1–135:6, 2015.

[88] Lenovo. Power manager. `http://support.lenovo.com`, 2015.

[89] J. Li and M. A. Danzer. Optimal charge control strategies for stationary photovoltaic battery systems. *Journal of Power Sources*, 258:365 – 373, 2014.

[90] S. Li, A. Khisti, and A. Mahajan. Privacy-optimal strategies for smart metering systems with a rechargeable battery. In *Proceedings of the American Control Conference (ACC)*, pages 2080–2085, 2016.

[91] K. Lim, A. Laclcner, P. Braatz, W. Smith Jr, J. Margerum, and H. Lim. Accelerated lifetime studies on commercial lithium-ion battery cells. In *Proceedings of the Symposium on Batteries for Portable Applications and Electrical Vehicles*, volume 18, pages 470–478, 1997.

[92] H. Lin, T. Liang, and S. Chen. Estimation of battery state of health using probabilistic neural network. *IEEE Transactions on Industrial Informatics*, 9(2):679–685, 2013.

[93] E. Liu and P. Cheng. Achieving privacy protection using distributed load scheduling: A randomized approach. *IEEE Transactions on Smart Grid*, 8(5):2460–2473, 2017.

[94] Los Angeles Department of Water and Power. Electric rate summary. `https://www.ladwp.com`, 2017.

[95] R. Mahamud and C. Park. Reciprocating air flow for li-ion battery thermal management to improve temperature uniformity. *Journal of Power Sources*, 196(13):5685 – 5696, 2011.

[96] N. Maluf, D. Ghantous, F. Berkowitz, and C. Peabody. Method and circuitry to adaptively charge a battery/cell using the state of health thereof. US Patent 9,121,910, 2015.

[97] A. R. Mandli, S. Ramachandran, A. Khandelwal, and K. Y. Kim. Methods for adaptive battery charging and electronic device thereof. US Patent App. 15/593,924, 2018.

[98] A. Marongiu, N. Nlandi, Y. Rong, and D. U. Sauer. On-board capacity estimation of lithium iron phosphate batteries by means of half-cell curves. *Journal of Power Sources*, 324:158 – 169, 2016.

[99] MathWorks. Simscape library 2018b - generic battery model. `https://de.mathworks.com/help/physmod/sps/powersys/ref/battery.html`, 2018.

[100] N. Matsumura, N. Otani, and K. Hamaji. Intelligent battery charging rate management. US Patent App. 12/059,967, 2009.

[101] N. Mattisson, P. Ungar, T. Greening, and J. Koller. Tracking fading battery capacity in a plugged-in portable electronic device. US Patent App. 13/791,328, 2014.

[102] P. McDaniel and S. McLaughlin. Security and privacy challenges in the smart grid. *IEEE Security & Privacy*, 7(3):75–77, 2009.

[103] D. Mehta, P. Sapun, and A.-K. Hamke. In-depth: eMobility 2018 - statista mobility market outlook - trend report. Technical report, Statista - The Statistics Portal, 2018.

[104] A. Millner. Modeling lithium ion battery degradation in electric vehicles. In *Proceedings of the IEEE Conference on Innovative Technologies for an Efficient and Reliable Electricity Supply (CITRES)*, pages 349–356, 2010.

[105] R. Mingant, J. Bernard, and V. Sauvant-Moynot. Novel state-of-health diagnostic method for li-ion battery in service. *Applied Energy*, 183:390 – 398, 2016.

[106] A. Molina-Markham, P. Shenoy, K. Fu, E. Cecchet, and D. Irwin. Private memoirs of a smart meter. In *Proceedings of the 2nd ACM Workshop on Embedded Sensing Systems for Energy-Efficiency in Building (BuildSys)*, pages 61–66, 2010.

[107] S. W. Moore and P. J. Schneider. A review of cell equalization methods for lithium ion and lithium polymer battery systems. *SAE Publication*, 2001.

[108] Morgan Stanley. Worldwide lithium-ion battery use in 2014, by application. Statista - The Statistics Portal, Statista `www.statista.com/statistics/606507/lithium-battery-use-globally-by-application/`, 2018.

[109] D. Z. Morris. Apple, responding to iPhone battery controversy, cuts replacement cost to $29. *Fortune Magazine*, 30 December 2017.

[110] S. Narayanaswamy, M. Kauer, S. Steinhorst, M. Lukasiewycz, and S. Chakraborty. Modular active charge balancing for scalable battery packs. *IEEE Transactions on Very Large Scale Integration (VLSI) Systems*, 25(3):974–987, 2017.

[111] K. S. Ng, C.-S. Moo, Y.-P. Chen, and Y.-C. Hsieh. Enhanced coulomb counting method for estimating state-of-charge and state-of-health of lithium-ion batteries. *Applied Energy*, 86(9):1506 – 1511, 2009.

[112] E. A. Oliver and S. Keshav. An empirical approach to smartphone energy level prediction. In *Proceedings of the 13th International Conference on Ubiquitous Computing (UbiComp)*, pages 345–354, 2011.

[113] S. Park, L. Zhang, and S. Chakraborty. Battery assignment and scheduling for drone delivery businesses. In *Proceedings of the IEEE/ACM International Symposium on Low Power Electronics and Design (ISLPED)*, pages 1–6, 2017.

[114] C. Pascual and P. Krein. Switched capacitor system for automatic series battery equalization. In *Proceedings of the Applied Power Electronics Conference (APEC)*, volume 2, pages 848–854, 1997.

[115] C. Pastor-Fernández, K. Uddin, G. H. Chouchelamane, W. D. Widanage, and J. Marco. A comparison between electrochemical impedance spectroscopy and incremental capacity-differential voltage as li-ion diagnostic techniques to identify and quantify the effects of degradation modes within battery management systems. *Journal of Power Sources*, 360:301 – 318, 2017.

[116] C. Pastor-Fernández, T. F. Yu, W. D. Widanage, and J. Marco. Critical review of non-invasive diagnosis techniques for quantification of degradation modes in lithium-ion batteries. *Renewable and Sustainable Energy Reviews*, 109:138 – 159, 2019.

[117] Peng Rong and M. Pedram. An analytical model for predicting the remaining battery capacity of lithium-ion batteries. *IEEE Transactions on Very Large Scale Integration (VLSI) Systems*, 14(5):441–451, 2006.

[118] G. P. Perrucci, F. H. P. Fitzek, and J. Widmer. Survey on energy consumption entities on the smartphone platform. In *Proceedings of the IEEE 73rd Vehicular Technology Conference (VTC Spring)*, pages 1–6, 2011.

[119] A. Pesaran, A. Vlahinos, and T. Stuart. Cooling and preheating of batteries in hybrid electric vehicles. In *Proceedings of the 6th ASME-JSME Thermal Engineering Joint Conference*, pages 1–7, 2003.

[120] A. Pröbstl, B. Islam, S. Nirjon, N. Chang, and S. Chakraborty. Intelligent chargers will make mobile devices live longer. *IEEE Design Test*, 2020.

[121] A. Pröbstl, P. Kindt, E. Regnath, and S. Chakraborty. Smart2: Smart charging for smart phones. In *Proceedings of the IEEE 21st International Conference on Embedded and Real-Time Computing Systems and Applications (RTCSA)*, pages 41–50, 2015.

[122] A. Pröbstl, S. Park, S. Narayanaswamy, S. Steinhorst, and S. Chakraborty. SOH-aware active cell balancing strategy for high power battery packs. In *Proceedings of the Design, Automation & Test in Europe Conference Exhibition (DATE)*, pages 431–436, 2018.

[123] A. Pröbstl, S. Park, S. Steinhorst, and S. Chakraborty. Cost/privacy co-optimization in smart energy grids. In *Proceedings of the Design, Automation & Test in Europe Conference Exhibition (DATE)*, pages 872–877, 2019.

[124] M. L. Puterman. *Markov decision processes: discrete stochastic dynamic programming*. John Wiley & Sons, 2009.

[125] Qnovo. Qnovo technology. `https://qnovo.com/technology/`, 2019.

[126] N. Ravi, J. Scott, L. Han, and L. Iftode. Context-aware battery management for mobile phones. In *Proceedings of the Sixth Annual IEEE International Conference on Pervasive Computing and Communications (PerCom)*, pages 224–233, 2008.

[127] T. Reddy. *Linden's Handbook of Batteries, 4th Edition*. McGraw-Hill Education, 2010.

[128] S. M. Rezvanizaniani, Z. Liu, Y. Chen, and J. Lee. Review and recent advances in battery health monitoring and prognostics technologies for electric vehicle (EV) safety and mobility. *Journal of Power Sources*, 256:110 – 124, 2014.

[129] Samsung. Battery life extender. `www.samsung.com`, 2014.

[130] F. Savoye, P. Venet, M. Millet, and J. Groot. Impact of periodic current pulses on li-ion battery performance. *IEEE Transactions on Industrial Electronics*, 59(9):3481–3488, 2012.

[131] S. Saxena, G. Sanchez, and M. Pecht. Batteries in portable electronic devices: A user's perspective. *IEEE Industrial Electronics Magazine*, 11(2):35–44, 2017.

[132] F. Schlachter. No moore's law for batteries. *Proceedings of the National Academy of Sciences*, 110(14):5273–5273, 2013.

[133] S. F. Schuster, T. Bach, E. Fleder, J. Müller, M. Brand, G. Sextl, and A. Jossen. Nonlinear aging characteristics of lithium-ion cells under different operational conditions. *Journal of Energy Storage*, 1:44–53, 2015.

[134] D. Sera, R. Teodorescu, and P. Rodriguez. PV panel model based on datasheet values. In *Proceedings of the IEEE International Symposium on Industrial Electronics (ISIE)*, pages 2392–2396, 2007.

[135] L. Serrao, S. Onori, A. Sciarretta, Y. Guezennec, and G. Rizzoni. Optimal energy management of hybrid electric vehicles including battery aging. In *Proceedings of the American Control Conference (ACC)*, pages 2125–2130, 2011.

[136] Y. Shi, K. Smith, R. Zane, and D. Anderson. Life prediction of large lithium-ion battery packs with active and passive balancing. In *Proceedings of the American Control Conference (ACC)*, pages 4704–4709, 2017.

[137] C. Sinai. coconutBattery. `https://www.coconut-flavour.com`, 2005 – 2019.

[138] S. Steinhorst, M. Kauer, A. Meeuw, S. Narayanaswamy, M. Lukasiewycz, and S. Chakraborty. Cyber-physical co-simulation framework for smart cells in scalable battery packs. *ACM Transactions on Design Automation of Electronic Systems (TODAES)*, 21(4):62:1–62:26, 2016.

[139] D. I. Stroe, M. Swierczynski, A. I. Stan, V. Knap, R. Teodorescu, and S. J. Andreasen. Diagnosis of lithium-ion batteries state-of-health based on electrochemical impedance spectroscopy technique. In *Proceedings of the IEEE Energy Conversion Congress and Exposition (ECCE)*, pages 4576–4582, 2014.

[140] G. Suri and S. Onori. A control-oriented cycle-life model for hybrid electric vehicle lithium-ion batteries. *Energy*, 96:644 – 653, 2016.

[141] K. Takei, K. Kumai, Y. Kobayashi, H. Miyashiro, N. Terada, T. Iwahori, and T. Tanaka. Cycle life estimation of lithium secondary battery by extrapolation method and accelerated aging test. *Journal of Power Sources*, 97:697–701, 2001.

[142] M. T. Tesfaye, M. Nardello, and D. Brunelli. Residential electrical consumption disaggregation on a single low-cost meter. In *Proceedings of the IEEE Workshop on Environmental, Energy, and Structural Monitoring Systems (EESMS)*, pages 1–6, 2017.

[143] Tesla. Powerwall: Technical specs. `https://www.tesla.com/powerwall`, 2017.

[144] M. Torchio, L. Magni, R. B. Gopaluni, R. D. Braatz, and D. M. Raimondo. LIONSIMBA: A Matlab framework based on a finite volume model suitable for li-ion battery design, simulation, and control. *Journal of The Electrochemical Society*, 163(7):A1192–A1205, 2016.

[145] A. E. Trippe, R. Arunachala, T. Massier, A. Jossen, and T. Hamacher. Charging optimization of battery electric vehicles including cycle battery aging. In *Proceedings of the IEEE PES Innovative Smart Grid Technologies, Europe (ISGT-Europe)*, pages 1–6, 2014.

[146] K. Uddin, S. Perera, W. Widanage, L. Somerville, and J. Marco. Characterising lithium-ion battery degradation through the identification and tracking of electrochemical battery model parameters. *Batteries*, 2(2):13, 2016.

[147] University of Massachusetts Amherst. Umass smart* home data set. `http://traces.cs.umass.edu/index.php/Smart/Smart`, 2017.

[148] USB Implementers Forum, Inc. *Battery Charging Specification - Revision 1.2*, 2012.

[149] R. Valentini, M. Levorato, and F. Santucci. Optimal aging-aware channel access and power allocation for battery – powered devices with radio frequency energy harvesting. *IEEE Transactions on Communications*, 66(11):5773–5787, 2018.

[150] K. Vatanparvar and M. A. Al Faruque. Battery lifetime-aware automotive climate control for electric vehicles. In *Proceedings of the 52nd Annual Design Automation Conference (DAC)*, pages 37:1–37:6, 2015.

[151] J. Vetter, P. Novák, M. Wagner, C. Veit, K.-C. Möller, J. Besenhard, M. Winter, M. Wohlfahrt-Mehrens, C. Vogler, and A. Hammouche. Ageing mechanisms in lithium-ion batteries. *Journal of Power Sources*, 147(1):269 – 281, 2005.

[152] J. Wang, P. Liu, J. Hicks-Garner, E. Sherman, S. Soukiazian, M. Verbrugge, H. Tataria, J. Musser, and P. Finamore. Cycle-life model for graphite-lifepo4 cells. *Journal of Power Sources*, 196(8):3942 – 3948, 2011.

[153] Y. Wang, X. Lin, Q. Xie, N. Chang, and M. Pedram. Minimizing state-of-health degradation in hybrid electrical energy storage systems with arbitrary source and load profiles. In *Proceedings of the Design, Automation & Test in Europe Conference Exhibition (DATE)*, pages 110:1–110:4, 2014.

[154] Z. Wei, F. Leng, Z. He, W. Zhang, and K. Li. Online state of charge and state of health estimation for a lithium-ion battery based on a data-model fusion method. *Energies*, 11(7):1810, 2018.

[155] X. Wu, D. Freese, A. Cabrera, and W. A. Kitch. Electric vehicles' energy consumption measurement and estimation. *Transportation Research Part D: Transport and Environment*, 34:52 – 67, 2015.

[156] Q. Xie, M. J. Dousti, and M. Pedram. Therminator: A thermal simulator for smartphones producing accurate chip and skin temperature maps. In *Proceedings of the IEEE/ACM International Symposium on Low Power Electronics and Design (ISLPED)*, pages 117–122, 2014.

[157] Q. Xie, J. Kim, Y. Wang, D. Shin, N. Chang, and M. Pedram. Dynamic thermal management in mobile devices considering the thermal coupling between battery and application processor. In *Proceedings of the IEEE/ACM International Conference on Computer-Aided Design (ICCAD)*, pages 242–247, 2013.

[158] Q. Xie, X. Lin, Y. Wang, M. Pedram, D. Shin, and N. Chang. State of health aware charge management in hybrid electrical energy storage systems. In *Proceedings of the Conference on Design, Automation & Test in Europe (DATE)*, pages 1060–1065, 2012.

[159] Q. Xie, D. Shin, N. Chang, and M. Pedram. Joint charge and thermal management for batteries in portable systems with hybrid power sources. *IEEE Transactions on Computer-Aided Design of Integrated Circuits and Systems (TCAD)*, 35(4):611–622, 2016.

[160] Q. Xie, S. Yue, M. Pedram, D. Shin, and N. Chang. Adaptive thermal management for portable system batteries by forced convection cooling. In *Proceedings of the Design, Automation & Test in Europe Conference Exhibition (DATE)*, pages 1225–1228, 2013.

[161] L. Yang, X. Chen, J. Zhang, and H. Poor. Cost-effective and privacy-preserving energy management for smart meters. *IEEE Transactions on Smart Grid*, 6(1):486–495, 2015.

[162] D. Zhang, S. Dey, H. E. Perez, and S. J. Moura. Real-time capacity estimation of lithium-ion batteries utilizing thermal dynamics. *IEEE Transactions on Control Systems Technology*, pages 1–9, 2019.

[163] J. Zhang and J. Lee. A review on prognostics and health monitoring of li-ion battery. *Journal of Power Sources*, 196(15):6007 – 6014, 2011.

[164] W. Zhe. Battery life doctor. `https://apps.apple.com/app/battery-life-doctor/id1165930552?mt=8&ign-mpt=uo%3D4`, 2016 – 2019.

[165] A. Zoha, A. Gluhak, M. Imran, and S. Rajasegarar. Non-intrusive load monitoring approaches for disaggregated energy sensing: A survey. *Sensors*, 12(12):16838–16866, 2012.

List of Tables

2.1 Aging parameters 28

3.1 SOH-aware balancing cell grouping rules 44
3.2 Determination of balancing currents for SOH-aware balancing 45

4.1 Results for cycle life improvement with smart charging 66
4.2 Power gap 75

5.1 Maximum and minimum costs 88
5.2 Parametrization for EES and PV sizes 89
5.3 Selected results of the cost/privacy co-optimization 91

6.1 Multi-scale evaluation selected results 110
6.2 Multi-scale evaluation results for target SOC variations 114
6.3 Multi-scale evaluation results for charge delay variations 115
6.4 Multi-scale evaluation results for balancing current variations 116

List of Figures

1.1 Battery discharge schematic 4
1.2 Battery cost development 8
1.3 Global Li-Ion battery market 9
1.4 CC-CV charging of a laptop battery 10

2.1 Battery degradation causes 20
2.2 Battery aging severity factor map 29

3.1 Overview of SOH-aware active cell balancing 35
3.2 Active cell balancing architecture operating principle 38
3.3 SOH development with SOH-aware cell balancing 39
3.4 Charge transfer efficiency model 42
3.5 Example of cell groupings in SOH-aware cell balancing 43
3.6 Comparison of balancing schemes with varying balancing current 46
3.7 Comparison of balancing schemes with varying normalized aging-speed 47
3.8 Mean number of cycles until EOL for random distributions of initial SOH . . . 48

4.1 Concept of an intelligent smartphone charger 53
4.2 Comparison of charging schedules 56
4.3 System abstraction layers in Android 58
4.4 Scatter plot of smartphone plug duration vs. plug time 61
4.5 Number of charge events for given charge duration 61
4.6 Bimodal log-normal probability density function fitted to data 63
4.7 Unimodal log-normal function fitted to data 64
4.8 Battery profile for smart charger usage 65
4.9 Bar plot showing the lifetime comparison for smart charging 66
4.10 Charging plot of individual user original and with aging mitigating measures . . 68
4.11 Smartphone plug time statistics 69
4.12 Mean squared error of plug predictors for individual users 70
4.13 Bar plot showing the performance of predictors 70
4.14 Error comparison of plug predictors 71
4.15 Intelligent charging protocol 72
4.16 Charge delay implementation 73
4.17 Hybrid charger 75
4.18 Battery replacement costs 76

5.1 Cost/Privacy Co-optimization overview 81
5.2 Grid power profile of cost optimal and water filling strategy 83
5.3 Load power probability distribution 85
5.4 Trade-off between privacy and the total cost of ownership 90
5.5 Cost components 91
5.6 Cost overhead 92

6.1 Multi-scale health management framework concept 97
6.2 Temperature variations and manufacturing inhomogeneities 101
6.3 Charge delays and SOC reduction 102
6.4 Framework implementation 105
6.5 Impact of charge delay on different pack qualities 107
6.6 Impact of cooling system on battery health 108
6.7 Multi-scale battery health management selected results 111
6.8 Multi-scale battery health management full results 113

Nomenclature

Symbol	Description	Unit
$\mathcal{A}$	Set of actions in Markov decision process	
a	Action in Markov decision process	
α	Smoothing factor in predictor	
B	Battery	
$\mathcal{B}$	Set of states in Markov decision process	
b	State in Markov decision process	
C	Cell capacity	A s
C_0	Usable battery capacity	A s
C_h	Capacity of healthier cell	A s
C_l	Capacity of less healthy cell	A s
C_N	Nominal battery capacity	A s
C_OSS	Parasitic output capacitance of the MOSFET	H
C_U	Unusable battery capacity	A s
D	Degradation parameter	
δ	Depth of discharge	
$\overline{T_\mathrm{plg}}$	Average duration a device remains plugged for charging	s
$\overline{T_\mathrm{plug,n}}$	Average duration a device remains plugged for charging for specific bin in predictor	s
ΔS	State of charge interval	
Δt	Time interval	s
$\Delta\theta$	Battery temperature difference	K
E_a	Activation energy	J
E_diss	Dissipated energy	J
E^cd	Dissipated energy by conduction in active cell balancing	J
E^sw	Dissipated energy by switching in active cell balancing	J
ε	End of life	
$\varepsilon_\%$	End of life in percent	%
η	Charge transfer direction and loss $\in \{-\gamma, 0, 1\}$	
E_tx	Transferred energy	J

Symbol	Description	Unit
γ	Efficiency	
H	Entropy	
$\mathcal{H}_P$	History of battery plug times	
$\mathcal{H}_S$	History of state of charge levels	
I	Static current	A
i	Time varying current	A
I_{b}	Balancing current of a battery	A
$I_{\mathrm{B,max}}$	Maximum balancing current of a battery	A
I_{C}	Accumulated load current of a battery including balancing current	A
I_{D}	Discharge load current of a battery	A
I_{EES}	Charge and discharge current of a stationary storage	A
$\mathcal{I}_{\mathrm{MI}}$	Mutual information	bit
ι_C	C-rate used to charge or discharge a battery	
$\iota_{C,\mathrm{max}}$	Maximum C-rate available to charge or discharge a battery	
I_{peak}	Peak balancing current	A
K_{a}	Constant in Suri et al. aging model, state of charge dependence	
κ	State of health	
K_{b}	Constant in Suri et al. aging model, state of charge dependence	
K_{c}	Constant in Suri et al. aging model, C-rate dependence	
K_{co}	Constant in Millner aging model, coefficient of throughput	
K_{ex}	Constant in Millner aging model, exponent of state of charge swing	
K_{pl}	Constant in Suri et al. aging model, power law exponent	
K_{soc}	Constant in Millner aging model, coefficient for mean state of charge	
K_{t}	Constant in Millner aging model, account for decay rate	
L	Inductor	H
$\mathcal{L}$	Set of load power states in Markov decision process	
l	Load power state in Markov decision process	
Λ_{EES}	Purchase cost of a stationary storage	USD
λ_{g}	Cost associated to buying and selling electricity to and from the grid	
$\lambda_{\mathrm{g,norm}}$	Normalized cost associated to buying and selling electricity	
λ_{h}	Cost associated to battery degradation	
$\lambda_{\mathrm{h,norm}}$	Normalized cost associated to battery degradation	
λ_j	Cost in category j (e.g. health, privacy, grid)	
$\lambda_{j,\mathrm{max}}$	Maximum cost in category j (e.g. health, privacy, grid)	
$\lambda_{j,\mathrm{min}}$	Minimum cost in category j (e.g. health, privacy, grid)	
$\lambda_{j,\mathrm{norm}}$	Normalized cost in category j (e.g. health, privacy, grid)	
λ_{p}	Cost associated to privacy	
$\lambda_{\mathrm{p,max}}$	Maximum cost for privacy	

Symbol	Description	Unit
$\lambda_{\mathrm{p,norm}}$	Normalized cost associated to privacy	
Λ_{SOH}	Loss in cost value of a stationary storage due to aging	USD
Λ_{USD}	Cost in dynamic energy pricing	USD
$\Lambda_{\mathrm{USD,peak}}$	Peak cost in dynamic energy pricing	USD
M	MOSFET switch	
m	Entry counter within bins in predictor	
M_{Ld}	Transition probability matrix for load power	
μ	Mean	
n	Bin index in predictor	
N_{bins}	Number of bins in predictor	
$N_{\mathrm{E,n}}$	Number of entries into specific bin n in predictor	
N_{G}	Number of energy generators	
N_{L}	Number of energy consuming loads	
N_{P}	Number of parallel connected cells in a pack	
N_{PE}	Number of detected plug events of a device	
N_{PS}	Number of energy prosumers	
N_{S}	Number of series connected cells in a pack	
N_{SOC}	Number of stored state of charge values in predictor	
N_{TP}	Effective number of throughput cycles	
ν	Placeholder for cell pairs grouped in active cell balancing	
$p(\cdot)$	Probability mass function	
P_{EES}	Stationary battery storage power	W
$P_{\mathrm{ESS,max}}$	Maximum stationary battery storage power	W
$P_{\mathrm{ESS,min}}$	Minimum stationary battery storage power	W
P_{g}	Grid power	W
$P_{\mathrm{g,max}}$	Maximum grid power	W
Φ_1	Charging phase	
Φ_2	Discharging phase	
π	Policy in Markov decision process	
P_{load}	Load power	W
P_{PV}	PV power	W
$P_{\mathrm{PV,out}}$	Output PV power	W
$\Pr$	Probability density function	
P_{target}	Target power	W
Q_0	Available battery charge	A s
Q_{bal}	Amount of battery charge required in for cell balancing	A s
Q_{cyc}	Amount of battery charge effectively discharged in one cycle	A s
$Q_{\mathrm{loss,\%}}$	Charge loss in percent	%
Q_{nom}	Nominal battery charge	A s

Symbol	Description	Unit
Q_{req}	Required battery charge	A s
Q_{rx}	Charge transferred by the source cell	A s
$Q_{\mathrm{tp,Ah}}$	Throughput battery charge	A h
Q_{tx}	Charge received by the destination cell	A s
$\mathcal{R}$	Set of rewards	
R	Reward for transitioning from one state to another	
r	Reward	
R_{gas}	Universal gas constant	$\mathrm{J\,K^{-1}\,mol^{-1}}$
ρ	Control signal in active cell balancing architecture	
$\mathcal{S}$	Set of state of charge states	
S	State of charge	
$\overline{S}$	Average state of charge	
S_{buf}	Buffer amount of charge level	
σ	State of charge swing	
S_{init}	Initial state of charge	
S_{med}	State of charge medium level	
S_{tar}	State of charge target level	
T	Time duration, time interval	s
t	Time	s
T_{buf}	Time buffer	s
T_{chg}	Time required to charge from current to target state of charge	s
T_{cycle}	Duration of a charge/discharge cycle	s
T_{del}	Time delay applied before starting the charge process	s
θ	Temperature	K
θ_{B}	Battery temperature	K
θ_{cell}	Battery cell temperature	K
θ_{EES}	Stationary battery storage temperature	K
θ_{in}	In-flowing temperature of a battery pack	K
θ_{max}	Maximum temperature	K
θ_{min}	Minimum temperature	K
θ_{out}	Out-flowing temperature of a battery pack	K
θ_{ref}	Reference battery temperature	K
t_{upprev}	Time of the previous unplug event	s
T_{life}	Shelf life of a battery at 25°C and 50% SOC until EOL	s
t_{now}	Current time stamp	s
T_{O}	Time duration of stationary storage operation	s
t_{OFF}	Turn-off time of switch	s
t_{ON}	Turn-on time of switch	s
T_{P}	Time duration of a trip	s
T_{plg}	Duration a device remains plugged for charging	s

Symbol	Description	Unit
t_{plg}	Plug time of a battery	s
t_{start}	Start time of the charging process of a battery	s
t_{up}	Unplug time of a battery	s
$\mathcal{U}$	Set of cloud cover states in Markov decision process	
u	Cloud cover state in Markov decision process	
V	Voltage	V
v_{a}	Aging speed in points per million and cycle: $\frac{1\times10^{-6}}{\text{cycle}} = 1$ ppmc	ppmc
w_{g}	Grid weight	
w_{h}	Battery aging weight	
w_{p}	Privacy weight	
w_{plug}	Weight in smart charging predictor	
$\mathcal{X}$	Random variable	
x	Random variable value	
ξ	Variance	
$\mathcal{Y}$	Random variable	
y	Random variable value	
$\mathcal{Z}$	Set of time-of-day states in Markov decision process	
z	Time-of-day state in Markov decision process	
ζ_{funct}	Severity factor in Suri et al. aging model	

Abbreviations

ANN Artificial Neural Network

API Application Programming Interface

BMS Battery Management System

CAEBAT Computer Aided Engineering for Batteries

CC Constant Current

CC-CV Constant-Current-Constant-Voltage

CV Constant Voltage

CPU Central Processing Unit

DOD Depth of Discharge

DSE Design Space Exploration

ECU Electronic Control Unit

EES Electrical Energy Storage

EIS Electrochemical Impedance Spectroscopy

EMA Exponential Moving Average

EOL End-of-Life

EV Electric Vehicle

GPU Graphics Processing Unit

GSM Global System for Mobile Communications

HEES Hybrid Electrical Energy Storage

HVAC Heating, Ventilation and Air Conditioning

IC Integrated Circuit

ID Identity

IoT Internet of Things

LCD Liquid Crystal Display

LCO Lithium Cobalt Oxide

LFP Lithium Iron Phosphate

Li-Ion Lithium-Ion

MDP Markov Decision Process

MOSFET Metal-Oxide-Semiconductor Field-Effect Transistor

NEDC New European Driving Cycle

NILM Non-Intrusive Load Monitoring

NMC Nickel-Mangan-Cobalt-Oxide

OCV Open Circuit Voltage

OAS Open Architecture Software

OS Operating System

PHEV Plug-In Hybrid Electric Vehicle

PV Photovoltaic

PWM Pulse Width Modulated

RAM Random Access Memory

RC Resistor-Capacitor

SEI Solid Electrolyte Interphase

SMA Simple Moving Average

SOA Safe Operating Area

SOC State-of-Charge

SOH State-of-Health

SVM Support Vector Machine

TPM Transition Probability Matrix

TRM Transition Reward Matrix

UP Utility Provider

USB Universal Serial Bus

VIBE Virtual Integrated Battery Environment

WLTP Worldwide Harmonized Light Vehicles Test Procedure